THE SEPARATIONS OF PICOLINE ISOMERS BY ENCLATHRATION

Emma Jane Tiffin

Dissertation presented for the Degree of Master of Science

in the Department of Chemistry

University of Cape Town

April 2019

Supervisors: Professor Luigi R Nassimbeni & Assoc. Professor Neil Ravenscroft

Declaration

I, Emma Jane Tiffin, hereby declare that the work on which this thesis is based is my original work (except where acknowledgements indicate otherwise) and that neither the whole work nor any part of it has been, is being, or is to be submitted for another degree in this or any other university. I authorise the University to reproduce for the purpose of research, either the whole or any portion of the contents, in any manner whatsoever.

Signed by candidate

Signature: Date: April 2019

Acknowledgements

My heartfelt thanks to:

Prof. Luigi Nassimbeni for all his understanding, guidance and wisdom. Also, for making sure I learned something new every day – even it means countless 10 cents forfeited. Thank you for sparking my curiosity and accompanying me on this adventure and, of course, the many gifts of chocolate.

To Assoc. Prof. Neil Ravenscroft for all his support and direction. Without his incredible attention to detail this dissertation would not have been possible. Thank you for always checking where I was.

To Nicole Sykes for her incredible patience, quick wit and enthusiasm in all endeavours. Your advice and support truly shaped this entire project. The laughs and conversations will be fondly remembered. Thank you for helping me have my life in control and inspiring me throughout my years in the Centre for Supramolecular Chemistry Research.

To everyone at the Centre for their camaraderie, advice and assistance with my research and writing.

To Dr Hong Su for the single crystal data collection and processing.

To Pete Roberts for the ^{1}H-NMR spectra collection.

To my family for their unfailing support, financial and otherwise, in my adventures with the picolines. Thank you for your proof reading, encouragement and indulgence.

Lastly, to my Gaga and Bill, whose love and support I will always cherish.

Publications

The work in this thesis has been published:

Tiffin E. J., Sykes N. M., Weber E., Ravenscroft N., Nassimbeni L. R. Enclathration of picoline isomers by (rac)-TADDOLs: structures, selectivity and thermal analysis. *Cryst. Growth Des.,* 2019, **19** (3), 1880-1887. DOI: 10.1021/acs.cgd.8b01853

Abstract

The chemical and physical properties of isomers make them difficult to separate using conventional methods. This renders the separation of isomers one of the more challenging obstacles in chemistry. In these cases, the supramolecular phenomenon of host-guest chemistry may be used in order to achieve separation.

In this investigation, the preferences of three TADDOL (α,α,α',α'-tetraphenyl-l,3-dioxolane-4,5-dimethanol) - derived host compounds towards the isomers of methyl-pyridines (picolines) were studied. Crystals of ten novel inclusion compounds were synthesised and their structural properties were further characterised using an array of techniques. Thermal analysis was also conducted on these and other TADDOL-derived inclusion compounds.

Binary competition experiments were performed with varying mole fractions of guests in the starting solution and detailed selectivity curves were generated. It was apparent that all three hosts discriminate between the picoline isomer guests. Notably, the three hosts display different preferences towards the picoline isomers and these results were rationalised by their resulting crystal structures, packing analysis, solubilities and correlated to their DSC results.

DSC results showed a correlation between the thermal stability of an inclusion compound and the preference of the host towards the certain isomer involved in the inclusion complex. Further discussion on the selectivity preferences with regard to solubilities and crystal growth times was conducted.

Abbreviations and Symbols

DNA	Deoxyribonucleic acid
CSD	Cambridge Structural Database
π – π	Pi – pi interaction
α-phase	The host compound in its non-porous phase (apohost)
β-phase	The host-guest complex
2PIC	2-picoline
3PIC	3-picoline
4PIC	4-picoline
PYR	Pyridine
TA	Tartaric acid
DBTA	O,O'-dibenzoyl tartaric acid
DTTA	O,O'-di-p-tolyl tartaric acid
TADDOL	α,α,α',α'-tetraaryl-l,3-dioxolane-4,5-dimethanol
H1	(4RS,5RS)-2,2-dimethyl-α,α,α',α'-tetrakis(p-tolyl)-1,3- dioxolane-4,5-dimethanol
H2	(4RS,5RS)-2,2-dimethyl-α,α,α',α'-tetrakis(p-fluorophenyl)-1,3-dioxolane-4,5-dimethanol
H3	(4RS, 5RS)-2,2-dimethyl-α,α,α',α'-tetraphenyl -1,3-dioxolane-4,5-dimethanol
K	Selectivity coefficient
X_A	Mole fraction of guest A in initial starting solution
X_B	Mole fraction of guest B in initial starting solution
Z_A	Mole fraction of guest A in the resulting crystal
Z_B	Mole fraction of guest B in the resulting crystal
SCXD	Single Crystal X-ray Diffraction
PXRD	Powder X-ray Diffraction
2θ	θ is the angle between the incident ray and the scattering planes
HSM	Hot Stage Microscopy
TGA	Thermogravimetric analysis
DSC	Differential Scanning Calorimetry
^{1}H-NMR	Proton Nuclear Magnetic Resonance
CCDC	The Cambridge Crystallographic Data Centre
a, *b*, *c*	Unit cell axes
α	Angle between the b and c unit cell axes
β	Angle between the a and c unit cell axes
γ	Angle between the a and b unit cell axes
Z	Number of formula units per unit cell
Z'	Reduced number of formula units per unit cell
T_{peak}	Peak temperature
T_{boil}	Boiling point temperature
T_{on}	Onset temperature

Atom Colours

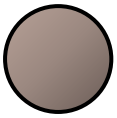

Carbon

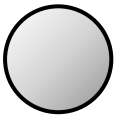

Hydrogen

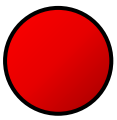

Oxygen

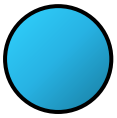

Nitrogen

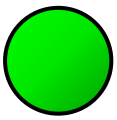

Fluorine

Table of Contents

Chapter 1. Introduction

1.1 Supramolecular Chemistry

Supramolecular chemistry is an extensive multidisciplinary field of chemistry, which attracts attention from a diverse range of researchers, including biochemists, physicists, mathematicians, engineers and medicinal chemists, along with many others. Supramolecular chemistry has been described as "chemistry beyond the molecule", and it encompasses chemical systems that are held together by intermolecular noncovalent interactions. Where traditional chemists focus on the covalent bond, supramolecular chemistry studies these weaker, reversible, intermolecular forces.[1,2] These supramolecular systems are diverse and potentially highly complex, ranging from simple host:guest compounds to programmable self-organising systems.

This branch of chemistry is relatively new, with the first simple supermolecules being described in the 1800s, followed by rapid advancements in the field occurring from the 1960s onwards.[3] The birth of X-ray crystallography allowed incredible insight into the structures of crystalline material, and the invention and proliferation of supercomputers has driven the growth of this field. A timeline of the history of supramolecular chemistry has been included in Figure 1.1, which gives a brief overview of the major contributions and discoveries in this field.

Supramolecular chemistry is present in almost all of the world around us, making up a large part of biological systems, including the iconic helix of DNA, along with furthering understanding of protein structures. This field has been instrumental in medicinal chemistry, primarily drug discovery, and plays a large part in synthetic chemistry. Its vibrant history culminates in the present time, where scientists are looking at the applications of these supramolecular discoveries and applying them to the fields of materials technology, catalysis, medicine and nanotechnology.[4]

1800s

There are multiple discoveries of supramolecular compounds beginning with chlorine hydrate by Sir Humphry Davy in **1810**. Inclusion compounds, including clathrates are identified and the basis of coordination chemistry is developed by Alfred Werner in **1893**. Emil Fischer proposes the *lock and key* concept for enzyme binding.

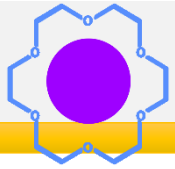

1960- 1990

The **1960s** usher in an explosion of supramolecular discoveries including the synthesis of Schiff base macrocycles in **1961** and **1964** by N. F. Curtis and Busch and Jager, respectively. Crown ethers were synthesised by Charles J. Pederson and Jean-Marie Lehn would synthesise the first cryptands, which are multidentate ligands that bind cations.

This **1960s** work would launch the field of "supramolecular chemistry" and Lehn coins this term in **1978**. In the **1970s** specialised host compounds and cyclodextrins are synthesised which lead to advances in host-guest chemistry. Vögtle and Weber synthesise podand hosts and develop specific nomenclature in **1981**.

Donald J. Cram, Charles J. Pedersen and Jean-Marie Lehn would go on to share the **1987** Nobel Prize in Chemistry for their supramolecular work.

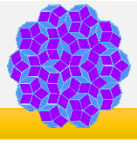

2010 -Present

The advances continue with Jean-Pierre Sauvage, Sir J. Fraser Stoddart and Bernard L. Feringa being awarded the Nobel prize in Chemistry, for the design and synthesis of molecular machines in **2016**. The field of nanomaterials is expanded with the publication of *Supramolecular Chemistry: from molecules to nanomaterials* by P. A. Gale and J. W. Steed in **2012**.

1900 - 1960

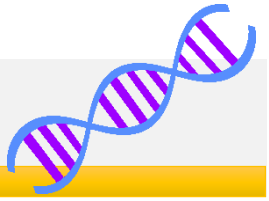

The supramolecular developments continue with these noncovalent interactions becoming more recognised leading to the inclusion of the Hydrogen Bond in Linus Pauling's **1939** book *The Nature of the Chemical Bond*. Inclusion compounds are further characterised and the term clathrate is introduced.

The development of X-ray crystallography allows for the structures of supramolecular compounds to be determined including β-quinol inclusion compounds by H. M Powell in **1945** and vitamin B_{12} by Dorothy Crowfoot Hodgkin in **1956**. The iconic structure of DNA by Watson and Crick is elucidated in the early **50s**.

1990 - 2010

The computational advancements of the **1990s** change the landscape for supramolecular chemistry. The Cambridge Structural Database adopted the "Crystallographic Information File" (CIF) in **1991** and the development of the Internet had great impacts on the sharing of information and online structural databases.

The publication of *Comprehensive Supramolecular Chemistry* by Atwood, Davies, MacNicol and Vögtle solidified supramolecular chemistry's development and presences as a prominent, state of the art field of chemistry. The advances in supercomputing in the **2000s** allowed for the solving of complex crystal structures and in-depth computational analysis is now possible using specialised software. Multiple Nobel prizes in Chemistry are awarded to scientists specialising in supramolecular work such as ion channels.

Figure 1.1: A timeline of the major events in the field of supramolecular chemistry.[1,3,4]

1.2 Host-Guest Chemistry

As described in the previous section, in the simplest description, a supermolecule is an association or noncovalent binding of at least two components to make a larger complex.[1] In a binding scenario, a component must be doing the binding and one must be the one being bound. In this case, a molecule that is doing the binding is termed a 'host' and the one being bound is the 'guest' molecule. The host is, generally, the larger molecule or compound and contains sites suitable for binding a guest. These sites need to be able to partake in intermolecular interactions to allow for complexation. A guest molecule is generally smaller, perhaps a cation or anion or simple compound, and it should contain receptors or moieties, which allow for the participation in intermolecular interactions. The host molecule is formally the one that possesses convergent bonding moieties, such as hydrogen bond donors, or Lewis basic donor atoms, and the guest possesses the divergent acceptor binding sites, such as Lewis acid metal cation or hydrogen bond acceptors.[1]

These noncovalent, intermolecular interactions encompass a large spectrum of forces that display a wide array of strengths and compositions. [5] These interactions are listed in Figure 1.2, with their respective strengths and some examples included. A supramolecular complex is likely to feature many of these interactions, and the interplay of these forces must be

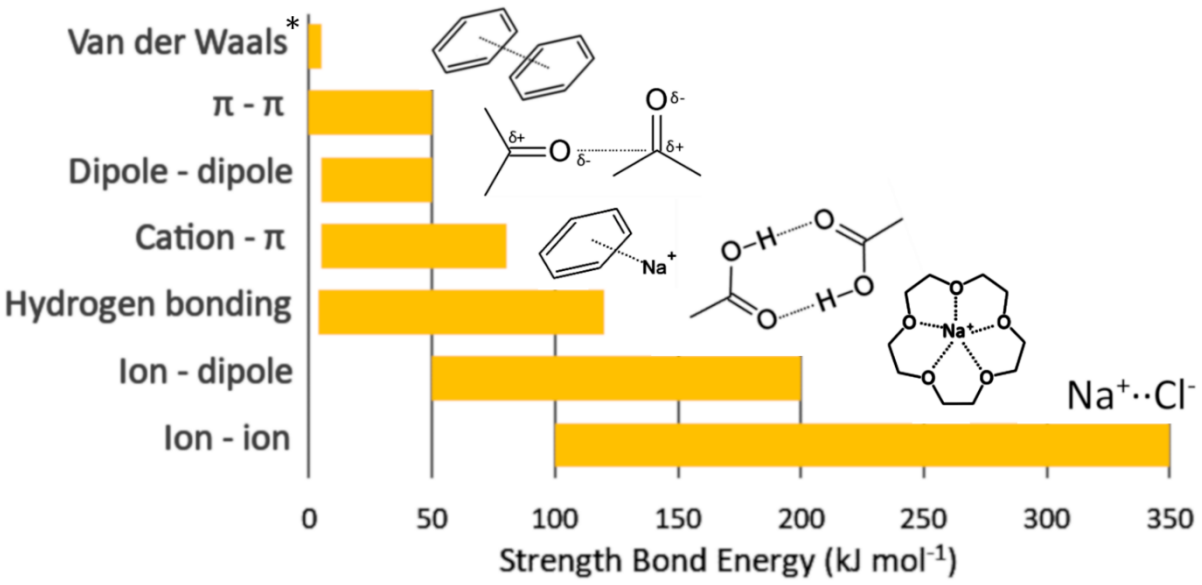

Figure 1.2: The strengths of the most common intermolecular interactions featured in host-guest compounds. * van der Waals forces have many examples including simple host-guest compounds which have not been pictured.[1]

considered when examining a supramolecular system. There are also solvation and hydrophobic effects to consider. These effects occur when the solvent (usually polar) exerts an exclusionary force on large molecules, which are then forced together and may look like they are held by attractive forces. These forces are hard to measure and their strength varies, so they have not been included in Figure 1.2. Similarly, Van der Waals forces are variable in strength and arise when the polarisation of an electron cloud by a nearby nucleus results in a weak attractive force. These likely contribute to the complexation of many host-guest compounds and their strength depends on the surface area of the compounds involved. Recent studies of anion – π interactions have been conducted, and these interactions have been identified in halide-arene complexes. However, these intermolecular forces appear to be relatively weak. This vast array of intermolecular interactions play a role in the formation of host-guest compounds and certain interactions can be almost guaranteed by utilising hosts with certain features.[1]

In order to classify host-guest compounds, it is important to look at the host used and the nature of the compound produced. There are two major classes of hosts. The first is a cavitand, where a host contains fixed intramolecular cavities and the guest compound can simply slot in forming a host-guest cavitate complex.[6,7] Examples include crown ethers, cyclodextrins, cyclophanes and cryptands.[8] The second is a clathrand, a host that possesses extramolecular binding sites which occur between two or more host molecules when in the solid state. These binding sites allow for host-guest compounds to be generated in the solid state and is termed a clathrate.[3] Clathrand hosts include water, urea, and other specialised host species, such as MacNicol's hexahosts. The formation of cavitate and clathrate host-guest compounds is outlined in Figure 1.3.[9,10]

In Figure 1.3, the yellow squares represent host molecules and the blue circles represent guests. The process a) shows the inclusion of the blue guests within the cavity present in the yellow hosts, and this allows for a host-guest cavitate complex to form. This complex can exist in solution or in the solid state, and examples of these are cyclodextrin compounds or crown ethers. The process b) shows the inclusion of guest molecules within cavities formed by the host molecules forming a lattice structure. These clathrates only exist in the solid state and the molecules are held in the lattice via intermolecular interactions.

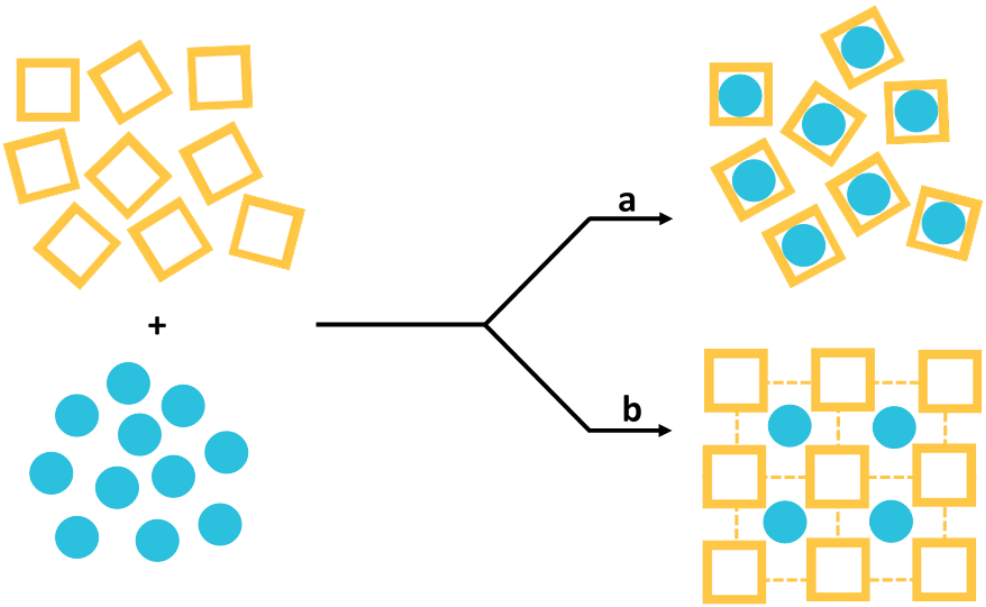

Figure 1.3: Schematic illustrating the differences between a cavitate and clathrate. (a) Shows the formation of a cavitate and (b) the formation of a clathrate due to a crystal lattice inclusion.

Many host-guest complexes form these lattice crystal clathrates. For example, water methane where the water molecules form a lattice cage around the methane molecules.[11]

Broadly, host-guest chemistry is founded on three main concepts, which have been defined over the history of supramolecular research:[12]

1. Molecules do not act if they do not bind, as was outlined by Paul Ehrlich in 1906. This explains the biological receptor, which does not become active unless it is bound by a substrate.
2. Emil Fischer's 1894 "lock and key" model describes that binding is selective and that only a molecule possessing the correct orientation can be bound by a certain receptor. This is referred to as complementarity, and underpins the idea of molecular recognition where a host can discern between a number of different guests.
3. Finally, that there needs to be some attraction or mutual affinity between the prospective host and guest molecules in order for selective binding to occur. This concept originated from the work of Alfred Werner on coordination chemistry in 1893.

These three concepts form the foundation of supramolecular host-guest chemistry. And Expansion on these ideas allows for further investigation of the drivers and potential applications for this particular phenomenon.

1.3 Selectivity and Host-Guest Chemistry

The concepts of complementarity and molecular recognition are important when considering whether a host will bind a particular guest. Molecular recognition describes the intermolecular interactions between two molecules and how they bind.[13] The degree of recognition between two molecules can be manipulated through specific host design, where hosts can be tailor-made to interact with specific moieties over others. This is a potentially powerful technique of selective inclusion, which has applications in separation chemistry. A guest that displays a higher degree of molecular complementarity towards a certain host over another guest will be preferentially included. This phenomenon is shown in Figure 1.4, where the purple square guest has more complementarity with the blue host than does the yellow circle. This yields a β-phase that includes the purple squares, but excludes the yellow circles. This allows for the potential separation of the two liquid guests in the starting mixture.

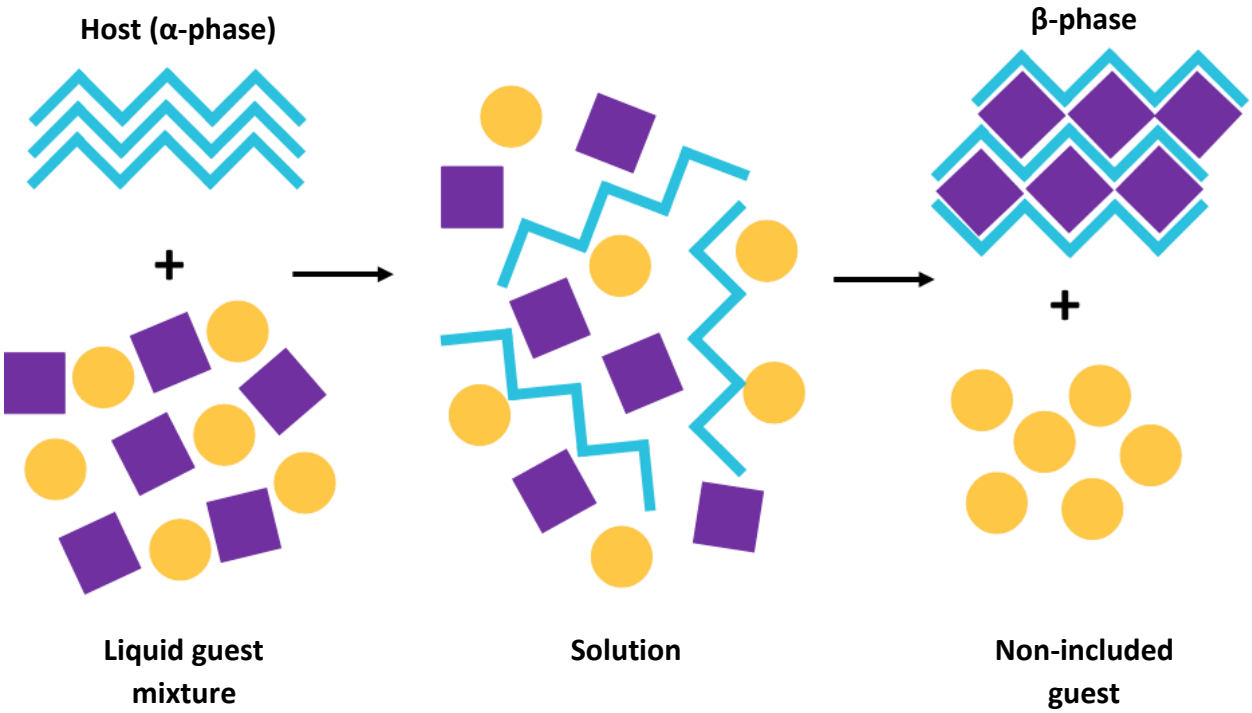

Figure 1.4: In this diagram the blue host preferentially selects the purple squares which are a 'better fit' for the resulting β-phase than the yellow circles.

Therefore, host-guest chemistry can be a useful technique when it comes to the separation of compounds that have similar physico-chemical properties. In these cases, traditional separation methods such as distillation, precipitation, solvent extraction or density columns fail, since these rely on notable differences in physical properties, such as boiling points or densities. Often the methods of drug synthesis or the by-products of chemical processes, such as in the petroleum industry, produce racemic mixtures or mixtures of stereoisomers, which are notoriously difficult to separate due to these similar physical properties. These separations are of importance since, when preparing drugs, one enantiomer may be useful and one may be harmful. This is true of Ethambutol where the (S,S)-(+)-enantiomer is used as a treatment for tuberculosis but the (R,R)-(–)-enantiomer causes blindness.[14] In industry, for example, the petroleum industry, the by-products are more valuable when they are pure, and therefore separation is often a high priority.

A well-known example are the isomers of xylene, which have boiling points ranging from 138.2°C to 144.4°C, and their separation via host-guest chemistry has been extensively studied.[15,16,17] Additionally, the formation of these inclusion compounds is reversible and, therefore, this process can be industrially useful. The included guests can be removed and extracted from the resulting β-phase, allowing the host compound to be recycled and reused for subsequent crystallisations. Selective inclusion has been used as a successful separation technique for constitutional isomers, stereoisomers, regioisomers and enantiomers. This method of separation has been used to separate the isomers of lutidine, phenylene diamine trimethoxybenzene and methyl and dimethypiperidines.[18, 19, 20, 21]

1.4 Guest Compounds Under Study

The guest compounds used for this investigation are the picolines: 2-, 3- and 4-methyl pyridine. These picolines have multiple uses, including as agrochemicals, solvents and in drug synthesis.[22,23] These isomers are difficult to separate conventionally, due to the similarity of their physical and chemical properties, which makes the usual separation techniques ineffective. Host-guest chemistry has been explored as a method of separation.[24] Pyridine has been included as a guest in this investigation, as it has previously been included in host-guest studies beside the picolines.[25] The guests are shown in Figure 1.5 with their physical properties in Table 1.1. The picolines have similar boiling points and are volatile liquids, which

makes their boiling point differences even more difficult to exploit, since their vapour pressures are high.[26] The melting points of the picoline guests seem to be well enough apart to achieve separation by fractional freezing. Unfortunately, it has been found that these picoline mixtures exhibit supercooling when the temperature of the individual compounds is taken below the anticipated freezing point, without them becoming solid.[27] This makes fractional freezing untenable as a method of separation.

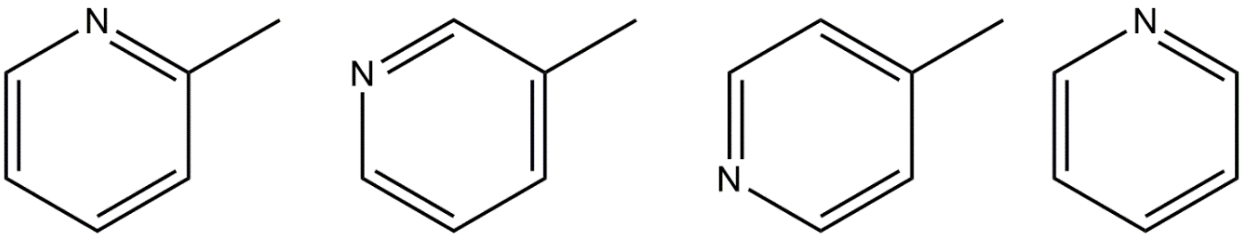

Figure 1.5: The guests used for this investigation from left: 2-picoline, 3-picoline, 4-picoline and pyridine.

Table 1.1: Properties of the guests utilised during this project.

Guest	Abbreviation	Density ($g \cdot mol^{-1}$) at 25 °C	Normal Boiling Point (°C)	Melting Point (°C)
2-Picoline	2PIC	0.943	129.4	-66.7
3-Picoline	3PIC	0.957	141.0	-18.0
4-Picoline	4PIC	0.957	145.0	+3.6
Pyridine	PYR	0.982	115.2	-41.6

The separation of close isomers has been the subject of study for many years and is highly relevant in industry. Volatile organic compounds are typically by-products of industrial processes and tend to be produced in mixtures; for example, the production of mixtures of picolines and lutidines from coal tar.[28] In order to make use of these chemicals, either for reuse or for sale, it is important to be able to separate the isomers. Pure compounds are nearly always worth more than mixtures and are, therefore, more commercially attractive. Therefore, the separation of the picoline isomers using host- guest chemistry is a viable path of investigation. This method is also industrially useful, as the method only requires the crystallisation of the host-guest compound in order to achieve separation. The crystalline material is then filtered off and the included guest is released by heating, allowing for the retrieval of the pure guest. The host compound can be retained and reused for subsequent crystallisations.[29]

As outlined when discussing host-guest interactions, these picoline guests contain a nitrogen atom, which is a hydrogen bond acceptor allowing for the formation of a hydrogen bond with hosts that feature hydrogen donor moieties. This, potentially, facilitates the formation of inclusion compounds and, if it is possible to produce host-guest compounds with each of these guests, then discriminatory behaviour can be investigated.

1.5 Host Compounds Under Study

A host molecule interacts with a guest through strong non-bonded interactions. This means that it is important for hosts to have various moieties, which facilitate this interaction. In most cases, the host has particular functional groups, which provide potential hydrogen donor capabilities that can interact with acceptor groups in the guest.[30] Examples of these host hydrogen donor groups include -OH or -NH_2, while acceptors would consist of oxygen or nitrogen atoms. This investigation will be utilising host compounds based on tartaric acid. Examples of these kind of compounds include tartaric acid itself, TA, O,O'-dibenzoyl tartaric acid (DBTA), and its related O,O'-di-p-tolyl tartaric acid (DTTA) derivatives and α,α,α',α'-tetraaryl-l,3-dioxolane-4,5-dimethanols (TADDOLs), which can be obtained in their chiral or racemic forms. This TADDOL structure is illustrated in Figure 1.6 and contains two hydroxyl groups and four aryl substituents. The chemistry of this TADDOL compound, and its many derivatives and analogues, has been the subject of previous reviews.[31] Their uses in asymmetric catalysis, synthesis, racemate resolution and separation of isomers in general make them highly relevant and important compounds for further study.[32]

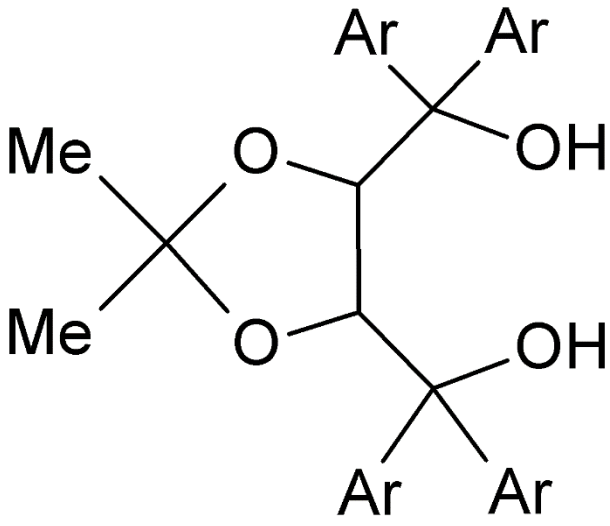

Figure 1.6: Structure of α,α,α',α'-tetraaryl-2,2-disubstituted 1,3-dioxolane-4,5-dimethanol (TADDOL).

This first host under investigation is (4RS,5RS)-2,2-dimethyl-α,α,α',α'-tetrakis(p-tolyl)-1,3-dioxolane-4,5-dimethanol ($C_{35}H_{38}O_4$, **H1**). It contains two hydroxyl groups that can function as hydrogen bond donors and accepters. The presence of the four phenyl rings also provides potential for CH···π and π···π interactions. The second TADDOL-based host is **H2** (4RS,5RS)-2,2-dimethyl-α,α,α',α'-tetrakis(p-fluorophenyl)-1,3-dioxolane-4,5-dimethanol, which contains fluorine atoms on the para positions of the phenyl rings. A previous investigation conducted by Benita Barton et al. explored the host potential of the (4RS, 5RS)-2,2-dimethyl-α,α,α',α'-tetraphenyl -1,3-dioxolane-4,5-dimethanol ($C_{31}H_{30}O_4$) towards the picoline guests. [25] This host is TADDOL-derived and lacks the methyl and fluoro groups present in **H1** and **H2**. This host produced host-guest compounds in the investigation conducted by Barton et al, and these compounds displayed hydrogen bonding and many π···π and CH···π interactions. This host was included for comparison and further study in this project as **H3**. These hosts are shown in Figure 1.7.

These host compounds are relatively straightforward to synthesise, with many potential routes available.[33,34] The primary starting compound is an acetonide of a tartrate, which is commercially available from many chemical companies and is synthesised from tartaric acid and dimethoxypropane. There are multiple avenues of preparing these TADDOLs from tartrates through acid catalysis by reacting them with aldehydes or ketones. These are then

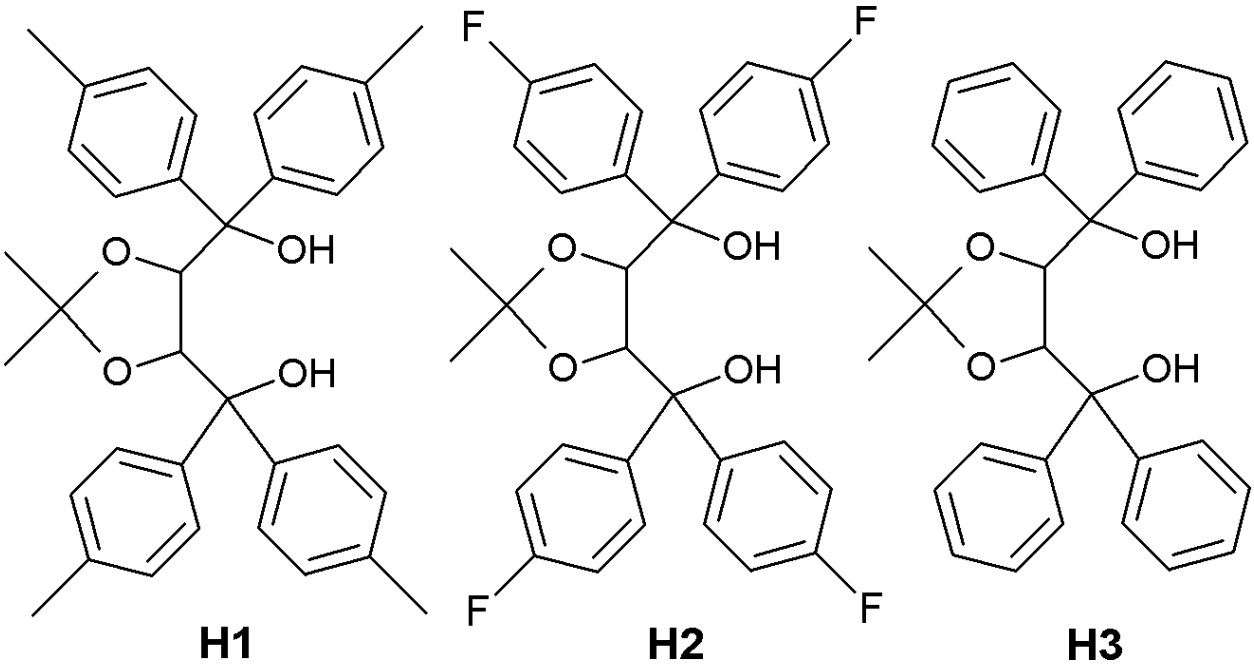

Figure 1.7: Structures of the three TADDOL Hosts used in this investigation, **H1** (4*RS*,5*RS*)-2,2-dimethyl-α,α,α',α'-tetrakis(p-tolyl)-1,3-dioxolane-4,5-dimethanol, **H2** (4*RS*,5*RS*)-2,2-dimethyl-α,α,α',α'-tetrakis(p-fluorophenyl)-1,3-dioxolane-4,5-dimethanol, and **H3** (4*RS*, 5*RS*)-2,2-dimethyl-α,α,α',α'-tetraphenyl -1,3-dioxolane-4,5-dimethanol.

subjected to treatment with aryl Grignard reagents to institute the desired aromatic groups. Transacetalisation is also an effective method of generating these compounds.[30]

These TADDOL compounds are numerous and diverse, and their propensity to crystallise has allowed for in-depth structural analysis, due to the insights that X-ray diffraction can provide. There are hundreds of structures, catalogued within the Cambridge Structural Database, which feature these compounds. It is known that crystals are easily obtained from crystallisations conducted in solvents that have hydrogen-bond accepting moieties.[35] This allows for the formation of TADDOL inclusion compounds, which is a key objective in the project.

In many cases, an intramolecular hydrogen bond forms between the hydroxyl, which then allows the second -OH group to form an intermolecular hydrogen bond. This motif is illustrated in Figure 1.8. These compounds form hydrogen bonds readily with guests that contain hydrogen-bond receptors. These lead to the formation of inclusion compounds and allow for potential purification through recrystallisation. These TADDOLs are excellent host compounds, and have been extensively explored as compounds for the separation of racemates and enantiomers via selective crystallisation.[36] Therefore, these hosts are viable for this particular project, as they are likely to generate inclusion compounds and have a history of being useful in separations. This history includes separating racemates and

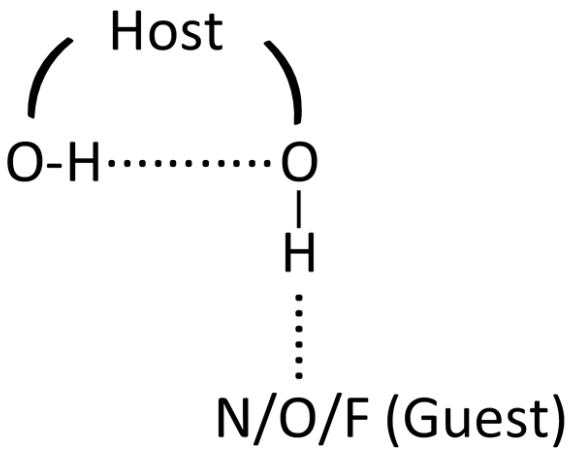

Figure 1.8: A motif showing the intramolecular hydrogen bond present in many inclusion compounds containing a TADDOL host. The hydrogen bond between a hydroxyl group of the host and a hydrogen accepter group present in the potential guest compound.

enantiomers. Various racemates have been separated using chiral TADDOLs, including amines and alcohols (which notably feature hydrogen bond accepting capabilities).[37]

These hosts can also be reused after separation. For example, subjecting an inclusion compound to heat can expel the included guest, and the pure host is retained for subsequent separations. This makes an industrial separation more cost-effective and greener, as there is less wastage and the recycling of the host saves material costs. All these hosts have a melting point between 198 °C and 220 °C. When separating via differential inclusion, if one guest is preferred over another, the crystals can be removed from the mixture and the included guest collected. The wide-ranging properties of these compounds as potential host compounds, and their history of use in separations, are the key reason why these compounds were selected for this project.

1.6 Competition Experiments

An objective of this project is to determine whether there is any discriminatory behaviour of the TADDOL hosts towards the different picolines. This preference is investigated by performing selectivity experiments and obtaining results, which are then analysed. These selectivity experiments are usually carried out by dissolving the host under study in an equimolar mixture of two guest (A and B) and allowing crystallisation to occur. The crystals are then collected and the amount of each guest present is quantified using ^{1}H-NMR analysis.

The selectivity of a host, H, with regard to guests A and B can be determined from the selectivity coefficient $K_{A:B}$ which is generated from the expression:

$$K_{A:B} = \frac{Z_A}{Z_B} \times \frac{X_B}{X_A}$$

X refers to the mole fraction of the guest in the starting solution and Z the mole fraction of the guest in resulting crystal ($X_A + X_B = 1$, $Z_A + Z_B = 1$).[38] Separation is deemed to be significantly useful if the selectivity coefficient is greater than 10. This selectivity coefficient is useful for equimolar solutions. However, a more comprehensive study of the selectivity can be gleaned from running a series of these binary competition experiments. This is accomplished by

exposing a host to a series of experiments, which feature varying guest molar ratios (X_A = 0, 0.1, 0.2 …. 1), and analysing the resulting mole fractions (Z_A and Z_B) present in the crystals.[39]

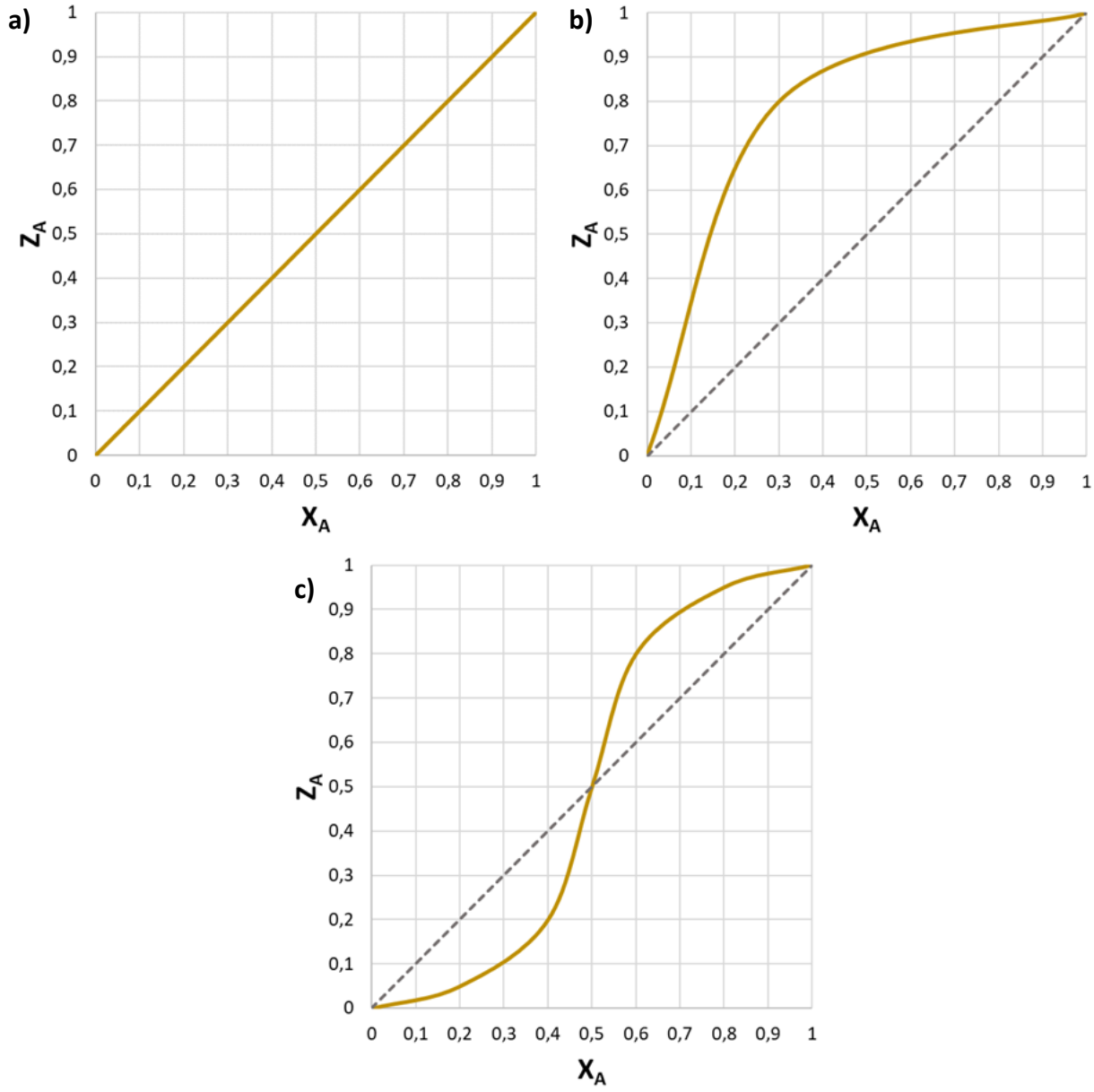

Figure 1.9: Typical selectivity profiles which are generated from competition experiments.

The series of results from the competition experiments allows the generation of a selectivity profile which plots Z_A versus X_A. This would give insight into a specific host's preference towards Guest A. Figure 1.9 depicts the most common selectivity profiles obtained from these kinds of competition experiments.[39]

In Figure 1.9a, there is no apparent selectivity since the points lie on $K_{A:B} = 1$, which means that the guests are expressed in the resulting crystal at the same proportion as that in the starting solution. This suggests that the crystal displays an equal preference for Guest A and Guest B. In Figure 1.9b, Guest A is preferentially enclathrated over guest B throughout the concentration range. Figure 1.9c depicts a system where the host prefers the guest which is in greater quantity in the starting solution. So, as the concentration of a certain guest in the initial solution increases, it is incorporated in higher proportions. This shows an example of a system where the two guests can be separated via selective enclathration. As always, not all systems will be as clear cut as these typical cases. However, by generating these selectivity plots, it is possible to investigate the selectivity preferences of these hosts towards the picoline guests.

1.7 Aims and Objectives

The aim of this project is to synthesise inclusion compounds of three host TADDOLs with the three isomers of picoline and pyridine. Additionally, if the synthesis of these inclusion compounds is achieved, then the aim is to use the phenomenon of host-guest chemistry to separate the guest compounds that display similar physico-chemical properties.

The three host compounds, **H1** (4RS,5RS)-2,2-dimethyl-α,α,α',α'-tetrakis(p-tolyl)-1,3-dioxolane-4,5-dimethanol, **H2** (4RS,5RS)-2,2-dimethyl- α,α,α',α'-tetrakis(p-fluorophenyl)-1,3-dioxolane-4,5-dimethanol, and **H3** (4RS, 5RS)-2,2-dimethyl-α,α,α',α'-tetraphenyl -1,3-dioxolane-4,5-dimethanol, were selected to separate the isomeric mixtures of 2-picoline (**2PIC**), 3-picoline (**3PIC**) and 4-picoline (**4PIC**).

The aim is to achieve a high degree of separation of the picoline isomers. In addition, the resulting analysis of the inclusion compounds and their selectivities can provide valuable insight into the use of TADDOL-derived hosts in selective inclusion studies. This may be pertinent in the further design of hosts for separation via host-guest chemistry.

1.8 References

1. Steed J. W., Atwood J. L. Supramolecular Chemistry: Concepts, 2nd Edition, 2009, John Wiley, Chichester, pp 2-48.

2. Lehn J.-M., Supramolecular Chemistry, 1st Edition, 1995, VCH: Weinheim.

3. Braga D., Grepioni F., Orpen A. G., Crystal Engineering: From Molecules and Crystals to Materials, 1999, Kluwer Academic Publishers, The Netherlands.

4. Gale P. A., Steed J.W. Supramolecular Chemistry: From Molecules to Nanomaterials, 2012, John Wiley, Chichester.

5. Toda F., Bishop R., Separations and Reactions in Organic Supramolecular Chemistry, 2004, John Wiley, Chichester, Vol 8.

6. Desiraju G. R., Crystal engineering: from molecule to crystal. *J. Am. Chem. Soc.*, 2013, **135**, 9952-9967, DOI: https://doi.org/10.1021/ja403264c.

7. Matsumoto K., Hayashi N., Heterocyclic Supramolecules II, 2009, Springer, London, New York.

8. Kamitori S., Hirotsu K. and Higuchi T., Crystal and molecular structures of double macrocyclic inclusion complexes composed of cyclodextrins, crown ethers, and cations. *J. Am. Chem. Soc.*, 1987, **109**, 2409-2414. DOI: https://doi.org/10.1021/ja00242a026.

9. Pivovar A. M., Holman K. T., Ward M. D., Shape-Selective Separation of Molecular Isomers with Tunable Hydrogen-Bonded Host Frameworks, *Chem. Mater.*, 2001, **13**, 3018–3031, DOI: https://doi.org/10.1021/cm0104452.

10. Maurin G., Serre C., Cooper A., Férey G., The new age of MOFs and of their porous-related solids, *Chem. Soc. Rev.*, 2017, **46**, 3104-3107, DOI: https://doi.org/10.1039/C7CS90049J.

11. Vysniauskas A., Bishnoi P.R., A kinetic study of methane hydrate formation. *Chem. Eng. Sci.*, 1983, **38**, 1061-1072, DOI: https://doi.org/10.1016/0009-2509(83)80027-X.

12. Behr J. P., The Lock and Key Principle. The State of the Art – 100 Years on, 2008, vol 17, John Wiley & Sons, Chichester.

13. Lehn J.M., Perspectives in supramolecular chemistry—from molecular recognition towards molecular information processing and self-organization., 1990, *Angew. Chem. Int. Ed.*, **29**, 1304-1319, DOI: https://doi.org/10.1002/anie.199013041.

14. Chhabra N., Aseri M.L., Padmanabhan D., A review of drug isomerism and its significance. *Int. J. Appl. Basic Med. Res.*, 2013, **3**, 16, DOI: https://doi.org/10.4103/2229516X.112233.

15. Campillo-Alvarado G., Vargas-Olvera E. C., Höpfl H., Herrera-España A. D., Sánchez-Guadarrama O., Morales-Rojas H., MacGillivray L. R., Rodríguez-Molina B., Farfán N., Self-Assembly of Fluorinated Boronic Esters and 4,4'-Bipyridine into 2:1 N→B Adducts and

Inclusion of Aromatic Guest Molecules in the Solid State: Application for the Separation of *o*,*m*,*p*‑Xylene, *Cryst. Growth Des.*, 2018, **18**, 2726-2743,

DOI: https://doi.org/10.1021/acs.cgd.7b01368

16. Barton B., Hosten E. C., Pohl P. L., Discrimination between o-xylene, m-xylene, p-xylene and ethylbenzene by host compound (R,R)-(–)-2,3-dimethoxy-1,1,4,4-tetraphenylbutane-1,4-diol, *Tetrahedron*, 2016, **72**, 8099-8105,

DOI: https://doi.org/10.1016/j.tet.2016.10.062.

17. Lusi M.,Barbour, L. J., Solid–vapor sorption of xylenes: prioritized selectivity as a means of separating all three isomers using a single substrate. *Angew. Chem. Int Ed.* 2012, **51** (16), 3928-3931. DOI: https://doi.org/10.1002/anie.201109084.

18. Bouanga Boudiombo J., Su H., Bourne S. A., Nassimbeni L. R., Separation of Trimethoxybenzene Isomers by Bile Acids, *Cryst. Growth Des.*, 2018, **18**, 424–430,

DOI: https://doi.org/10.1021/acs.cgd.7b01423.

19. Caira M. R., Horne A., Nassimbeni L. R., Okuda K., Toda F., Selective inclusion of phenylenediamine isomers by 1, 1-bis(4-hydroxyphenyl)cyclohexane, *J. Chem. Soc., Perkin Trans. 2*, 1995, 1063-1067, DOI: https://doi.org/10.1039/P29950001063.

20. Bouanga Boudiombo J., Su H., Bourne S. A., Weber E., Nassimbeni L. R., Separation of Lutidine Isomers by Selective Enclathration, *Cryst. Growth Des.*, 2018, **18**, 2620-2627,

DOI: https://doi.org/10.1021/acs.cgd.8b00251.

21. Sykes N. M., Su H., Weber E., Bourne S. A., Nassimbeni L. R., Selective Enclathration of Methyl- and Dimethylpiperidines by Fluorenol Hosts, *Cryst. Growth Des.*, 2017, **17**, 819–826, DOI: https://doi.org/10.1021/acs.cgd.6b01661.

22. Sato S., Sakamoto T., Miyazawa E., Kikugawa Y., One-pot reductive amination of aldehydes and ketones with α-picoline-borane in methanol, in water, and in neat conditions., *Tetrahedron*, 2004, **60**(36), 7899-7906,

DOI: https://doi.org/10.1016/j.tet.2004.06.045.

23. Shimizu S., Watanabe N., Kataoka T., Shoji T., Abe N., Morishita S., Ichimura, H., Pyridine and pyridine derivatives. *Ullmann's Encyclopedia of Industrial Chemistry*., 2000,

DOI: https://doi.org/10.1002/14356007.a22_399.

24. Caira M.R., Horne A., Nassimbeni L.R. Toda F., Inclusion and separation of picoline isomers by a diol host compound. *J. Mater. Chem.*,1997, **7**(10), 2145-2149.

DOI: https://doi.org/10.1039/A703221H.

25. Barton B., Hosten E. C., Jooste D. V., Comparative investigation of the inclusion preferences of optically pure versus racemic TADDOL hosts for pyridine and isomeric methylpyridine guests, *Tetrahedron*, 2017, **73**, 2662,

DOI: https://doi.org/10.1016/j.tet.2017.03.049.

26. Herington E.F.G., Martin J.F., Vapour pressures of pyridine and its homologues. *Transactions of the Faraday Society*, 1953, **49**, 154-162.

27. Bowman R. S., (1949), *US2459146A*, retrieved from https://patents.google.com/patent/US2459146A/en, 15 April 2019.

28. Coulson E.A., Jones J.I., Studies in coal tar bases. I. Separation of β-and γ picolines and 2: 6-lutidine. *J. Chem. Soc. Indust.*, 1946, **65**(6), 169-175,

DOI: https://doi.org/10.1002/jctb.5000650605.

29. Apel, S., Lennartz, M., Nassimbeni, L.R. and Weber, E., Weak Hydrogen Bonding as a Basis for Concentration-Dependent Guest Selectivity by a Cyclophane Host., *Chem. Eur. J.*, 2002, **8**(16), 3678-3686,

DOI: https://doi.org/10.1002/1521-3765(20020816)8:16<3678::AID-CHEM3678>3.0.CO;2-4.

30. Weber E., Shape and Symmetry in the Design of New Hosts, in *Comprehensive Supramolecular Chemistry*, Vol 6, Atwood J. L., Davies J. E. D., MacNicol D. D., Vögtle F., 1996, Elsevier Science, Oxford, pp. 535-592.

31. Seebach D., Beck A. K., Heckel A., TADDOLs, Their Derivatives, and TADDOL Analogues: Versatile Chiral Auxiliaries, *Angew. Chem. Int. Ed.*, 2001, **40**, 92-138.

DOI: https://doi.org/10.1002/1521-3773(20010105)40:1<92::AID-ANIE92>3.0.CO;2-K.

32. Eißmann D., Katzsch F., Weber E., Synthesis and solvent sorption characteristics of new types of tartaric acid, lactic acid and TADDOL derived receptor compounds, *Tetrahedron*, 2015, **71**(40), 7695-7705, DOI: https://doi.org/10.1016/j.tet.2015.07.061.

33. Carmack M., Kelley C.J., Synthesis of optically active Cleland's reagent [(-)-1, 4-dithio-L-threitol]., *J. Org. Chem.,* 1968, **33**(5), 2171-2173, DOI: https://doi.org/10.1021/jo01269a123

34. Seebach D., Crass G., Wilka E.M., Hilvert D., Brunner E., Three new chiral aminoethers from tartaric acid for improved asymmetric syntheses with organolithium reactions. *Helv. Chim. Acta*, 1979, **62**(8), 2695-2698, DOI: https://doi.org/10.1002/hlca.19790620819.

35. Toda F., Molecular recognition. *Bioorg. Chem.*, 1991, **19**(2), 157-168,

DOI: https://doi.org/10.1016/0045-2068(91)90032-K.

36. Toda F., Tanaka K., Design of a new chiral host compound, trans-4, 5-bis (hydroxydiphenylmethyl)-2, 2-dimethyl-1, 3-dioxacyclopentane. An effective optical resolution of bicyclic enones through host-guest complex formation. *Tetrahedron Lett.*, 1988, **29**(5), 551-554, DOI: https://doi.org/10.1016/S0040-4039(00)80147-1.

37. Weber E., Dörpinghaus N., Wimmer C., Stein Z., Krupitaky H., Goldberg I., New Crystalline Hosts Based on Tartaric Acid. Synthesis, Inclusion Properties, and X-ray Structural Characterization of Interaction Modes with Alcohol Guests, *J. Org. Chem.*, 1992, **57**, 6825-6833, DOI: https://doi.org/10.1021/jo00051a029.

38. Pivovar A.M., Holman K.T., Ward M.D., Shape-selective separation of molecular isomers with tunable hydrogen-bonded host frameworks. *Chem. Mater.*, 2001, **13(9)**, 3018-3031, DOI: https://doi.org/10.1021/cm0104452.

39. Báthori N. B., Nassimbeni L. R., In *Supramolecular Chemistry: From Molecules to Nanomaterials*, 2012, John Wiley, Chichester, pp 3009-3016.

Chapter 2. Experimental

The materials and methods utilised in the course of this project are identified in this chapter. The instrumentation, techniques, procedures and further analyses are outlined.

2.1. Host and Guest Compounds

The three host compounds under investigation are (4*RS*,5*RS*)-2,2-dimethyl-α,α,α',α'-tetrakis(p-tolyl)-1,3- dioxolane-4,5-dimethanol ($C_{35}H_{38}O_4$, **H1**), (4*RS*,5*RS*)-2,2-dimethyl-α,α,α',α'-tetrakis(p-fluorophenyl)-1,3-dioxolane-4,5-dimethanol ($C_{31}H_{26}F_4O_4$, **H2**) and(4*RS*, 5*RS*)-2,2-dimethyl-α,α,α',α'-tetraphenyl-1,3-dioxolane-4,5-dimethanol ($C_{31}H_{30}O_4$, **H3**). Previous studies utilised **H3** to synthesise host-guest complexes with pyridine and picoline guests. This host was included for comparison purposes. These compounds were synthesised by Professor Edwin Weber from the Institute for Organic Chemistry, TU, Bergakademie Freiberg, Leipziger Strasse 29, D-09596, Freiberg/Sachs, Germany, and were used without

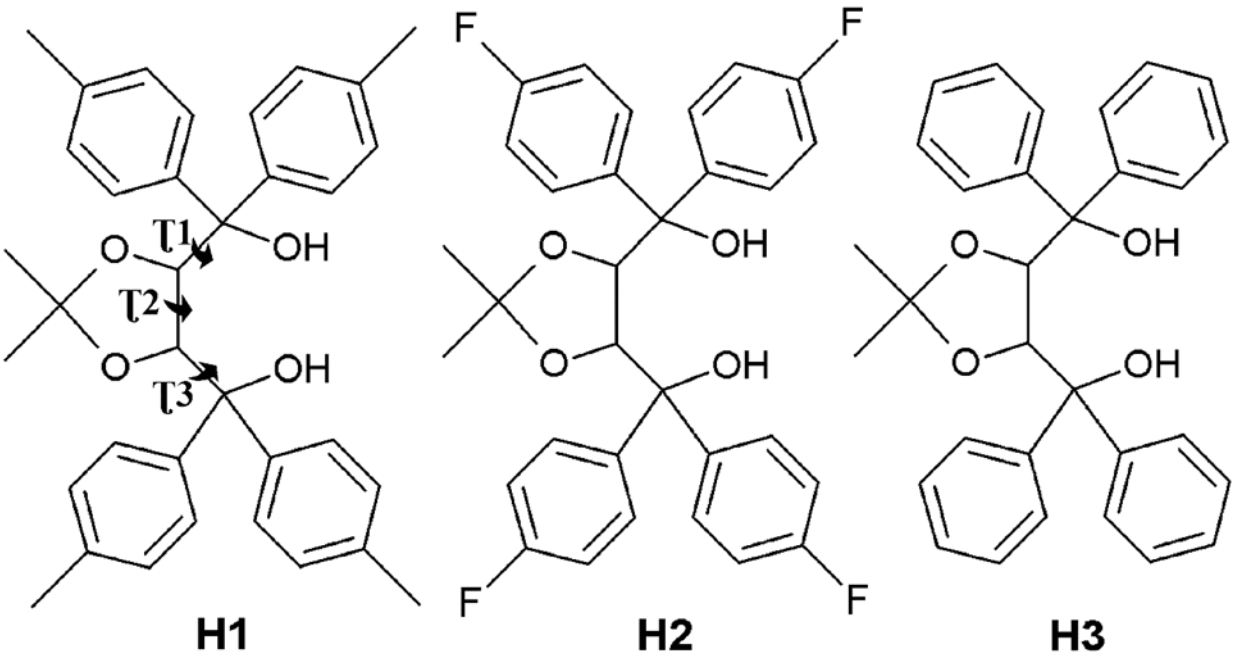

Figure 2.1: Structures of the TADDOL hosts, **H1** (4*RS*,5*RS*)-2,2-dimethyl-α,α,α',α'-tetrakis(p-tolyl)-1,3-dioxolane-4,5-dimethanol, **H2** (4*RS*,5*RS*)-2,2-dimethyl-α,α,α',α'-tetrakis(p-fluorophenyl)-1,3-dioxolane-4,5-dimethanol, and **H3** (4*RS*, 5*RS*)-2,2-dimethyl-α,α,α',α'-tetraphenyl -1,3-dioxolane-4,5-dimethanol along with the pyridine and methylpyridine (picoline) guests. The torsion angles in each structure are Ƭ1 = O1-C1-C2-C3, Ƭ2 = C1-C2-C3-C4 and Ƭ3 = O4-C4-C3-C2.

further purification. These hosts show the characteristic two hydroxyl groups and the four bulky aromatic groups of the TADDOL-type hosts (TADDOL = α,α,α',α'-tetraphenyl-1,3-dioxolane-4,5-dimethanol). These are shown in Figure 2.1.

This host contains hydrogen donor groups along with the aromatic groups. This combination of moieties allows for a diversity of potential interactions between host and guest molecules: for example, hydrogen bonding between the hydrogen bond donor (hydroxyl) groups of the host and hydrogen bond acceptor (nitrogen) of the guest. All three compounds possess aromatic rings and, therefore, π···π and C-H···π interactions are also possible.

The guest compounds utilised for this investigation are the picoline isomers and pyridine. These reagents were supplied by Sigma-Aldrich. These four compounds have been previously studied as guests in separation using host-guest chemistry.[1] These made them good candidates for this study, as it was likely that the previously described host compounds would form host:guest complexes with these guests. While pyridine is neither isomeric nor very similar in physical properties, it has previously been included in sepration studies and it was included in this project in order to further study the potential selectivity behaviour of the hosts.

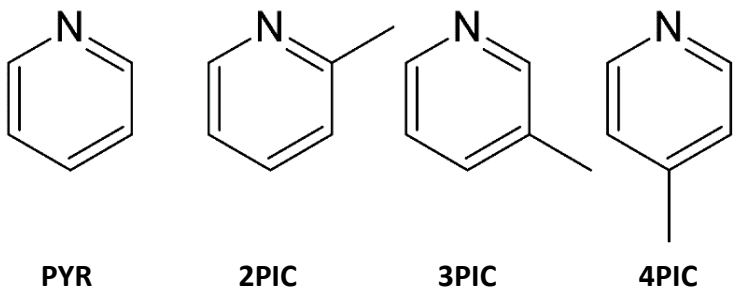

Figure 2.2: Structures of the methylpyridine (picoline) guests and pyridine.

Table 2.1: Physical properties of the guests utilised during this project.

Guest	Abbreviation	Density ($g \cdot mol^{-1}$) at 25 °C	Normal Boiling Point (°C)
2-Picoline	2PIC	0.943	129.4
3-Picoline	3PIC	0.957	141.0
4-Picoline	4PIC	0.957	145.0
Pyridine	PYR	0.982	115.2

2.2 Crystal Growth

The desired host-guest compounds were prepared using the slow evaporation method of crystallisation. The host compound (40 mg) was dissolved in 1.5 ml of the single guest or binary mixtures. The solution was left to stir for 5 minutes in order to facilitate the dissolution of the host. Each host-guest solution was left in a vial with the cap removed at room temperature to evaporate. After a number of days, small block-shaped crystals grew in the bottom of the vial. These were collected for further analysis.

The formation of crystalline material using vapour diffusion was also explored, with the host and guest in two separate smaller vials sealed within a larger container. The setup was conducted in such a way that the smaller vials did not touch each other, in order to mitigate against the guest liquid 'creeping' into the host powder Figure 2.3. The volatile nature of the guest, and the difference in vapour pressures, has the guest diffusing into the powder of the host, resulting in oversaturation and the formation of crystalline material.

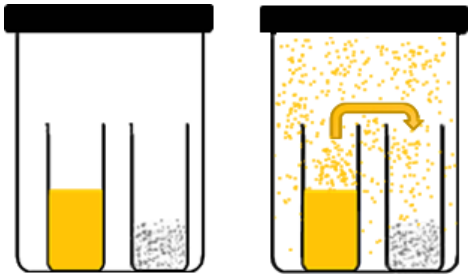

Figure 2.3: Vapour diffusion setup (left) and (right) showing guest (yellow) diffusing into the powder of the host.

2.3 Competition Experiments

Competition experiments were used to study the selectivity of the host towards a certain guest. In these experiments, a host is exposed to varying ratios of a binary mixture of potential guests. The resulting crystals are then analysed and the amount of each guest included in the crystal is determined. One can then see which guests are preferred at certain concentrations in comparison to another guest. This allows insight into the host's selectivity and comparisons can be drawn between guests and a selectivity profile generated. In this investigation, the hosts were dissolved in binary mixtures of picoline guests of known mole

fractions. The fractions would be varied over an interval of 0 to 100% of the starting solution. A schematic showing a setup of a competition experiment can be seen in Figure 2.4. X_A and X_B would be the two guests under study in the selectivity experiment outlined in this Figure.

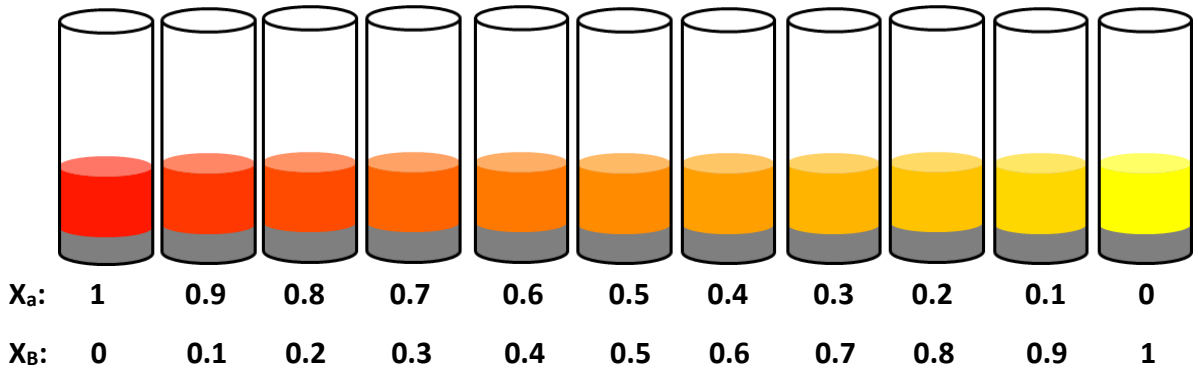

Figure 2.4: Setup of competition experiment where the mole fractions of Guest A (X_A) and Guest B (X_B) are varied.

A suitable method was used to characterise the amount of each guest compound in the resulting crystals. This was done using ^{1}H-NMR, as often the host is not perfectly selective and the resulting samples contain a mixture of guests. The proton signals can be used to determine the presence of each guest and their respective ratios in the sample.

Once the respective ratios in each sample have been determined, a selectivity profile can be created for each binary set of guests.

2.4 X-ray Diffraction

X-ray diffraction was the primary technique used for determining the structures of synthesised crystals. This method also allowed for comparison between structures and characterisation of various intra- and intermolecular interactions.

2.4.1 Single Crystal X-ray Diffraction

Single crystal X-ray Diffraction (SXRD) is an important tool for elucidating the structure of a crystalline material. The resulting information obtained from the diffraction yielded important structural information, such as geometry, interatomic distances and angles. The results show the packing and the overall stoichiometry of the inclusion compounds. Further information, such as crystal systems and space groups, is also provided. Specialised computer software was used to compute and refine the data provided by the diffractometer.

A suitable crystal was selected from the mother liquor. A good crystal is of an appropriate size (at least 0.1 mm in all directions) and clarity. This was checked visually using polarised light microscopy, accomplished by rotating the crystal under the microscope and looking for extinguishing, thus proving that the crystal is single and clear. The crystal was then immersed in paratone oil and mounted onto a loop in preparation for diffraction.

All crystal data were collected on a Bruker KAPPA APEX II DUO single crystal X-ray diffractometer with graphite monochromated MoKα radiation (λ = 0.7107 Å), generated by a Bruker K780 generator (50 kV, 30 mA) at -100 °C using an Oxford cryostream 700.[2] The data computation and cell refinement were performed using SAINT-Plus[3] followed by XPrep[4] which uses systematic absences in order to derive the space group. SADABS[5] was used to correct for Lorentz polarisation and absorption effects present in intensity data. These data were verified by the refinement results, after which XPREP was used to process and prepare the input data for the programmes, SHELXS-2017, SHELXT-2015 and SHELXL-2017/1 (Sheldrick, 2017).[6, 7] These programmes were linked with the graphical interface X-Seed to solve and refine the crystal structures.[8] The O-H bonds of the resulting structures were fixed using the method of Lusi and Barbour.[9]

2.4.2 Computing Packages

Other software utilised in the determination, analysis and refinement of crystal structures included the following:

- The Cambridge Structural Database (CSD) was used to search through potentially relevant structures that had already been published. This included searching for previous reports of the host and/or similar hosts, along with determining whether the structures being synthesised were novel. Similar searches were conducted for the guests, and for literature dealing with the separation of picolines. This prevented potential overlap in experiments and provided insight into suitable methods and directions of inquiry. The WEB CSD, located online and constantly updated, was also consulted for more recent works.[10]
- LAYER was used to determine the space group symmetry of the structures.[7]
- PLATON was used to characterise the intermolecular interactions and geometrical relationships.[11]

- Mercury was used to generate pictures of the asymmetric unit, unit cell, packing and void spacing, along with providing certain calculations such as void volumes.[10]
- Hirshfeld surface plots were prepared using Crystalexplorer, which allows quantification of various intermolecular interactions of the crystal structure.[12, 13, 14]

Note that X-Seed was the graphical interface for SHELXS-2097 and LAYER.

2.4.3 Powder X-ray Diffraction

Powder X-ray diffraction (PXRD) is an analytical method, which can be used to follow characteristic phase changes for solid crystalline compounds. This allows for ease of identification of solid material, as predicted powder patterns can be generated from known crystal structures, which is a powerful tool for comparison and identification. Samples need to be in powder form, so crystal samples must be ground up to allow for this characterisation. These patterns were collected on a Bruker D8 Advance diffractometer equipped with a Lynxeye detector and using CuKα-radiation (λ = 1.5406 Å) at 298 K. The powdered sample was placed on a zero background sample holder and scanned over a 2θ range of 4° - 40°. The X-rays were produced by a current flow of 40 mA and accelerating voltage of 30 kV. The generated data were captured by gnuplot and saved as text files, in order to obtain the PXRD patterns.

The computing software, Mercury v5.40 was used to calculate the PXRD patterns from the single crystal data. The X-ray source of λ = 1.5406 Å was kept consistent when generating the calculated plots. This was used to determine whether the single crystal data obtained from a crystal were truly representative of the bulk experimental sample.

2.5 Thermal Analysis

2.5.1 Hot Stage Microscopy

In some cases, hot stage microscopy (HSM) was used to observe the thermal events resulting from heating. These events included solvent release, crystal colour changes, melt and decomposition. Samples were observed using a Nikon SMZ- 10 stereoscopic microscope fitted with a Linkam THMS600 hot stage and a Linkham TP92 temperature control unit. The samples were mounted on a glass cover slip and immersed in silicone oil, and images were captured with a real-time Sony Digital Hyper HAD colour video camera.

2.5.2 Thermogravimetric Analysis

Thermogravimetric analysis (TGA) records the change in mass of a sample as a function of temperature. During this analysis, the sample is exposed to a nitrogen atmosphere and a thermobalance monitors the mass of a sample as it is subjected to an increase in temperature.

Thermogravimetric samples were prepared by removing the crystals from their mother liquor, patting dry using filter paper and lightly grinding into a powder. TGA was performed after obtaining PXRD traces of the samples, in order to maximise the mass of sample for the experiment. Each sample, consisting of 4 mg to 8 mg, was heated from room temperature (≈ 20 °C) to 350 °C at 10 °C·min^{-1}. This method was used extensively to confirm and quantify guest and solvent present in crystals.

The machine used a TA-Q500 Thermogravimetric Analyser, and the resulting traces were analysed using TA Instruments *Universal Analysis 2000* software (v4.5A TA Instrument-Waters LLC). This was operated with a dry nitrogen purge gas flow rate of 60 cm^3 min^{-1}.[15]

2.5.3 Differential Scanning Calorimetry

Differential Scanning Calorimetry (DSC) is a technique that measures the difference in heat flow to a sample compared to a reference as a function of temperature. This provides insight into the nature of energetic events, which occur during the heating or cooling of a sample; for example, guest release, melting, crystallisation or polymorphic transitions. These events would be described as either endothermic or exothermic, depending on whether energy is absorbed or released during the event. This is translated into a heat flow vs temperature graph, which allows analysis of the various peaks occurring due to thermal events.

DSC samples were prepared in the same way as the TGA samples. Standard aluminium pans were used and between 1 and 2 mg of powdered samples weighed out and sealed with a pierced aluminium lid. A reference pan containing no sample was prepared in the exact same way. The sample and reference were subjected to heating from room temperature to 250 °C at a rate of 10 °C·min^{-1}. The machine used was a TA DSC25 Discovery operating a nitrogen purge gas flow rate of 60 cm^3 min^{-1} and the software used to process the traces was Trios v4.1.133073.[16]

2.6 Proton Nuclear Magnetic Resonance Spectroscopy (^{1}H-NMR)

Proton Nuclear Magnetic Resonance (^{1}H-NMR) Spectroscopy was used to confirm the presence of both host and guest and their respective stoichiometry in the crystals. This identifies the isomer(s) that have been included in the crystals, as the proton signals are unique for each guest. The ratio of which guests are present is also quantified using various peak integration methods.

The samples were prepared by removing the crystals from the mother liquor, drying on filter paper and dissolving them in D_6-DMSO. The spectra were captured using a Bruker Ultrashield 400 Plus (400 MHz) spectrometer. The raw data were analysed using the programme TopSpin 3.5 pl 7 © 2007 Bruker BioSpin. The spectra were referenced to the D_6-DMSO solvent peak at 2.50 ppm.[17]

2.7 Solubility Experiments

The solubility of each host compound in each of the liquid guests was investigated by performing approximate solubility experiments. A small sample of the host, approximately 10 mg, was placed in a vial and a stirrer bar added. This experimental set up was weighed and the combined mass noted. The liquid guest was added incrementally, and left to stir, until all the host powder had dissolved. The mass of the added liquid was determined and the amount of solvent required to dissolve 1 g of host was calculated.

2.8 Microscopy

The morphology, colour and appearance of crystals grown during this project were examined using microscopy. This allowed for comparisons and images of the crystals to be examined. Photographs were taken with an Axiocam 105 colour camera attached to a Zeiss SteREO Discovery V8 microscope and processed using the ZEN 2 (blue edition) programme (Carl Zeiss Microscopy GmbH, 2011).

2.9 References

1. Barton B., Hosten E. C., Jooste D. V., Comparative investigation of the inclusion preferences of optically pure versus racemic TADDOL hosts for pyridine and isomeric methylpyridine guests, *Tetrahedron*, 2017, **73**, 2662, DOI: https://doi.org/10.1016/j.tet.2017.03.049.

2. Bruker AXS Inc., APEX2, Version 1.0-27, Bruker AXS Inc, Madison, Wisconsin, USA.

3. Bruker AXS Inc., Program SAINT, Version 7.60a, Bruker AXS Inc., Madison, Wisconsin, USA, 2006.

4. Bruker AXS Inc., XPREP, Version 5.1, Bruker AXS Inc., Madison, Wisconsin, USA, 1997.

5. Sheldrick G. M., Program SADABS, Version 2.05, University of Göttingen, Germany, 2007.

6. Sheldrick G. M. SHELXL-97: Program for the refinement of crystal structure; University of Göttingen: Göttingen, Germany, 1997.

7. Sheldrick, G. M., A short history of SHELX, *Acta Crystallogr. A.*, 2008, **64**, 112-122.

DOI: https://doi.org/10.1107/S0108767307043930.

8. Barbour L.J., X-Seed—A software tool for supramolecular crystallography, *J. Supramol. Chem.*, 2001, **1**, 189-191. DOI: https://doi.org/10.1016/S1472-7862(02)00030-8.

9. Lusi M., Barbour L. J., Determining Hydrogen Atom Positions for Hydrogen Bonded Interactions: A Distance-Dependent Neutron-Normalized Method, *Cryst. Growth Des.*, 2011, **11** (12), 5515–5521, DOI: https://doi.org/10.1021/cg201087s.

10. Cambridge Structural Database and Cambridge Structural Database system, Version 5.40 (updates to April 2019), Cambridge Crystallographic Data Centre, University Chemical Laboratory, Cambridge, England, 2019.

11. Speck, A L, PLATON, A multipurpose crystallographic tool, 1980-2000.

12. McKinnon J. J., Spackman M. A., Mitchell A. S. Novel tools for visualizing and exploring intermolecular interactions in molecular crystals, *Acta Crystallogr.*, 2004, **B60**, 627-668, DOI: https://doi.org/10.1107/S0108768104020300.

13. Spackman M. A., McKinnon J. J. Fingerprinting intermolecular interactions in molecular crystals, *CrystEngComm.*, 2002, **4**, 378-392, DOI: http://dx.doi.org/10.1039/B203191B.

14. Spackman M. A., McKinnon J. J., Jayatilaka D., Electrostatic potentials mapped on Hirshfeld surfaces provide direct insight into intermolecular interactions in crystals, *CrystEngComm.*, 2008, **10**, 377-388, DOI: http://dx.doi.org/10.1039/B715227B.

15. TA Instruments, Universal Analysis version 4.5A, Waters LLC, 2000.

16. TA Instruments, Trios v4.1.133073.

17. Bruker Biospin, pl 7, Bruker AXS Inc., Madison, Wisconsin, USA, 2007.

Chapter 3. Novel Host-Guest Structures

3.1 Introduction

Ten novel inclusion compounds were prepared, using three different host compounds. The first host, (4*RS*,5*RS*)-2,2-dimethyl-α,α,α',α'-tetrakis(p-tolyl)-1,3- dioxolane-4,5-dimethanol (**H1**) forms inclusion compounds **H1·2PIC**, **H1·3PIC**, **H1·4PIC** and **H1·PYR**.

A second host, (4*RS*,5*RS*)-2,2-dimethyl-α,α,α',α'-tetrakis(p-fluorophenyl)-1,3-dioxolane-4,5-dimethanol (**H2)**, is similar to **H1**, but has fluorine atoms at the para positions on the phenyl rings. Once again, four novel inclusion compounds **H2·2PIC**, **H2·3PIC H2·4PIC** and **H2·PYR** were synthesised and characterised.

A third host, (4*RS*, 5*RS*)-2,2-dimethyl-α,α,α',α'-tetraphenyl-1,3-dioxolane-4,5-dimethanol, is similar to **H1** and **H2**, but lacks the methyl or fluorine groups on the phenyl rings. Structures of **H3** with 3-,4-picoline and pyridine were reported by Barton et al., but in the case of the inclusion compound formed with **H3** and 2-picoline, the authors were unable to obtain a good quality crystal for single crystal X-ray diffraction.[1] This structure, **H3·2PIC**, was synthesised during the course of this investigation and the structure elucidated. The **H3** and 4-picoline host-guest compound synthesised by Barton contained waters of crystallisation and, therefore, another aim for this project was to determine whether a compound could be synthesised containing just the host and guest compound. This was achieved, and a novel **H3·(1.5)4PIC** host-guest compound was achieved. All of the inclusion compounds reported by Barton were resynthesised during this investigation.

The host used in this investigation are shown in Figure 3.1. Once the inclusion compounds were synthesised, the structures were elucidated and the compounds were further studied, using an array of analytical methods focusing on their structural and thermal properties.

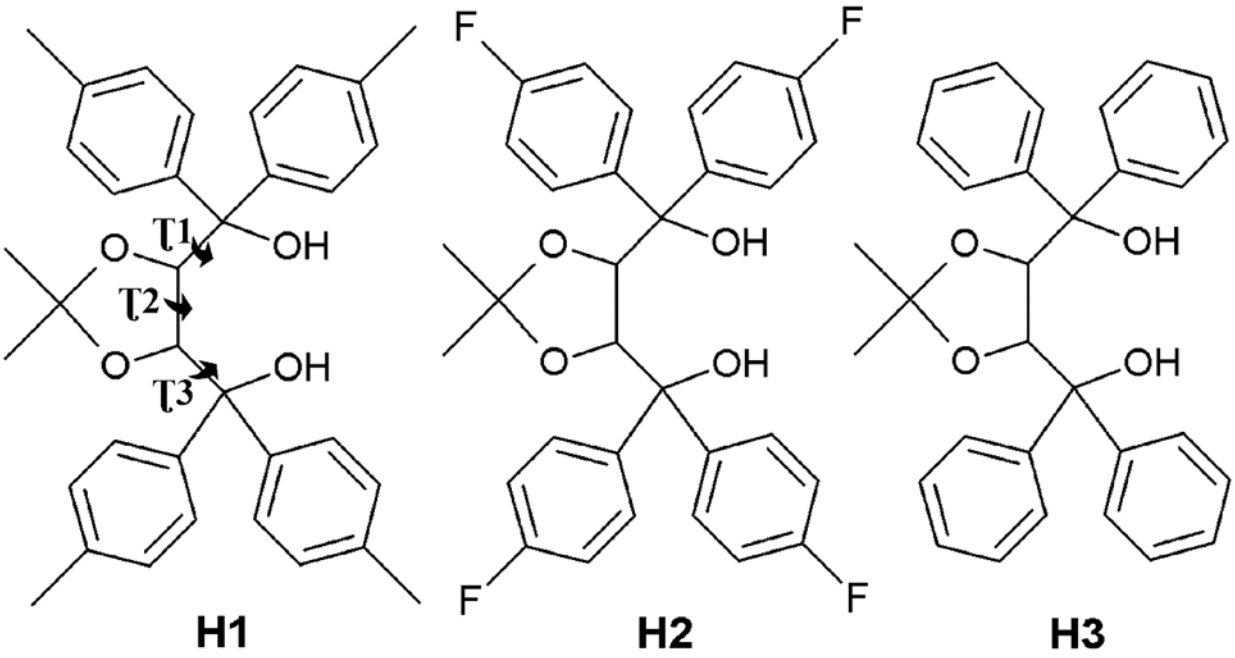

Figure 3.1: Structures of the TADDOL hosts, **H1** (4*RS*,5*RS*)-2,2-dimethyl-α,α,α',α'-tetrakis(p-tolyl)-1,3-dioxolane-4,5-dimethanol, **H2** (4*RS*,5*RS*)-2,2-dimethyl-α,α,α',α'-tetrakis(p-fluorophenyl)-1,3-dioxolane-4,5-dimethanol, and **H3** (4*RS*, 5*RS*)-2,2-dimethyl-α,α,α',α'-tetraphenyl -1,3-dioxolane-4,5-dimethanol along with the pyridine and methylpyridine (picoline) guests. The torsion angles in each structure are Ƭ1 = O1-C1-C2-C3, Ƭ2 = C1-C2-C3-C4 and Ƭ3 = O4-C4-C3-C2.

3.2 Preparation of Inclusion Compounds

All inclusion compounds were prepared via slow evaporation. Approximately 50 mg of the host compound was dissolved in a single liquid guest (1.5 ml), the solution stirred for five minutes until clear, and left on the benchtop to evaporate at room temperature (25 °C).

In the synthesis of **H3·(1.5)4PIC**, the liquid guest was dried using distillation and a highly saturated solution was left in a sealed desiccator. In all cases, clear crystalline material appeared after a few days, depending on the combination of host and guest used. Powders were also obtained by utilising vapour diffusion. This was accomplished by leaving 50 mg of host and 2 ml of guest in separate, open vials sealed in jars for a month.

All crystals obtained were block-shaped and colourless, and were observed using a microscope. These photographs in Figure 3.2 were taken under polarised light and the differences in crystal and background colours are due to the analysers being at different angles each time. The crystals show birefringence and, by using this microscope, single crystals can be identified, as they extinguish upon rotation of the polarisers. **H1·3PIC** in Figure 3.2 is slightly yellow due to excess 3-picoline in the solution.

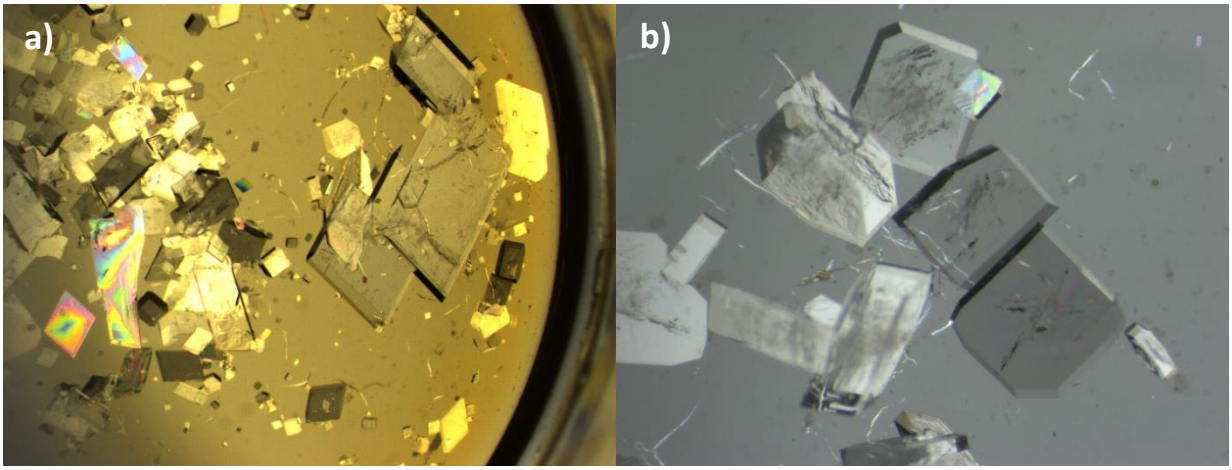

Figure 3.2: Images showing the habit of the crystals obtained during the course of this investigation. All hosts generated block shaped crystals which were colourless. The left image shows **H1·3PIC** and right shows **H3·2PIC**.

3.3 Analysis of Inclusion Compounds

Once obtained, these compounds were subjected to various analyses, such as single crystal X-ray diffraction (SCXD), powder X-ray diffraction (PXRD), proton nuclear magnetic resonance (^{1}H-NMR) spectroscopy and thermal analysis, including hot stage microscopy (HSM), thermalgravimetric Analysis (TGA) and differential scanning calorimetry (DSC). Enclathration was confirmed using all of these techniques.

A suitable crystal was selected for SCXD and remaining crystals were removed from the mother liquor and patted dry on filter paper. The crystals were then ground for PXRD analysis with the samples then being utilised for TGA and DSC analysis, followed by ^{1}H NMR spectroscopy. As all of the potential crystals that could crystallise out of the prepared solutions would be novel, the first avenue of analysis was SCXD.

3.4 Structural Analysis of H1·2PIC

3.4.1 Single Crystal X-ray Diffraction Analysis

A colourless block-shaped crystal, with dimensions of 0.30 x 0.35 x 0.41 mm^3, was selected for single crystal X-ray diffraction analysis. These crystals appeared in the vial after only 24 hours. The data were collected on a Bruker DUO APEX II^2 diffractometer at -100 °C. **H1·2PIC** crystallises in the triclinic crystal system with the space group $P\bar{1}$. The resulting structure was refined to R_1 = 0.0488 and wR_2 = 0.216, and the asymmetric unit contains one **H1** molecule and one **2PIC** guest with an overall molecular formula of 615.81 $g.mol^{-1}$ and the unit cell contains two of these units giving Z = 2. This shows a host:guest ratio of 1:1, which was subsequently confirmed using thermal and ^{1}H-NMR spectroscopic methods. The crystal data and refinement details are shown in Table 3.1.

Table 3.1: Crystal Data for **H1·2PIC**.

Compound	H1·2PIC
CCDC	1881574
Structural formula	C_{41} H_{45} NO_4
Molecular mass ($g·mol^{-1}$)	615.81
Data collection temp. (K)	173
Crystal system	Triclinic
Space group	$P\bar{1}$
a (Å)	11.177(2)
b (Å)	11.199(2)
c (Å)	15.093(3)
α(°)	75.81(3)
β(°)	85.06(3)
γ(°)	68.82(3)
Volume ($Å^3$)	1707.9(7)
Z/Z'	2/1
Dc, calc density ($g·cm^{-3}$)	1.197
θ range (°)	1.392-28.292
Reflections collected	27619
No. data I>2 σ (I)	8446
Final R Indices R_1, wR_2, [I>2 σ (I)]	0.0488, 0.216
Goodness-of-fit on F^2	1.050

a)

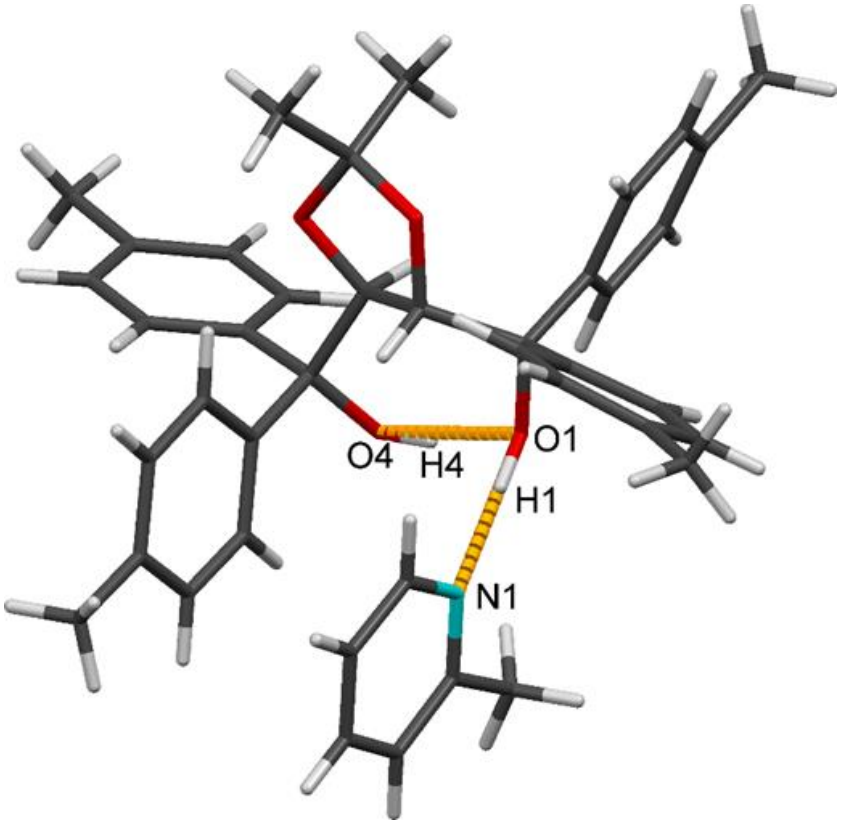

b)

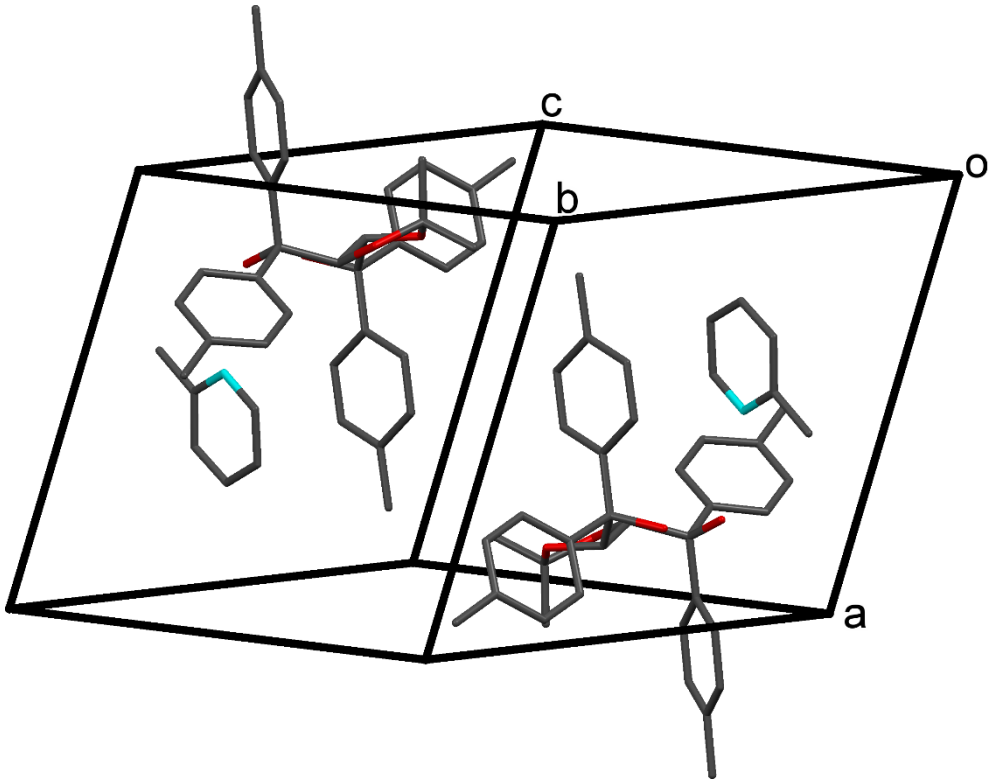

Figure 3.3: a) The asymmetric unit of **H1·2PIC** with the hydrogen bonds shown in orange b) The unit cell of **H1·2PIC** showing the two asymmetric units.

This structure is characterised by two hydrogen bonds, one intramolecular (O-H···O) within the host and one intermolecular (O-H···N) connecting the host to the guest. This is shown in Figure 3.3a. The unit cell contains two host:guest pairs and is pictured in Figure 3.3b. The O-H bond lengths were fixed during refinement using the method of Lusi and Barbour.[2] The details of the hydrogen bonds are shown in Table 3.2.

Table 3.2: Hydrogen bond interactions in **H1·2PIC.**

Donor (D)	Acceptor (A)	D···A (Å)	D-H(Å)	D···A (Å)	<D-H···A(°)
O4	N1	2.735(2)	0.988(5)	1.760(7)	169(2)
O1	O4	2.722(2)	0.974(5)	1.762(2)	168(2)

The guest packing (Figure 3.4) shows grey host molecules, with hydrogens omitted for clarity, and blue, space-filled guests. The guests form layers and the voids are shown in Figure 3.5 and were calculated using a probe radius of 1.2 Å and grid spacing of 0.7 Å. These voids have a kinked, zig-zag shape and are discrete cavities containing two guests each. The voids make up 15.1% of the unit cell volume, with a total void volume of 258 $Å^3$ per unit cell.

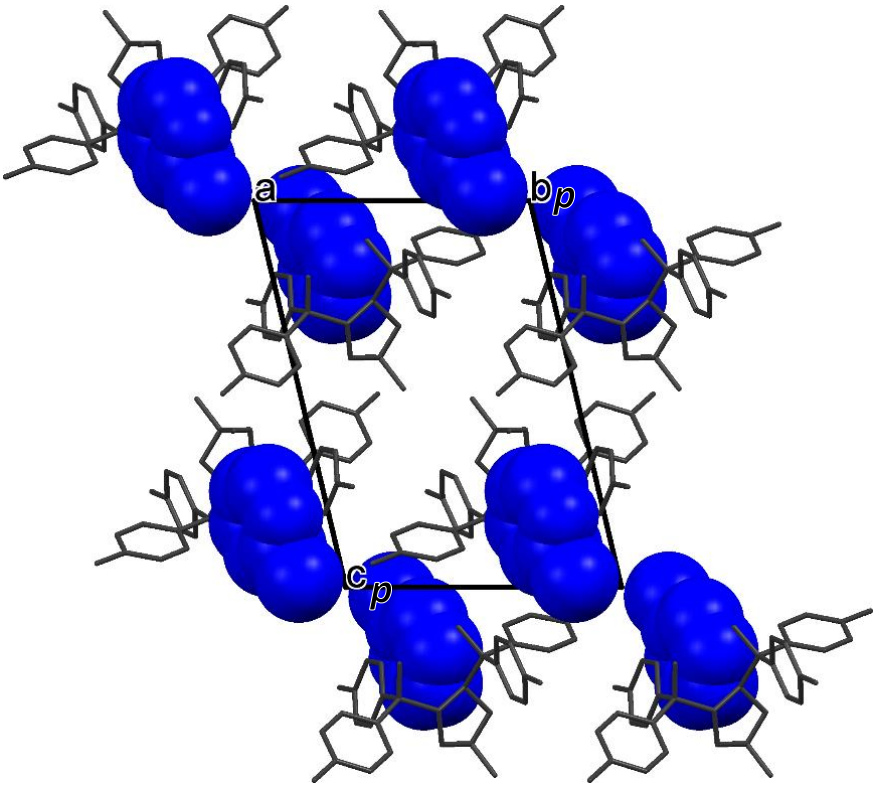

Figure 3.4: The packing of **H1·2PIC** viewed down [001].

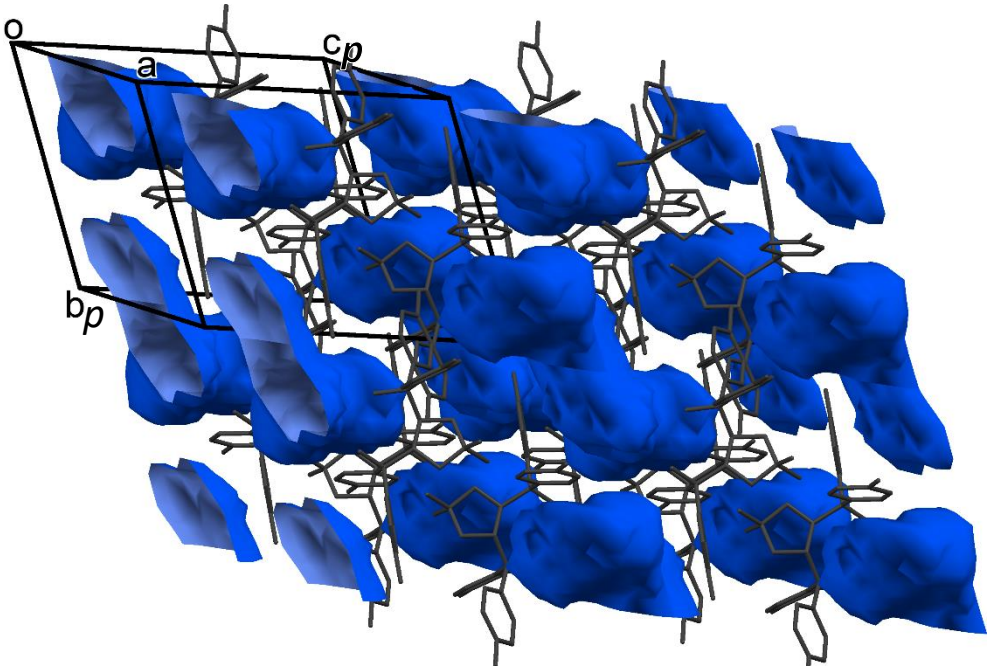

Figure 3.5: The void space of **H1·2PIC**.

3.4.2 Hirshfeld Surface Analysis

The non-bonded interactions of the **H1·2PIC** host-guest system were analysed using the program CrystalExplorer.[3] The Hirshfeld surface was generated around the guest molecule and points were mapped. A point on the Hirshfeld surface shows the distance to the nearest atom within the molecule (d_i) and the distance to the nearest atom on the neighbouring molecule (d_e). By plotting these points, a fingerprint plot is generated. These distances and their respective density give insight into the relationship between the guest molecule and its direct environment within the crystal. This is valuable as these fingerprint plots allow for easy identification and interpretation of intermolecular interactions.

The fingerprint plot for **H1·2PIC** (Figure 3.6a) shows that the majority of the interactions stem from H···H for H1·2PIC, followed by H···C and C···H, with the N···H interactions only making up 7.5%. The breakdown of these interactions is shown in Figure 3.6b. This shows the percentages of the overall interactions within the fingerprint. However, it must be noted that the percentages do not necessarily correspond to bond strength. As the strongest interaction

is clearly the H-N hydrogen bond, due to the minimisation of d_i and d_e, but the H-N interaction makes up only 7.5% of all the interactions present in the host:guest surface.

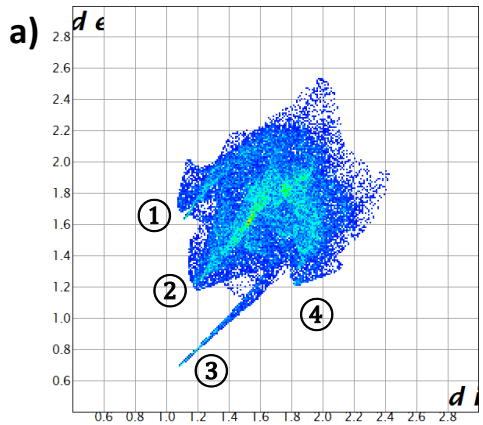

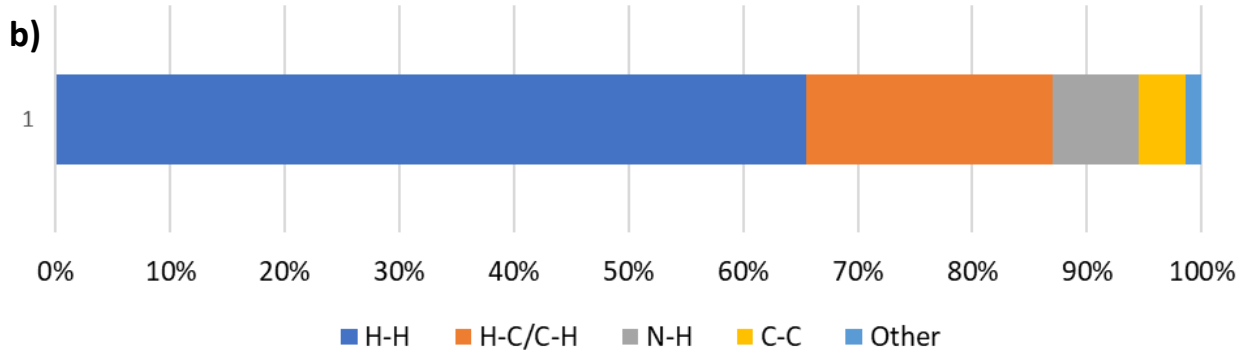

Figure 3.6: a) Fingerprint plot with the 2-picoline guest molecule as target. Spikes correspond to;
1) H···C 2) H···H 3) N···H and 4) C···H other smaller interactions are not labelled.

b) The breakdown of the intermolecular interactions between the host and the 2-picoline guest.

3.4.3 Intra- and Intermolecular Interactions

Due to the nature of this host and guest, containing a multitude of aromatic rings, there are many π···π and CH···π interactions present in **H1·2PIC**. It is expected that the more host π-pyridyl guest π interactions present in the crystal structure, the more stable the guest is in the inclusion complex. Though these interactions are generally weak, a large number of them will have noticeable effects on the stability of the inclusion compound. The PLATON programme was used to generate these interactions.[4]

Table 3.3 shows the labelling of the generated centroids of the aromatic rings present in **H1·2PIC**, with Table 3.4 listing the C-H···π interactions. Table 3.5 shows the π···π interactions. However, as there were so many, only strong contacts (under 5 Å) were included. The interaction that is the strongest is, unsurprisingly, between one of the host phenyl rings and the pyridyl of the guest.

Short contacts present within the inclusion compound were noted. These non-bonded interactions were regarded as significant when their interatomic distances were less than the sum of the van der Waals radii given by Bondi: H = 1.20 Å, C = 1.70 Å, O = 1.52 Å, N = 1.53 Å and F = 1.47 Å.[5]

Table 3.3: The generated centroids for **H1·2PIC** and their corresponding atoms.

Centroid	Nature	Atom 1	Atom 2	Atom 3	Atom 4	Atom 5	Atom 6
Cg 1	Host	O2	C2	C3	O3	C29	-
Cg 2	Host	C5	C6	C7	C8	C9	C10
Cg 3	Host	C11	C12	C13	C14	C15	C16
Cg 4	Host	C17	C18	C19	C20	C21	C22
Cg 5	Host	C23	C24	C25	C26	C27	C28
Cg 6	Guest	N1	C36	C37	C38	C39	C40

Table 3.4: C-H···π interactions in **H1·2PIC**

Nature	C(I)-H(J) ··· Cg(k)	Symmetry Operator	H···Cg (Å)	Angle (°)
Host-Host	C(30)-H(30B) ··· Cg(2)	2-x, -y, 1-z	2.80	146
Guest-Host	C(39)-H(39) ··· Cg(4)	1-x, 1-y, -z	2.75	168
Host-Guest	C(33)-H(33C) ··· Cg(6)	1+x, y, z	3.00	125

Table 3.5: π···π interactions in **H1·2PIC**

Nature	Cg(I)-Cg(J)	Symmetry operator	Cg-Cg (Å)
Host-Guest	Cg(3)-Cg(6)	1+x, y, z	4.693(2)
Host-Guest	Cg(2)-Cg(6)	2-x, -y, 1-z	4.992(2)
Host-Host	Cg(5)-Cg(4)	x, y, z	4.880(2)
Host-Guest	Cg(5)-Cg(6)	x, y, z	3.893(2)

Table 3.6: Summary of shortest intermolecular contacts

Nature	Contact	C(I)-H(J) ··· Cg(k)	Symmetry Operator	Length (Å)
Host-Guest	H···C	H(1) ··· C(36)	x, y, z	2.63
Host-Host	C···H	C(27) ··· H(33A)	-1+x, 1+y, z	2.74
Host-Guest	H···C	H(1) ··· C(40)	x, y, z	2.76
Host-Guest	C···H	C(10) ··· H(36)	x, y, z	2.86
Host-Host	C···H	C(9) ··· H(30B)	2-x, -y, 1-z	2.87
Host-Host	H···H	C(21) ··· H(35A)	1+x, y, z	2.88
Host-Host	H···H	H(18) ··· H(33A)	-1+x, 1+y, z	2.39
Host-Host	H···C	H(22) ··· C(21)	2-x, 1-y, -z	2.89

3.4.4 Powder X-ray Diffraction Analysis

The predicted and experimental PXRD traces for **H1·2PIC** are shown in Figure 3.7. These patterns show strong similarities and confirm that the single crystal is representative of the bulk crystalline material. In addition, these patterns closely resemble the PXRD trace of **H1·2PIC** grown through vapour diffusion and, therefore, shows two avenues of **H1·2PIC** preparation. This method of preparing crystalline material utilising vapour diffusion requires no solution and a reduced amount of guest liquid and is, therefore, potentially greener than slow evaporation.

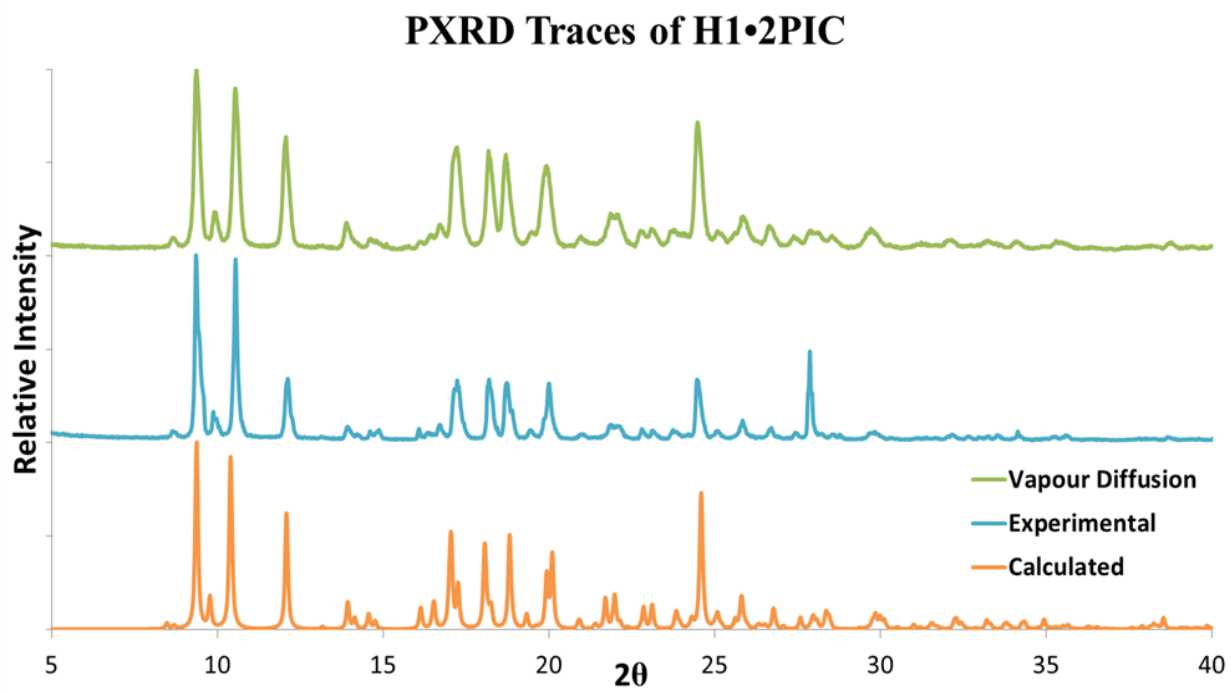

Figure 3.7: PXRD patterns of **H1·2PIC,** grown by vapour diffusion (green), slow evaporation crystals (blue) and compared to the trace calculated from the crystal structure (orange).

3.5 Structural Analysis of H1·3PIC, H1·4PIC and H1·PYR

3.5.1 Single Crystal X-ray Diffraction Analysis

H1·3PIC, **H1·4PIC** and **H1·PYR** are isomorphous and, consequently, share many of the same features and are, therefore, presented together for comparison and brevity. As is the case with **H1·2PIC**, these host-guest compounds all crystallise in a triclinic crystal system and $P\bar{1}$ space group. The cell parameters are similar to those of **H1·2PIC** but the **H1·3PIC, H1·4PIC** and **H1·PYR** guests reside in channels, which contrasts with the discrete cavities present in **H1·2PIC.** As with **H·2PIC**, the host:guest ratio was modelled with a 1:1 ratio, and this was confirmed using ^{1}H NMR spectroscopy and thermal analysis. Once again, the O···H bond lengths were fixed and the crystal data and refinement details are shown in Table 3.7.

Table 3.7: Crystal Data for **H1·3PIC**, **H1·4PIC** and **H1·PYR**

Compound	H1•3PIC	H1•4PIC	H1•PYR
CCDC	1881573	1881572	1881570
Structural formula	$C_{41}H_{45}NO_4$	$C_{41}H_{45}NO_4$	$C_{40}H_{43}NO_4$
Molecular mass (g·mol^{-1})	615.78	615.78	601.75
Crystal Size	0.18 x 0.29 x 0.44	0.13 x 0.25 x 0.27	0.28 x 0.35 x 0.46
Data collection temp. (K)	173	173	173
Crystal system	Triclinic	Triclinic	Triclinic
Space group	$P\bar{1}$	$P\bar{1}$	$P\bar{1}$
a (Å)	10.327(2)	10.398(2)	10.240(2)
b (Å)	10.761(2)	10.944(2)	10.819(2)
c (Å)	17.899(4)	17.935(4)	17.846(4)
α(°)	76.85(3)	73.47(3)	74.29(3)
β(°)	91.04(3)	85.90(3)	88.68(3)
γ(°)	63.48(3)	63.00(3)	63.34(3)
Volume (Å^3)	1716.5(8)	1716.4(8)	1689.8(7)
Z/Z'	2/1	2/1	2/1
D calc density (g·cm^{-3})	1.191	1.176	1.183
θ range (°)	2.750-28.330	2.3745-26.410	2.240-34.584
Reflections collected	23099	20057	29152
No. data I>2 σ (I)	8550	8772	13239
Final R Indices R_1, [I>2 σ (I)]	0.0484	0.0836	0.0573
Goodness-of-fit on F^2	1.047	0.993	1.047

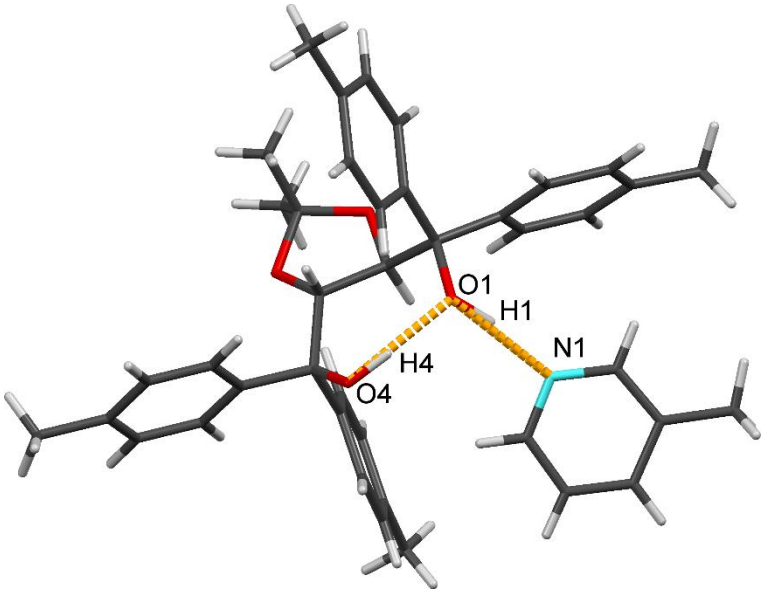

Figure 3.8: The asymmetric unit of **H1·3PIC** which is analogous to those of **H1·4PIC** and **H1·PY**.

The hydrogen bonding in all three of these inclusion compounds is analogous to that described above in **H1·2PIC**, with one intramolecular (O-H···O) bond connecting the two host oxygen atoms and one intermolecular (O-H···N) bond connecting host to the nitrogen of the guest. These interactions are summarised in Table 3.8. An example of an asymmetric unit is shown in Figure 3.8 with **H1·3PIC**. The packing and void spaces are different from that seen in **H1·2PIC** and have been included. The packing diagram in Figure 3.9 displays the isostructural nature of the three compounds and shows guests arranged in layers. Once the guests are removed and the void spaces mapped, the channels can be seen. This is shown in Figure 3.10 and are different from the discrete cavities that are exhibited in **H1·2PIC.** These three structures show channels running down [010].

Table 3.8: Hydrogen-bonding interactions in **H1·3PIC**, **H1·4PIC** and **H1·PY**.

	Donor (D)	Acceptor (A)	D···A (Å)	D-H(Å)	H···A (Å)	<D-H···A (°)
H1·3PIC	O4	N1	2.693(2)	0.939(5)	1.782(8)	163(2)
	O1	O4	2.697(2)	0.951(5)	1.747(5)	177(2)
H1·4PIC	O4	N1	2.717(4)	0.922(5)	1.808(1)	169(4)
	O1	O4	2.679(3)	0.952(5)	1.746(1)	166(4)
H1·PY	O4	N1	2.772(2)	0.892(5)	1.909(8)	162(2)
	O1	O4	2.711(1)	0.951(5)	1.769(6)	170(2)

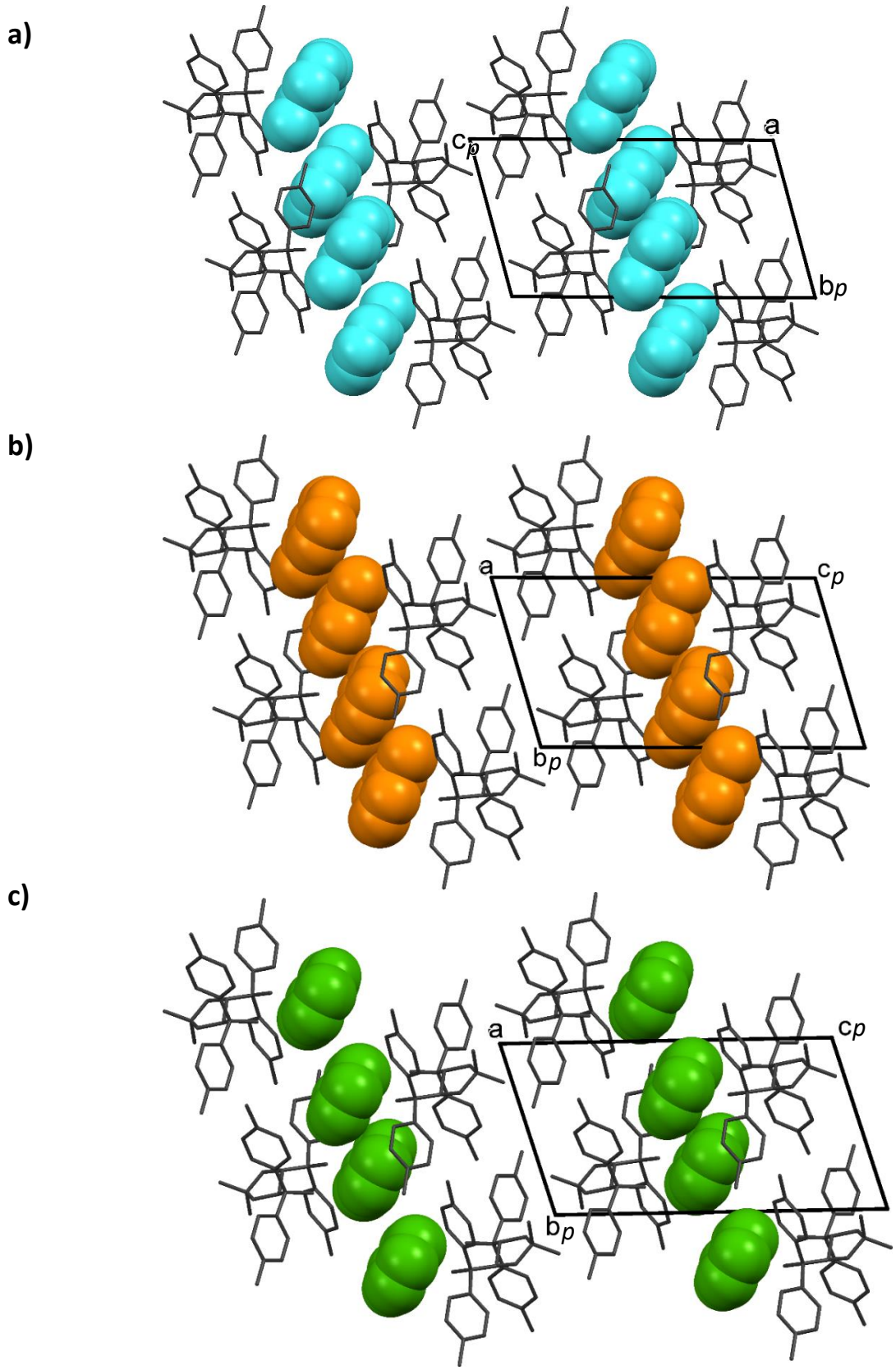

Figure 3.9: The packing of a) **H1·3PIC** b) **H1·4PIC** and c) **H1·PYR**.

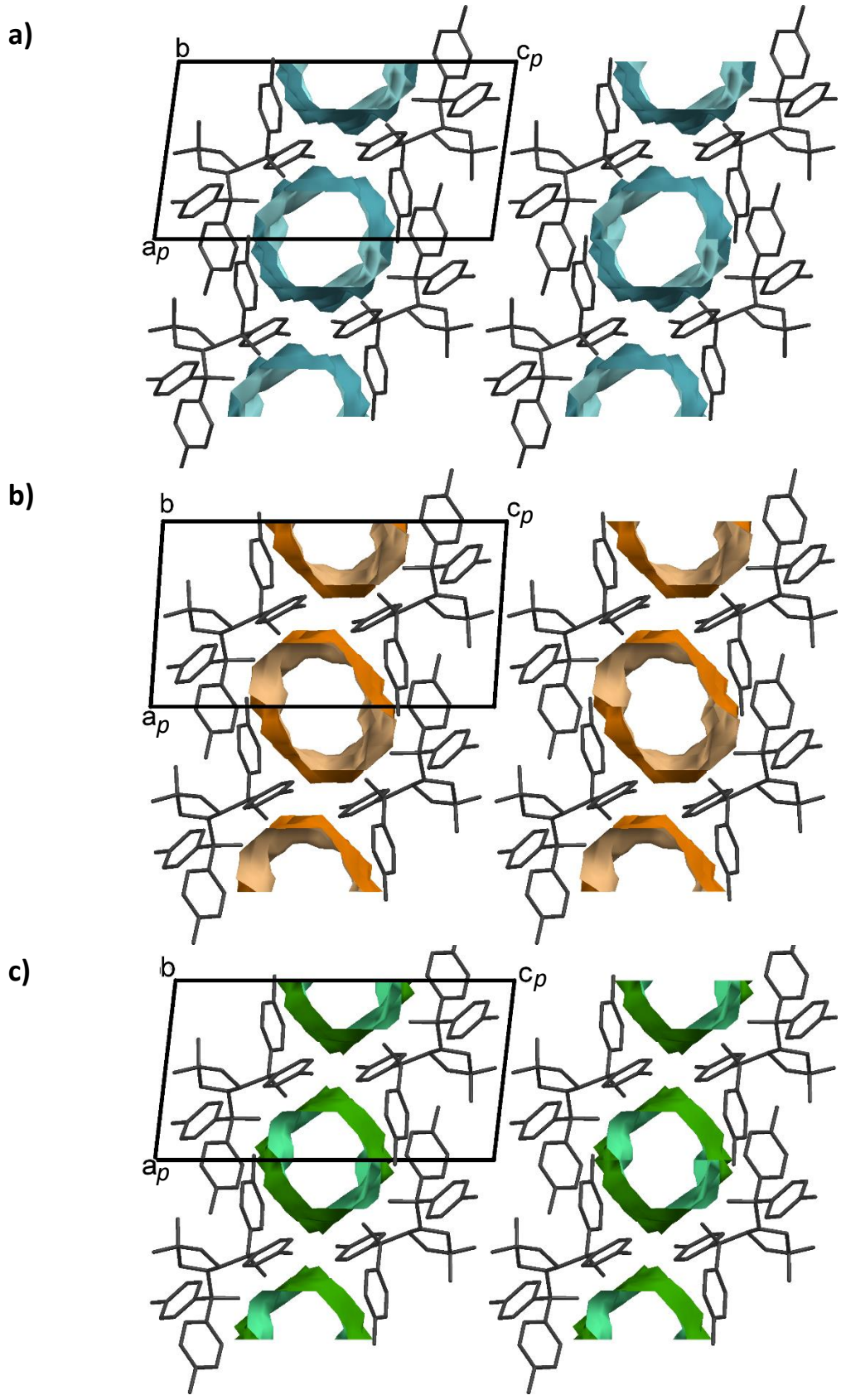

Figure 3.10: The voids of a) **H1·3PIC** b) **H1·4PIC** and c) **H1·PYR** with the channels down [010].

The channels present in **H1·3PIC**, **H1·4PIC** and **H1·PYR** may be a consequence of shifting of the guests, which could blend the discrete cavities resulting in the formation of channels. It is interesting that the pyridine guest would also exhibit this feature when crystallised with **H1**, despite lacking the methyl group that is characteristic of the other two guests. The percentage and the volume of void space in each unit cell are shown in Table 3.9.

Table 3.9: Void percentage and volume for each unit cell.

	H1·3PIC	**H1·4PIC**	**H1·PY**
% voids space	16.9	16.2	16.9
Volume (Å³)	293	278	294

3.5.2 Hirshfeld Surface Analysis

Once again, the Hirshfeld surface was generated around the guest molecules and the interactions calculated. **H1·3PIC**, **H1·4PIC and H1·PYR** are isomorphous and, as described above, have many similarities in crystal structure and packing, which makes comparison tricky. However, the three guests have different structures and this should translate into differences in the intermolecular interactions hightlighted in the fingerprint plots.

The fingerprint plots for **H1·3PIC**, **H1·4PIC** and **H1·PYR** are shown in Figure 3.11a, 3.11b and 3.11c, respectively. The labels correspond to peaks showing ① H···C ②H···C ③H···H ④N···H and ⑤ C···H. The breakdown of the individual interactions is shown in Figure 3.11d. The majority of interactions are H···H and H···C/C···H with the hydrogen bonding coming in third. Overall, there are some differences in the composition of interactions with **H1·3PIC** showing a higher percentage of C···C interactions, compared to the other structures.

The fingerprint plot for the **H1·4PIC** structure (Figure 3.11b) is interesting, as there is a sharp spike corresponding to peak ②. This indicates a H···O interaction, which was attributed to a hydrogen atom on the methyl group of the guest interacting with an oxygen atom of a host molecule outside of the asymmetric unit. This interaction makes the **H1·4PIC** compound potentially more stable than **H1·3PIC** and **H1·PYR**, which lack this sharp peak. This contact is illustrated in Figure 3.11e.

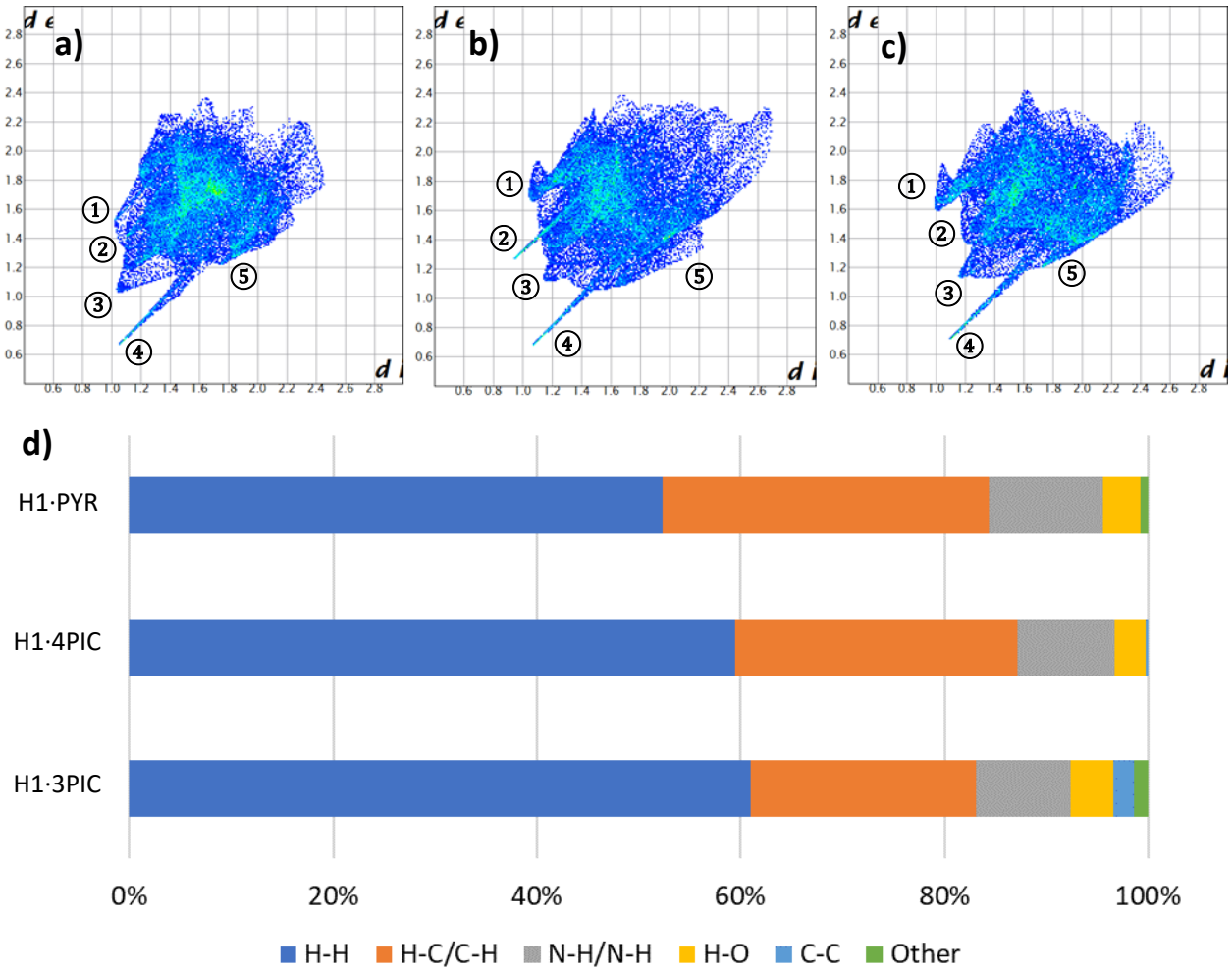

Figure 3.11: Fingerprint plots of a) **H1·3PIC**, b) **H1·4PIC** and c) **H1·PYR.** d) The breakdown of the individual interactions present in each generated Hirshfeld fingerprint plot. e) The unique O···H contact in **H1·4PIC**.

3.5.3 Intra- and Intermolecular Interactions

Once again, due to the nature of this host and guest, containing a multitude of aromatic rings, many π···π and CH···π interactions are present in **H1·3PIC**, **H1·4PIC** and **H1·PYR**. The PLATON programme was used to generate these interactions. The generated centroids for the three host:guest complexes are outlined in Table 3.10. Table 3.11 shows the π···π interactions. These interactions are numerous and the majority are not strong (>4 Å). Therefore, only the strongest contact in each host:guest complex is listed. **H1·3PIC** has one strong π···π contact, which corresponds to guest:guest interactions, while the strongest π···π contacts in **H1·4PIC** and **H1·PYR** correspond to a host-guest interaction within the unit cell. Table 3.12 summarises the CH···π interactions in all three structures. These are generally similar across the structures. **H1·3PIC** has slightly fewer interactions than do the other two structures, however, this may not be significant. The shortest contacts in the three structures are listed in Table 3.13 and, for brevity, only the interactions that are shorter than 95% of the sum of the van der Waals radii outlined by Bondi are included.

Table 3.10: The generated centroid (Cg) for the guests of **H1·3PIC, H1·4PIC** and **H1·PYR** and their corresponding atoms.

Centroid	Nature	Atom 1	Atom 2	Atom 3	Atom 4	Atom 5	Atom 6
Cg 1	Host	O2	C2	C3	O3	C29	-
Cg 2	Host	C5	C6	C7	C8	C9	C10
Cg 3	Host	C11	C12	C13	C14	C15	C16
Cg 4	Host	C17	C18	C19	C20	C21	C22
Cg 5	Host	C23	C24	C25	C26	C27	C28
Cg 6	Guest	N1	C36	C37	C38	C39	C40

Table 3.11: Strong π···π interactions in **H1·3PIC**, **H1·4PIC** and **H1·PYR**.

Structure	Cg(I)-Cg(J)	Symmetry	Cg-Cg (Å)
H1·3PIC	Cg(6)-Cg(6)	1-x, -y, -z	3.956(2)
H1·4PIC	Cg(2)-Cg(6)	x, y, z	4.681(2)
H1·PYR	Cg(3)-Cg(6)	x, y, z	4.631(2)

Table 3.12: C-H···π interactions in **H1·3PIC**, **H1·4PIC** and **H1·PYR**.

Structure	Nature	C(I)-H(J) ··· Cg(k)	Symmetry Operator	H···Cg (Å)	Angle (°)
H1·3PIC	Host-Host	C(13)-H(13) ··· Cg(5)	1+x, y, z	2.87	162
H1·3PIC	Host-Host	C(19)-H(19) ··· Cg(2)	-1+x, y, z	2.86	178
H1·3PIC	Host-Host	C(31)-H(31A) ··· Cg(3)	x, y, z	2.99	140
H1·4PIC	Host-Host	C(15)-H(15) ··· Cg(5)	1+x, y, z	2.98	159
H1·4PIC	Host-Host	C(19)-H(19) ··· Cg(2)	-1+x, y, z	2.97	165
H1·4PIC	Host-Host	C(33)-H(33B) ··· Cg(6)	1+x, -1+y, z	2.94	166
H1·4PIC	Guest-Host	C(36)-H(36) ··· Cg(2)	x, y, z	2.61	146
H1·PY	Host-Host	C(7)-H(7) ··· Cg(5)	1+x, y, z	2.96	156
H1·PY	Host-Host	C(19)-H(19) ··· Cg(3)	-1+x, y, z	2.91	163
H1·PY	Guest-Host	C(39)-H(39) ··· Cg(2)	2-x, 2-y, -z	2.97	140
H1·PY	Guest-Host	C(40)-H(40) ··· Cg(3)	x, y, z	2.52	150

Table 3.13: Summary of shortest intermolecular contacts in **H1·3PIC**, **H1•·PIC** and **H1·PYR**.

Structure	Nature	Contact	C(I)-H(J) ··· Cg(k)	Symmetry Operator	Length (Å)
H1·3PIC	Host-Guest	H···C	H(1) ··· C(36)	x, y, z	2.53
H1·3PIC	Host-Guest	C···H	C(18) ··· H(36)	x, y, z	2.69
H1·3PIC	Host-Guest	H···H	H(32A) ··· H(37)	1+x, y, z	2.25
H1·4PIC	Host-Guest	O···H	O(4) ··· H(41C)	-x, 1-y, 1-z	2.32
H1·4PIC	Host-Guest	H···C	H(1) ··· C(40)	x, y, z	2.65
H1·4PIC	Host-Guest	H···C	H(1) ··· C(36)	x, y, z	2.73
H1·4PIC	Host-Guest	H···C	H(6) ··· C(36)	1-x, 1-y, 1-z	2.39
H1·PY	Host-Guest	H···C	H(1) ··· C(40)	x, y, z	2.70
H1·PY	Host Guest	C···H	C(15) ··· H(40)	x, y, z	2.75

3.5.4 Powder X-ray Diffraction Analysis

As described for **H1·2PIC**, the crystals **H1·3PIC**, **H1·4PIC and H1·PYR** were ground up and PXRD traces recorded. The experimental traces have a significant number of peaks, in common with the calculated pattern, confirming that the single crystals used to determine the structure were representative of the bulk sample. The experimental and calculated traces are shown in the plots included in Figure 3.12.

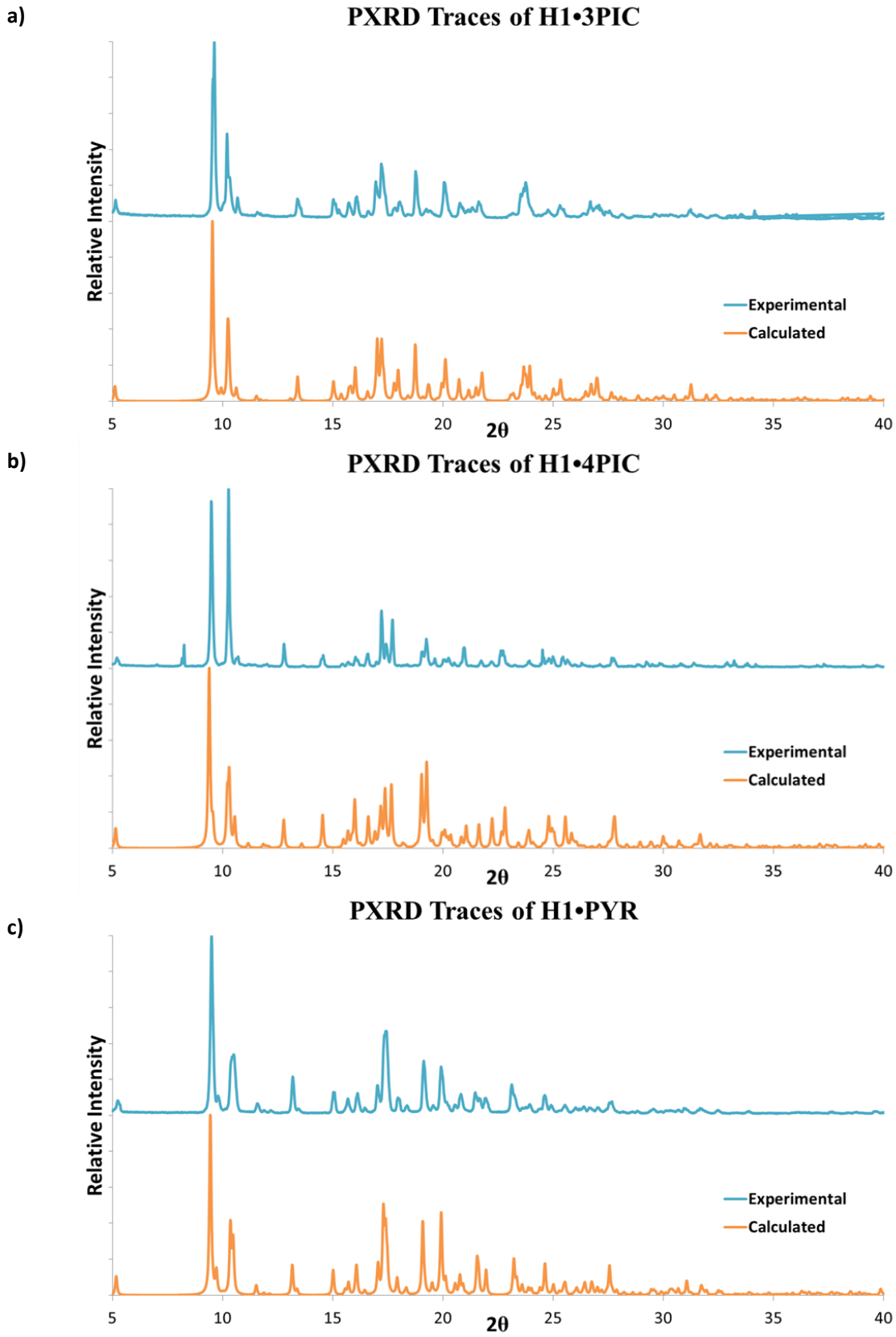

Figure 3.12: PXRD traces of a) **H1·3PIC** b) **H1·4PIC** and c) **H1·PYR**.

3.6 Structural Analysis of H2·2PIC

3.6.1 Single Crystal X-ray Diffraction Analysis

A colourless plate-shaped crystal, with dimensions of 0.08 x 0.28 x 0.45 mm^3, was selected for single crystal X-ray diffraction analysis. The data were collected on a Bruker DUO APEX II^2 diffractometer at -100 °C. **H2·2PIC** crystallises in the monoclinic crystal system with the space group $P2_1/n$.

The resulting structure was refined to R_1 = 0.0536 and wR_2 = 0.1128 and the asymmetric unit contains two **H2** molecules and two **2PIC** guests and the unit cell contains eight of these units giving a Z = 8 with Z' =2. This shows a host:guest ratio of 2:2, which was subsequently confirmed using thermal and ^{1}H NMR spectroscopic methods. The crystal data and refinement details are shown in Table 3.14.

Table 3.14: Crystal Data for **H2·2PIC**.

Compound	H2·2PIC
CCDC	1881576
Structural formula	$C_{37}H_{33}F_4NO_4$
Molecular mass (g·mol^{-1})	631.64
Data collection temp. (K)	173
Crystal system	Monoclinic
Space group	$P2_1/n$
a (Å)	19.316(4)
b (Å)	16.178(3)
c (Å)	22.229(4)
α(°)	90
β(°)	113.86(3)
γ(°)	90
Volume (Å^3)	6353.0(3)
Z/Z'	8/2
D calc density (g·cm^{-3})	1.321
θ range (°)	2.365-22.820
Reflections collected	52405
No. data I>2 σ (I)	15797
Final R Indices R_1, [I>2 σ (I)]	0.0536
Goodness-of-fit on F^2	1.011

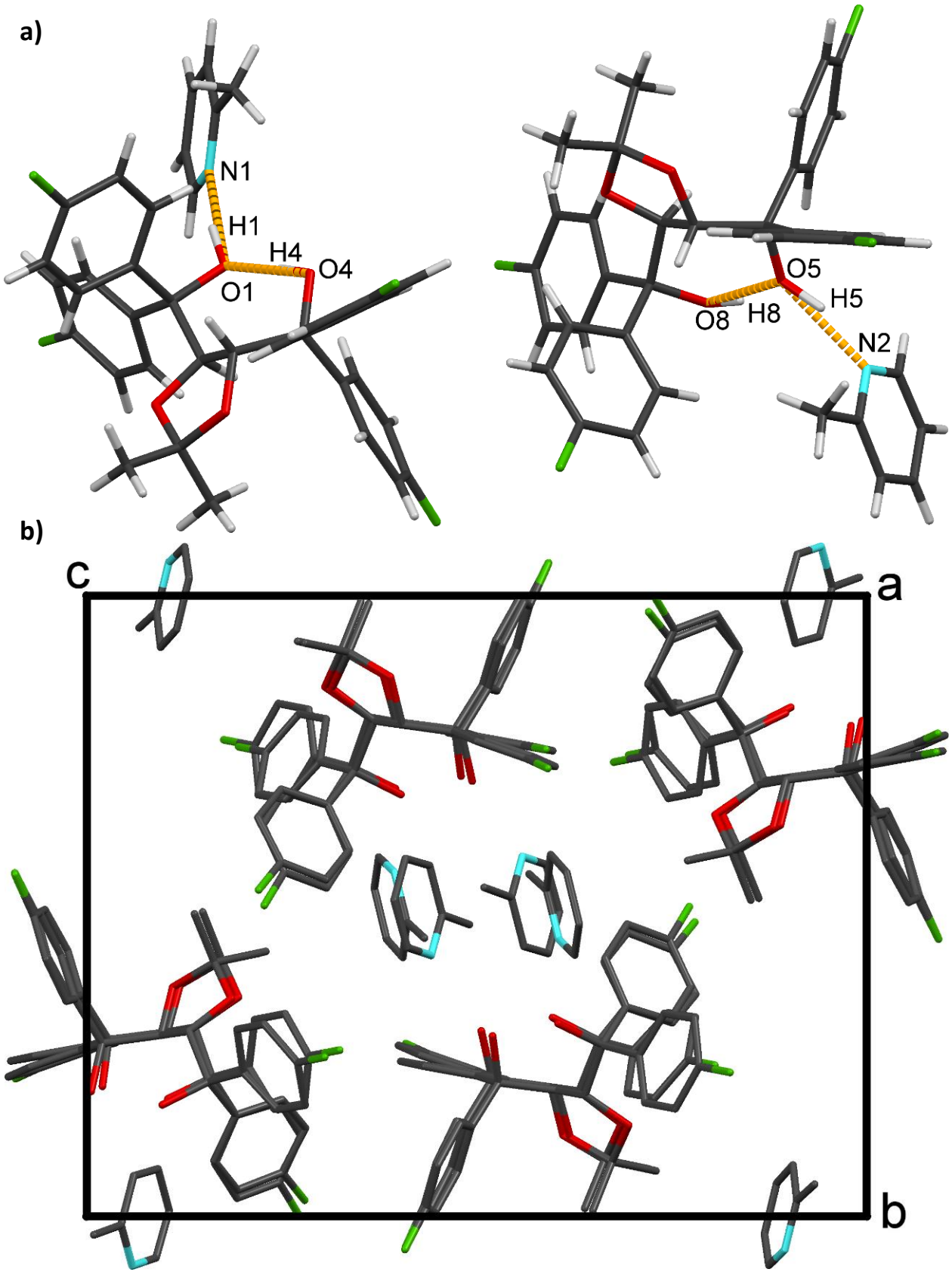

Figure 3.13: a) The asymmetric unit of **H2·2PIC** b) the unit cell of **H2·2PIC**.

This structure has two crystallographically independent host-guest pairs within the asymmetric unit with O···N hydrogen bonds of 2.640 (0.002) Å and 2.664 (0.002) Å. This host is characterised by fluorine atoms on the para-positions of the host phenyl rings and allows for fluorine-fluorine interactions. This particular structure exhibits an F···F intermolecular interaction of 2.91 Å between the two host molecules within the asymmetric unit. The structure also displays the O-H···N hydrogen bonds present in the **H1** host-guest compounds. The asymmetric unit and unit cell have been included in Figure 3.13a and 3.13b, respectively. The unit cell shows the presence of eight guests and when the view is down [100] the grouping of four guests in the centre of the cell can be seen. These guests form the channels which become clear when the packing and void spaces are mapped.

The packing of the **H2·2PIC** structure indicates the guests lie in zig-zag layers down [100]. These layers can be seen in Figure 3.14, which shows the view down [010]. The guests were once again removed and the voids were calculated with a probe radius of 1.2 Å and grid spacing of 0.7 Å. This showed the kinked layers and the resulting channels which formed down [100], as is seen in Figure 3.15. The voids make up 20.1 % of the total volume, with the total void volume within the unit cell being 1273.86 $Å^3$.

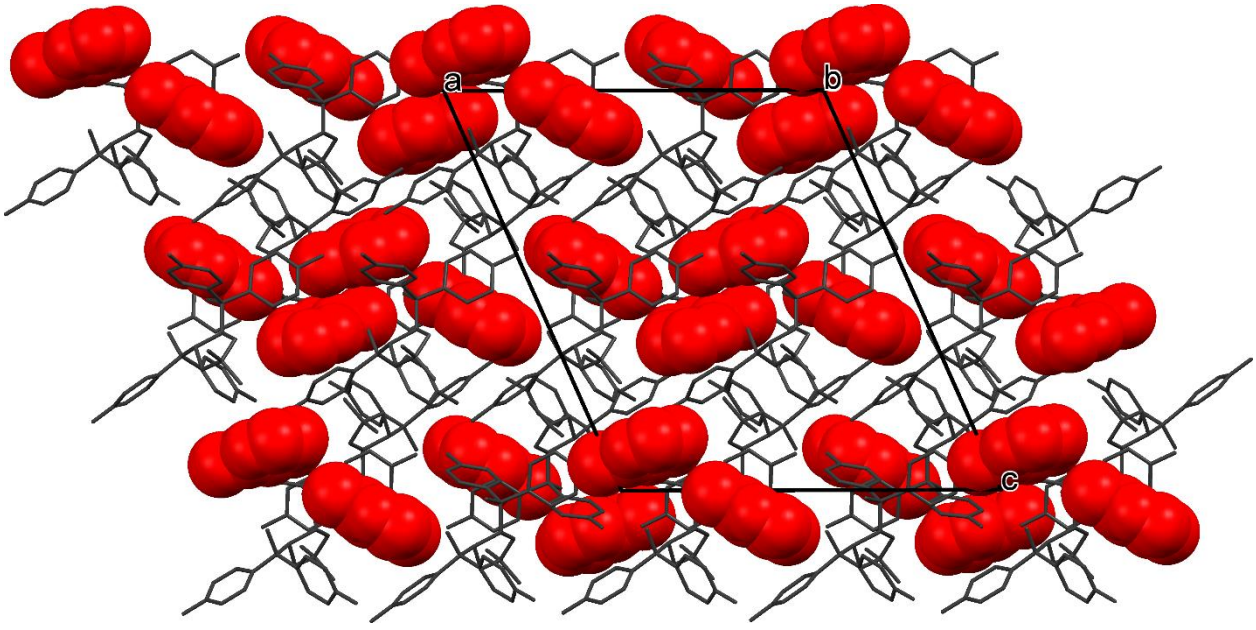

Figure 3.14: The packing of **H2·2PIC** with the layers along [100].

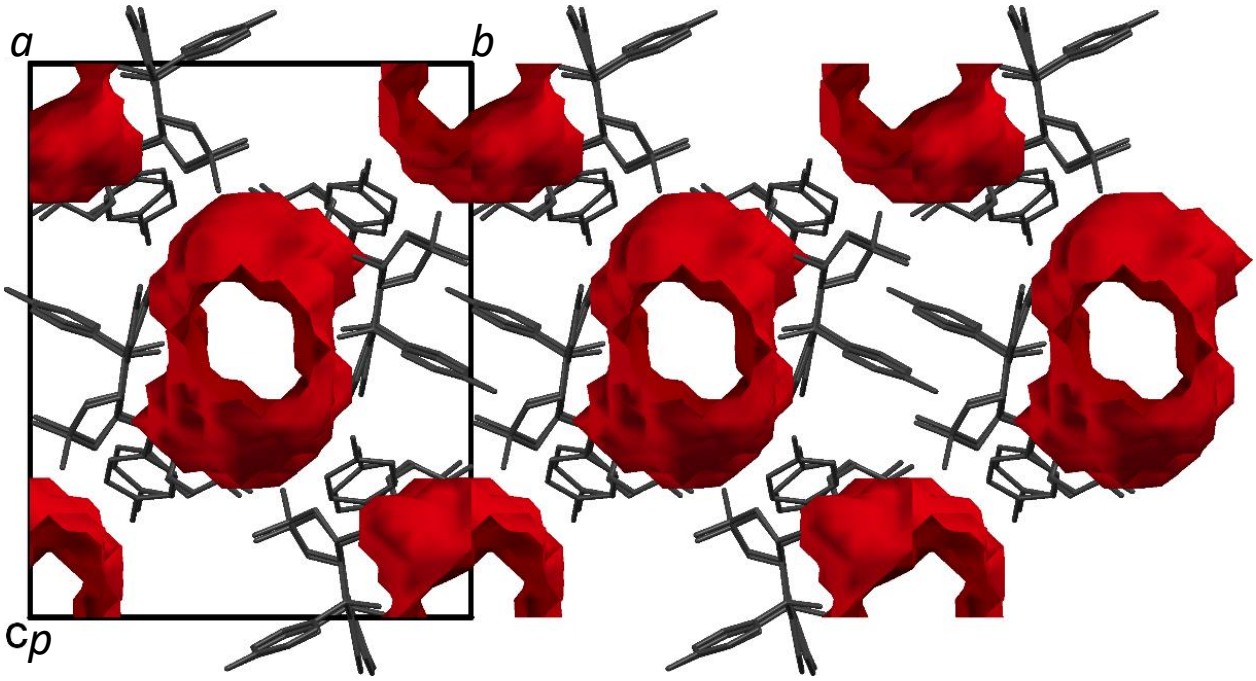

Figure 3.15: The channels present in **H2·2PIC** down [100].

3.6.2 Hirshfeld Surface Analysis

The non-bonded interactions of the **H2·2PIC** host-guest system were analysed using the programme CrystalExplorer. The Hirshfeld surface was generated around each the guest molecules, A and B, and points were mapped. A fingerprint plot was generated for each guest and the interactions catalogued. Since there are two unique guests in this system, this analysis will highlight the differences in intermolecular interactions that characterise the guests. The fingerprint plots and interaction breakdowns for the guests of **H2·2PIC** are shown in Figure 3.16.

The two guests are in relatively similar environments and, as before, the majority of interactions are H···H and C···H/H···C. The second guest has some further weaker interactions, which result in the fingerprint plot spreading out to the top right. The addition of the fluorine atoms on the para positions of the phenyl groups results in the addition of H···F interactions in this host-guest complex, which make up a significant percentage of the overall number of interactions. There are some minor C···F included in the 'other' component and they are more numerous in guest A.

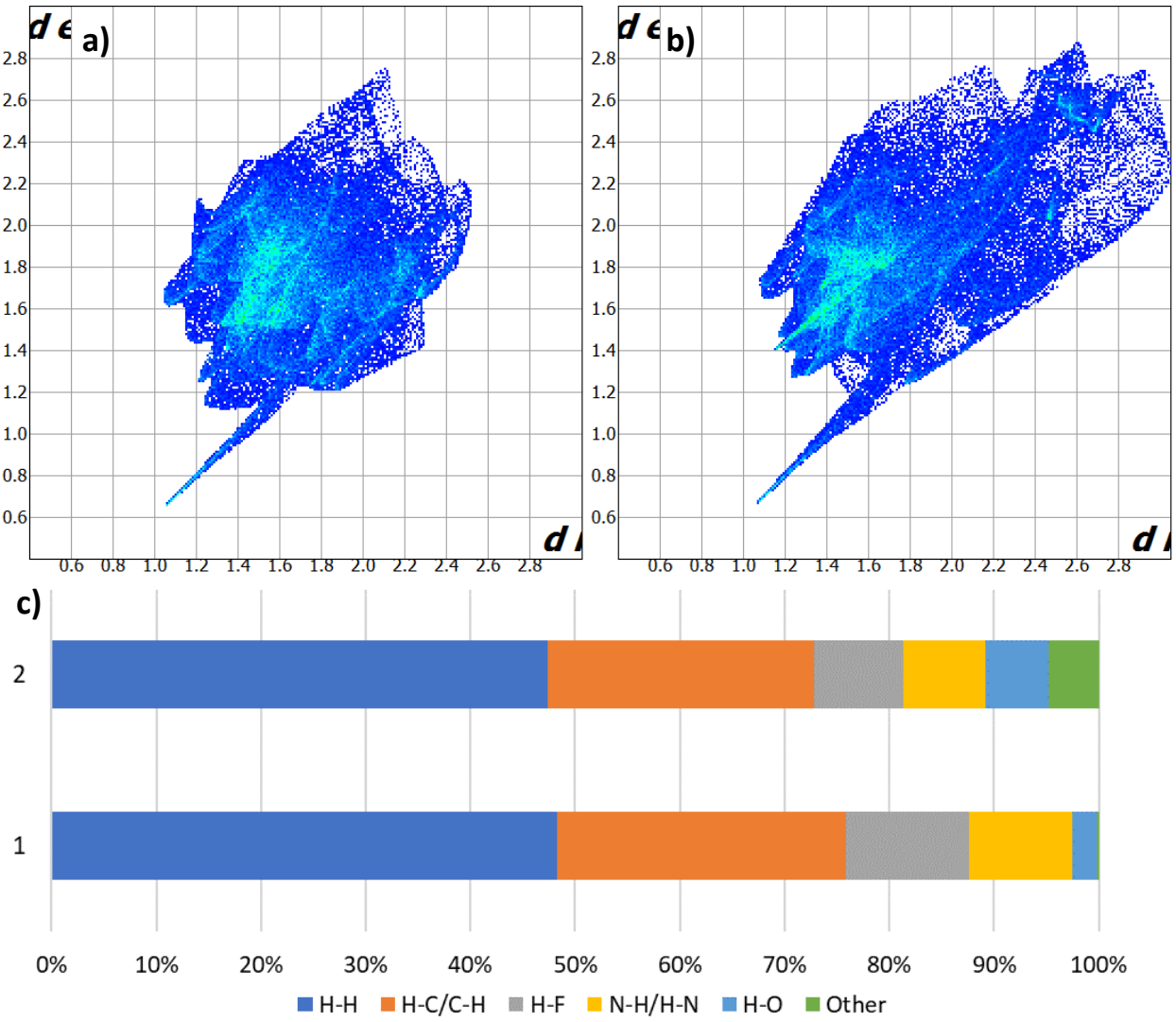

Figure 3.16: The Hirshfeld fingerprint plots for the two guests present in the asymmetric unit of **H2·2PIC** a) guest A b) guest B. c) shows the breakdown of the intermolecular interactions for each guest.

3.6.3 Intra- and Intermolecular Interactions

Each host:guest pair has a multitude of potential intra- and intermolecular interactions, due to the diversity of their substituents resulting in many possible contacts. The presence of two hosts and two guests also results in many more interactions than those present in the previously described structures. The PLATON programme was used to generate these interactions. The ubiquitous hydrogen bonds, which are characteristic of these complexes, are also present in **H2·2PIC** and are described in Table 3.15. The asymmetric unit contains two

hosts and two guests and, therefore, there are multiple centroids, five per host and one per guest, which have been included in Table 3.16.

The C-H·· π interactions shorter than 3.0 Å were calculated and included in Table 3.17. Table 3.18 lists the π··· π interactions shorter than 5.0 Å. Table 3.19 contains the intermolecular short contacts, which includes interactions whose intermolecular distances are less than the sum of the van der Waals radii given by Bondi. These include F···F, F···H, O···H, H···H, C···H and C···F. There is a F···F contact of 2.91 Å, which connects the two hosts within the asymmetric unit. Interestingly, all these short contacts involve Host A and there are no notable intermolecular short contacts between Host B and either of the guests (apart from the hydrogen bond connecting O5 of Host B to the N2 of Guest B).

Table 3.15: Hydrogen-bonding interactions in **H2·2PIC**.

Pair	Donor (D)	Acceptor (A)	D···A (Å)	D-H(Å)	H···A (Å)	<D-H···A (°)
A	O1	N1	2.664(2)	1.028(5)	1.651(6)	167(2)
	O4	O1	2.635(2)	0.983 (6)	1.651(8)	173(2)
B	O5	N2	2.640(2)	1.050(5)	1.664(14)	153(2)
	O8	O5	2.631(2)	0.986(5)	1.670(9)	164(2)

Table 3.16: The generated centroids for **H2·2PIC** and their corresponding atoms.

Centroid	Nature	Atom 1	Atom 2	Atom 3	Atom 4	Atom 5	Atom 6
Cg 1	Host A	O2	C2	C3	O3	C29	-
Cg 2	Host A	C5	C6	C7	C8	C9	C10
Cg 3	Host A	C11	C12	C13	C14	C15	C16
Cg 4	Host A	C17	C18	C19	C20	C21	C22
Cg 5	Host A	C23	C24	C25	C26	C27	C28
Cg 6	Host B	O6	C39	C40	O7	C66	-
Cg 7	Host B	C42	C43	C44	C45	C46	C47
Cg 8	Host B	C48	C49	C50	C51	C52	C53
Cg 9	Host B	C54	C55	C56	C57	C58	C59
Cg 10	Host B	C60	C61	C62	C63	C64	C65
Cg 11	Guest A	N1	C32	C33	C34	C35	C36
Cg 12	Guest B	N2	C69	C70	C71	C72	C73

Table 3.17: C-H···π interactions in **H2·2PIC**.

Nature	C(I)-H(J) ··· Cg(k)	Symmetry Operator	H···Cg (Å)	Angle (°)
Host A-Host B	C(31)-H(31A) ··· Cg(10)	1-x, 2-y, 1-z	2.97	177
Guest A-Host A	C(36)-H(36) ··· Cg(3)	x, y, z	2.86	134
Host B-Host A	C(67)-H(67C) ··· Cg(2)	1-x, 1-y, 1-z	2.97	171
Guest B-Host A	C(70)-H(70) ··· Cg(4)	$\frac{3}{2}$ – x, $\frac{1}{2}$ + y, $\frac{3}{2}$ -z	2.93	130

Table 3.18: π···π interactions in **H2·2PIC**.

Nature	Cg(I)-Cg(J)	Symmetry operator	Cg-Cg (Å)
Host A- Guest B	Cg(2)-Cg(12)	$\frac{3}{2}$+x, -$\frac{1}{2}$ +y, $\frac{3}{2}$-z	4.919(2)
Host A- Guest A	Cg(3)-Cg(11)	x, y, z	4.729(2)
Host A- Guest B	Cg(4)-Cg(12)	$\frac{3}{2}$+x, -$\frac{1}{2}$ +y, $\frac{3}{2}$-z	4.761(2)
Host B-Host B	Cg(7)-Cg(8)	x, y, z	4.772(2)
Host B- Host B	Cg(9)-Cg(7)	-$\frac{1}{2}$ +x, $\frac{3}{2}$-y, -$\frac{1}{2}$ +z	4.919(2)
Host B- Host B	Cg(10)-Cg(9)	x, y, z	4.840(2)
Guest B-Host A	Cg(12)-Cg(2)	$\frac{3}{2}$ -x, $\frac{1}{2}$ +y, $\frac{3}{2}$ -z	4.919(2)

Table 3.19: Summary of shortest intermolecular contacts in **H2·2PIC**.

Nature	Contact	C(I)-H(J) ··· Cg(k)	Symmetry Operator	Length (Å)
Host A - Guest A	H···C	H(1) ··· C(36)	x, y, z	2.49
Host A - Host A	F···H	F(4) ··· H(16)	1-x,2-y,1-z	2.46
Host A - Guest A	H···C	H(1) ··· C(32)	x, y, z	2.70
Host A - Host B	H···F	H(7) ··· F(7)	$\frac{1}{2}$+x, $\frac{3}{2}$ -y, $\frac{1}{2}$+z	2.52
Host A- Host B	O···H	O(3) ··· H(50)	$\frac{3}{2}$ -x, $\frac{1}{2}$ +y, $\frac{3}{2}$ -z	2.61
Host A - Host B	F···H	F(1) ··· H(56)	1+x, y, z	2.57
Host A - Guest B	C···H	C(22) ··· H(70)	$\frac{3}{2}$ -x, -$\frac{1}{2}$+y, $\frac{3}{2}$ -z	2.81
Host A - Host B	H···O	H(27) ··· O(6)	$\frac{3}{2}$ -x, $\frac{1}{2}$ +y, $\frac{3}{2}$ -z	2.65
Host A - Host B	C···F	C(7) ··· F(7)	$\frac{1}{2}$ +x, $\frac{3}{2}$ -y, -$\frac{1}{2}$ +z	3.13
Host A - Guest A	C···C	C(12) ··· C(36)	x, y, z	3.36
Host A - Host B	F···F	F(4) ··· F(8)	x, y, z	2.91
Host A - Guest B	F···H	F(3) ··· H(73)	$\frac{1}{2}$ +x, $\frac{3}{2}$ -y, -$\frac{1}{2}$ +z	2.65
Host A - Host B	H···C	H(31A) ··· C(63)	1-x, 2-y, 1- z	2.88
Host A - Guest B	C···H	C(17) ··· H(70)	$\frac{3}{2}$ -x, -$\frac{1}{2}$ +y, $\frac{3}{2}$ -z	2.89
Host A - Host B	H···H	H(21) ··· H(53)	$\frac{1}{2}$ +x, $\frac{3}{2}$ -y, -$\frac{1}{2}$ +z	2.39

3.6.4 Powder X-ray Diffraction Analysis

A PXRD trace was calculated from the single crystal data and was compared to the trace obtained experimentally. The powder was obtained by removing the crystals from solution, patting dry and lightly crushing. The experimental trace is a close match with the trace calculated from the single crystal and, therefore, the single crystal can be considered representative of the bulk sample. The traces are included in Figure 3.17.

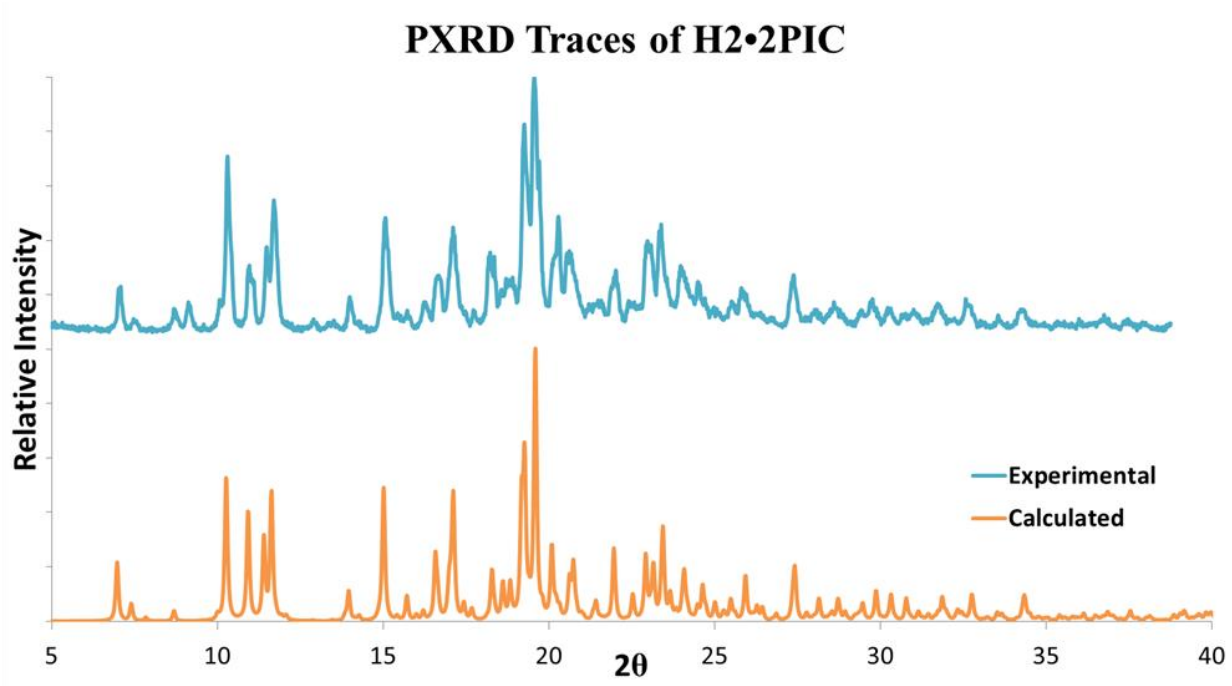

Figure 3.17: The PXRD traces for **H2·2PIC** with blue showing the experimental trace obtained for the crushed crystals and orange corresponding to the trace calculated from the data obtained from the single crystal.

3.7 Structural Analysis of H2·3PIC

3.7.1 Single Crystal X-ray Diffraction Analysis

A colourless block-shaped crystal, with dimensions of 0.15 x 0.16 x 0.23 mm^3, was selected for single crystal X-ray diffraction analysis. The data were collected on a Bruker DUO APEX II[2] diffractometer at -100 °C. **H2·3PIC** crystallises in the triclinic crystal system with the space group $P\bar{1}$.

The resulting structure was refined to R_1 = 0.0549 and wR_2 = 0.1349 and the asymmetric unit contains two **H2** molecules and two **3PIC** guests and the unit cell contains four of these units giving a Z = 4 with Z' =2. This shows a host:guest ratio of 2:2, which was subsequently confirmed using thermal analysis and ^{1}H NMR spectroscopic methods. The crystal data and refinement details are shown in Table 3.20.

Table 3.20: Crystal Data for **H2·3PIC**.

Compound	H2·3PIC
CCDC	1881571
Structural formula	$C_{37}H_{33}F_4NO_4$
Molecular mass (g·mol^{-1})	631.64
Data collection temp. (K)	173
Crystal system	Triclinic
Space group	$P\bar{1}$
a (Å)	12.534(3)
b (Å)	17.007(3)
c (Å)	17.088(3)
α(°)	118.73(3)
β(°)	92.96(3)
γ(°)	98.58(3)
Volume (Å^3)	3126.2(14)
Z/Z'	4/2
D calc density (g·cm^{-3})	1.342
θ range (°)	2.370-28.065
Reflections collected	26927
No. data I>2 σ (I)	15450
Final R Indices R_1, [I>2 σ (I)]	0.0550
Goodness-of-fit on F^2	0.997

As with **H2·2PIC**, **H2·3PIC** has an asymmetric unit containing two host and two guest molecules. One of the guests lies entrapped within a host dimer, and this is shown in Figure 3.18a. The phenyl rings of the hosts form a cage-like arrangement which encloses a guest. The second guest is not encased.

Figure 3.18b shows a view of the unit cell down [100] and the stacking of the guests in the lower left and upper right of the figure can be seen. The hydrogen atoms in Figure 18b have been omitted for clarity. These stacks of 3-picoline guests form the basis of the layers and channels which become apparent in Figures 3.19a and 3.19b. Figure 3.19a illustrates the layers of the guests along [100]; the guests are space filled and coloured yellow with hosts remaining grey and, once again, hydrogens have been omitted. The channels were mapped and are shown in Figure 3.19b. The guests were removed and the voids were calculated with a probe radius of 1.2 Å and grid spacing of 0.7 Å.

The structure also shows the host dimers forming a rectangular lattice around the guests. This results in slightly restricted channels running through the centre of the two hosts within each unit cell. Later, when the thermal analysis is outlined, it is possible to see the two steps of guest loss, which is due to the entrapment of one of the guests.

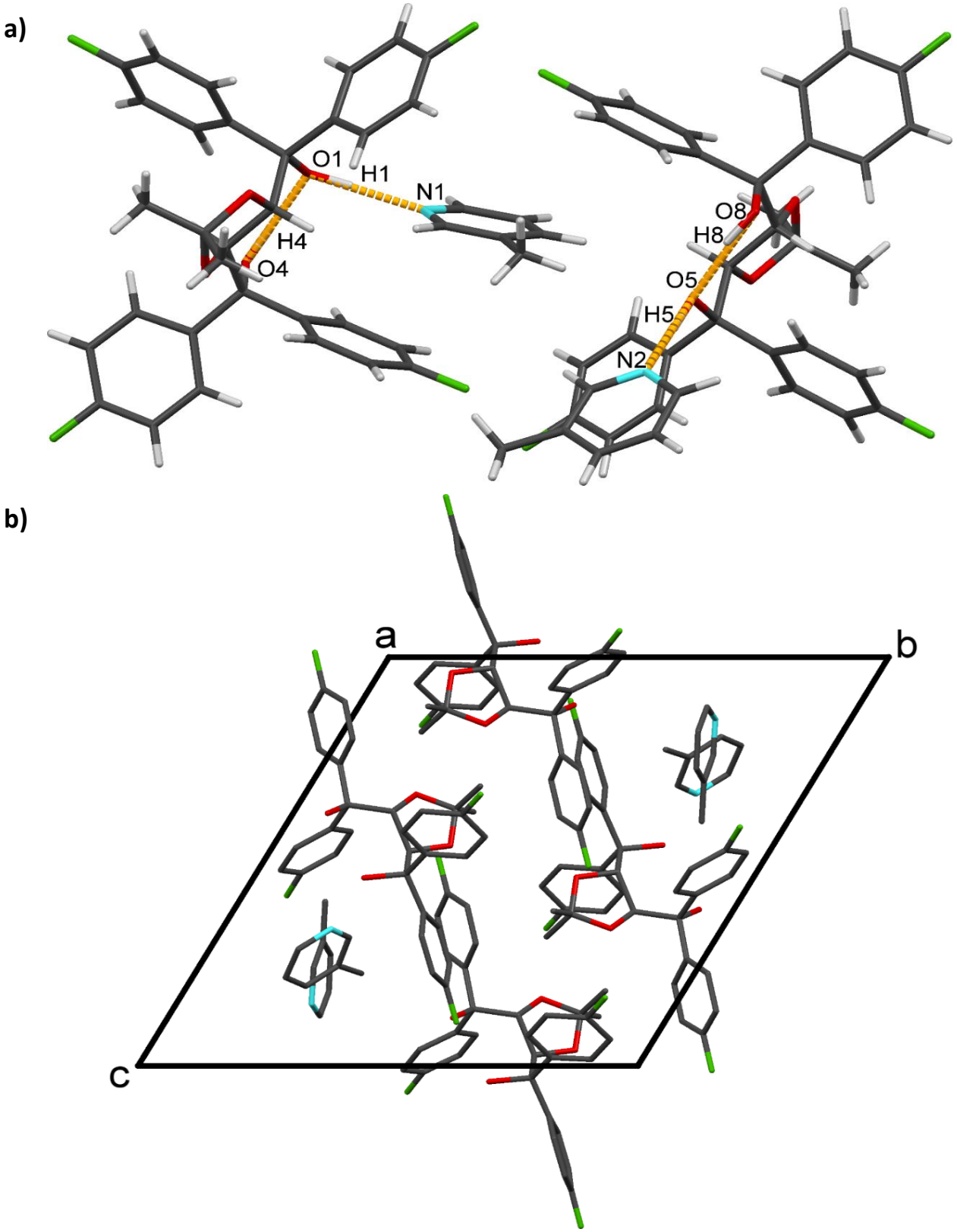

Figure 3.18: a) Asymmetric unit of **H2·3PIC** with one guest enclosed in the host dimer. The second guest is held loosely in the crystal lattice. The hydrogen bonds have been labelled. b) Shows the unit cell down [100] with Z= 4. Hydrogen atoms have been omitted for clarity in b.

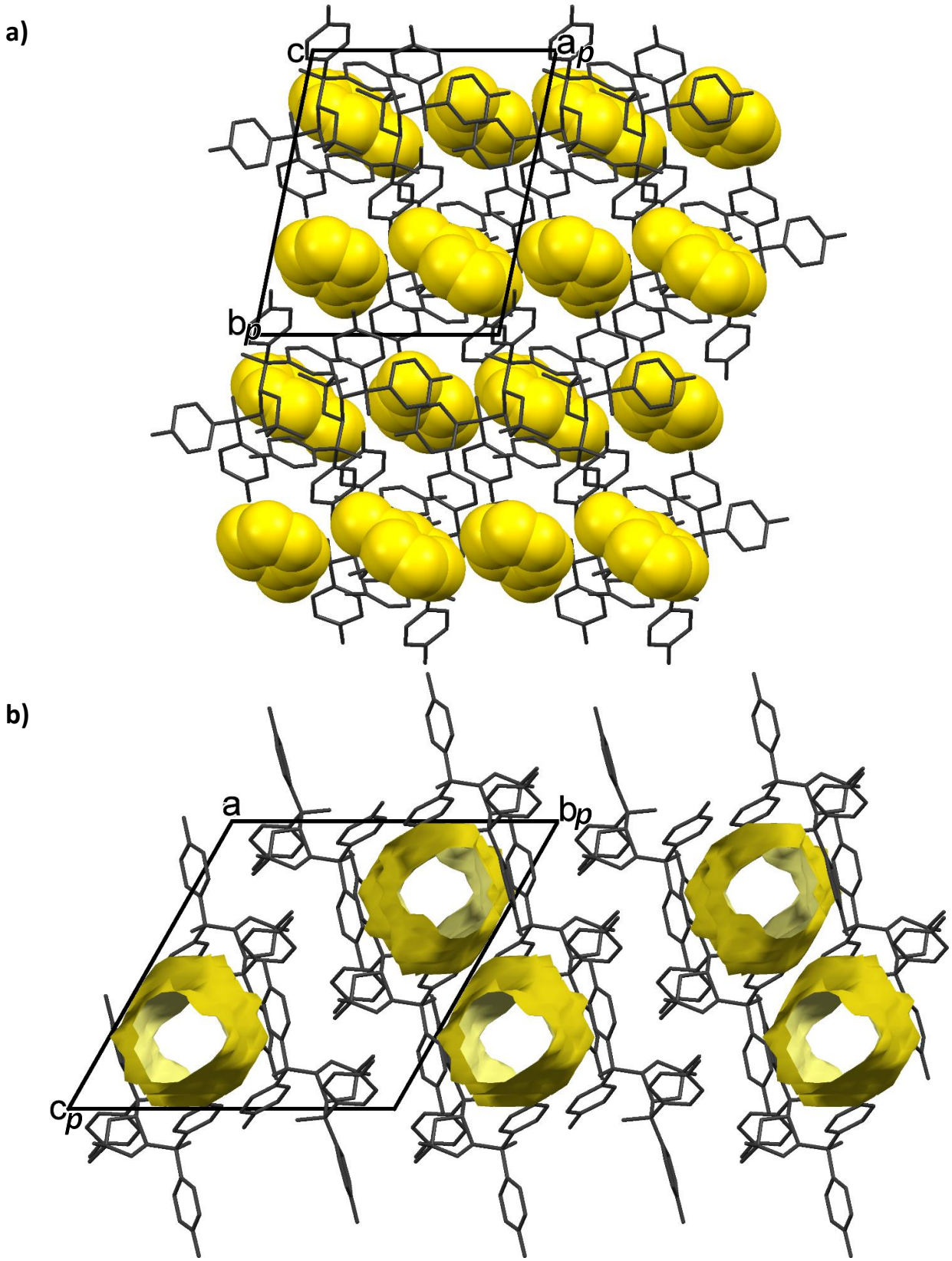

Figure 3.19: a) Packing of **H2·3PIC** showing the yellow space-filled guests. The view is down [001]. b) The channels down [100] are shown when the guests are removed. Hydrogen atoms are omitted for clarity.

3.7.2 Hirshfeld Surface Analysis

The non-bonded interactions of the **H2·3PIC** host-guest system were analysed using the program CrystalExplorer. The Hirshfeld surface was generated around the guest molecules and points were mapped. A fingerprint plot was generated for each guest and the interactions catalogued. Since there are two guests in this system, this analysis will highlight the differences in intermolecular interactions that characterise the guests. The fingerprint plots for the guests of **H2·3PIC** are shown in Figure 3.20.

Guest 2 is the guest which is held in the centre of the host dimer and there is a greater percentage of C-H/H-C bonds present in guest 2 than guest 1. Guest 1 contains a higher

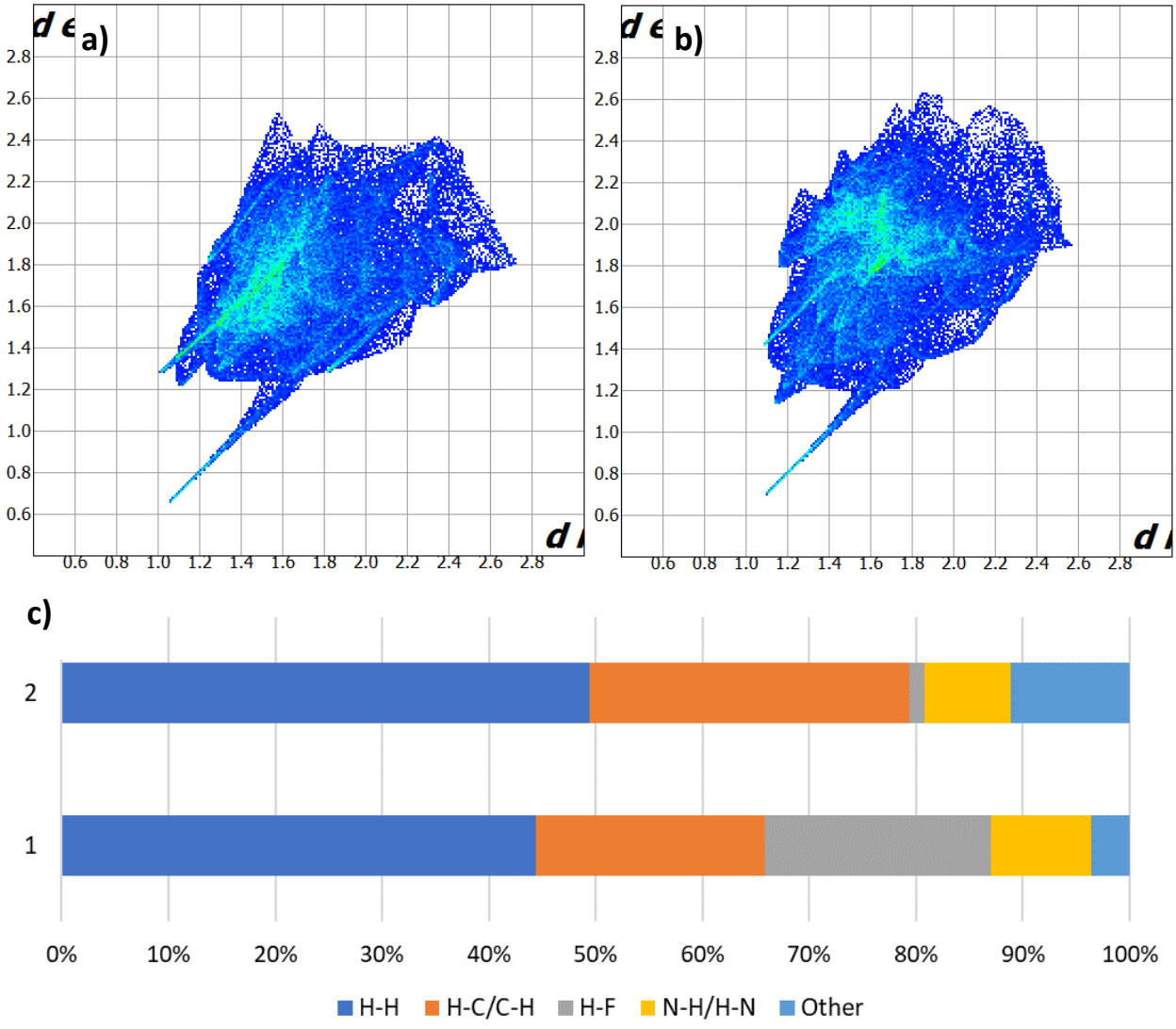

Figure 3.20: The Hirshfeld fingerprint plots of the two guests present in the asymmetric unit of **H2·3PIC** a) guest 1 b) guest 2. c) shows the breakdown of the intermolecular interactions for each guest.

percentage of H···F bonds, and this is consistent with the generated short contacts, which indicate that the guest outside of the host dimer experiences more H···F bonds than its entrapped counterpart. The entrapment may also explain why this guest has a greater majority of H···H and C···H/H···C interactions, as the location of the guest within the host dimer would promote these types of interactions.

3.7.3 Intra- and Intermolecular Interactions

This structure is consistent with those previously discussed, as it exhibits four hydrogen bonds, two per host:guest pair. The PLATON programme wa, once again, used to generate these interactions. The specifics of those bonds are captured in Table 3.21. There are two host and two guest molecules within the asymmetric unit, and the atoms comprising the generated centroids have been listed in Table 3.22. Cg 1 – Cg 10 refer to the two host molecules and Cg 11 and Cg 12 refer to the two guests. Note that guest 2 (Cg11) is the guest that is entrapped within the host dimer. Table 3.23 shows X-H···Cg (H···Cg < 3Å) and Y-X···Cg (X···Cg < 4Å) interactions of which there is only one of each. The first is an interaction between a guest CH and a phenyl ring of Host 2, and the second is a C···F interaction with the pyridyl ring of a guest. This is consistent with the position of Guest 2 within the dimer formed by the two hosts. Table 3.24 lists the strongest π··· π interactions present within the complex. Two of the shortest and, therefore, strongest are between Host 2 and Guest 2, with another interaction of similar strength between Host 1 and Host 2.

All of these interactions are within the asymmetric unit, aside from one interaction between Host B and Guest B. This may be a consequence of the dimerisation. Table 3.25 lists the short contacts present in **H2·3PIC**; these were included when the distance between the atoms was less than the sum of their respective van der Waals radii (outlined by Bondi). As with **H2·2PIC**, there is a diversity of interactions that include H···O, F···H, C···H, etc. Notably, all of these interactions involve Host 2, with the majority of interactions involving Host-Host interactions which is consistent with the host dimer present in the asymmetric unit.

Table 3.21: Hydrogen-bonding interactions in **H2·3PIC**.

Pair	Donor (D)	Acceptor (A)	D···A (Å)	D-H(Å)	H···A (Å)	<D-H···A (°)
1	O5	N2	2.675(3)	1.018(5)	1.665(7)	173(3)
	O8	O5	2.666(2)	0.977(5)	1.714(9)	164(2)
2	O1	N1	2.765(3)	0.972(5)	1.794(6)	177(3)
	O4	O1	2.705(2)	0.974(5)	1.758(9)	163(2)

Table 3.22: The generated centroids for **H2•3PIC** and their corresponding atoms.

Centroid	Nature	Atom 1	Atom 2	Atom 3	Atom 4	Atom 5	Atom 6
Cg 1	Host A	O2	C2	C3	O3	C29	-
Cg 2	Host A	C5	C6	C7	C8	C9	C10
Cg 3	Host A	C11	C12	C13	C14	C15	C16
Cg 4	Host A	C17	C18	C19	C20	C21	C22
Cg 5	Host A	C23	C24	C25	C26	C27	C28
Cg 6	Host B	O6	C39	C40	O7	C66	-
Cg 7	Host B	C42	C43	C44	C45	C46	C47
Cg 8	Host B	C48	C49	C50	C51	C52	C53
Cg 9	Host B	C54	C55	C56	C57	C58	C59
Cg 10	Host B	C60	C61	C62	C63	C64	C65
Cg 11	Guest A	N1	C32	C33	C34	C35	C36
Cg 12	Guest B	N2	C69	C70	C71	C72	C73

Table 3.23: Y-X···π interactions in **H2·3PIC**.

Nature	Y(I)-X(J) ··· Cg(k)	Symmetry Operator	X···Cg (Å)	Angle (°)
Guest A- Host A	C(35)-H(35) ··· Cg(4)	2-x, 2-y, 1-z	2.95	146
Host B- Guest A	C(57)-F(7) ··· Cg(11)	x, y, z	3.91	82.65

Table 3.24: π···π interactions in **H2·3PIC** less than 5 Å.

Nature	Cg(I)-Cg(J)	Symmetry operator	Cg-Cg (Å)
Host A- Guest A	Cg(3)-Cg(11)	x, y, z	4.451(2)
Host A- Host A	Cg(5)-Cg(4)	x, y, z	4.931(2)
Host A- Guest A	Cg(5)-Cg(11)	x, y, z	4.128(2)
Host B- Guest B	Cg(7)-Cg(12)	x, y, z	4.904(2)
Host B– Host B	Cg(9)-Cg(10)	x, y, z	4.871(2)
Host B- Host A	Cg(9)-Cg(11)	x, y, z	4.468(2)
Host B- Guest B	Cg(9)-Cg(12)	1-x, 1-y, -z	4.889(2)

Table 3.25: Summary of shortest intermolecular contacts in **H2·3PIC**.

Nature	Contact	Y(I)··· X(k)	Symmetry Operator	Length (Å)
Host A – Host B	H···O	H(31A) ··· O(7)	x, y, 1+z	2.68
Host A- Host B	H···F	H(18) ··· F(6)	1+x, y, 1+z	2.41
Host A- Host B	O···H	O(3) ··· C(67C)	x, y, 1+z	2.46
Host A- Host B	F···H	F(2) ··· H(61)	1+x, y, 1+z	2.46
Host A- Guest A	H···C	H(1) ··· C(32)	x, y, z	2.73
Host A- Host A	O···H	O(2) ··· H(9)	2-x, 1-y, 1-z	2.56
Host A- Guest A	C···H	C(16) ··· H(32)	x, y, z	2.75
Host A- Guest B	F···H	F(1) ··· H(73)	1-x, 1-y, -z	2.54
Host A- Guest A	H···C	H(1) ··· C(36)	x, y, z	2.77
Host A- Guest A	C···C	C(16) ··· C(32)	x, y, z	3.29
Host A- Guest B	O···H	O(1) ··· H(71)	1+x, y, z	2.68
Host A- Guest B	C···C	C(12) ··· C(71)	1+x, y, z	3.37
Host A- Host B	C···F	C(18) ··· F(6)	1+x, y, 1+z	3.14
Host A- Host B	H···F	H(6) ··· F(5)	2-x, 2-y, 1-z	2.65

3.7.4 Powder X-ray Diffraction Analysis

A PXRD trace was generated from the single crystal data and was compared to the trace obtained experimentally. The powder was obtained by removing the crystals from the mother liquor and lightly crushing to produce a uniform powder. The two traces were compared to ensure the single crystal was represented of the bulk sample. These traces are shown in Figure 3.21 and share many common peaks, which indicates that the single crystal used for data collection is representative of the bulk sample.

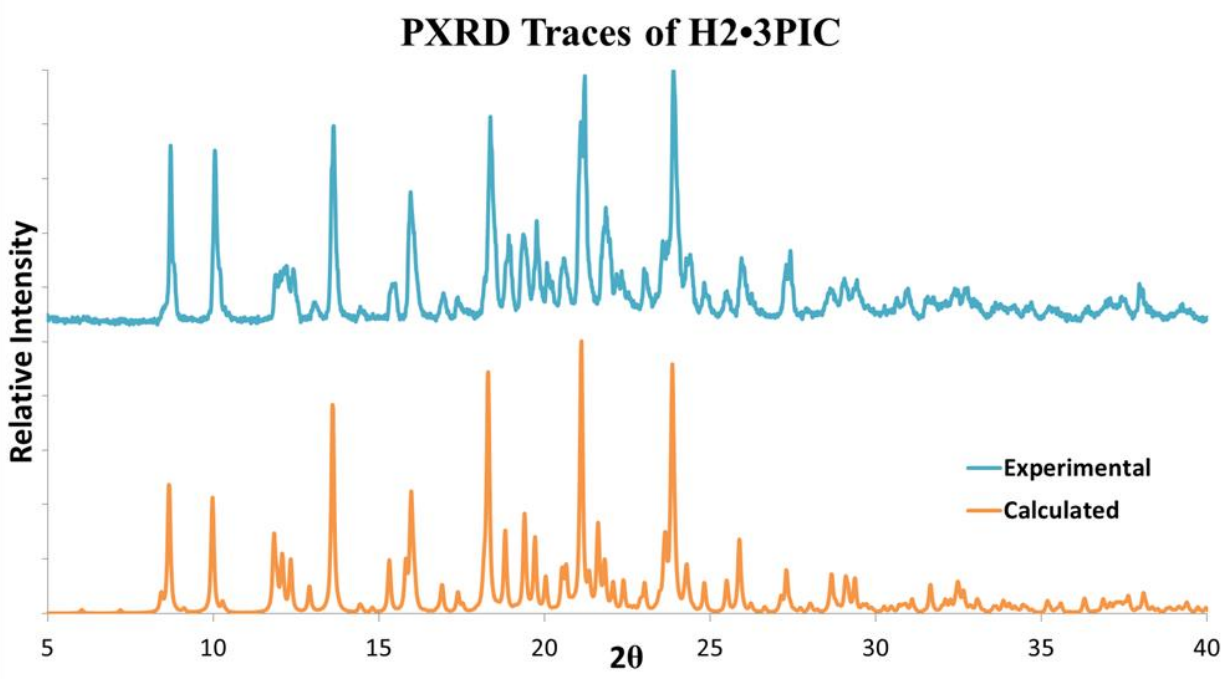

Figure 3.21: PXRD traces of **H2·3PIC** with the calculated (orange) trace obtained from the SXRD data and the experimental (blue) from the sample.

3.8 Structural Analysis of H2·4PIC

3.8.1 Single Crystal X-ray Diffraction Analysis

A colourless block-shaped crystal of dimensions 0.12 x 0.13 x 0.14 mm^3 was selected and subjected to single crystal X-ray diffraction analysis. The data were collected on a Bruker DUO APEX II^2 diffractometer at -100 °C. **H2·4PIC** crystallises in the monoclinic crystal system with the space group $P2_1/n$. The resulting structure was refined to R_1 = 0.0466 and wR_2 = 0.0967 and unlike **H2·2PIC** and **H2·3PIC** the host:guest ratio is 1:1 with one host and one guest molecule within the asymmetric unit. This was confirmed using thermal and ^1H NMR spectroscopic methods. The crystal data and refinement details are shown in Table 3.26.

Table 26: Crystal Data for **H2·4PIC**.

Compound	H2·4PIC
CCDC	1881575
Structural formula	$C_{37}H_{33}F_4NO_4$
Molecular mass (g·mol^{-1})	631.64
Data collection temp. (K)	173
Crystal system	Monoclinic
Space group	$P2_1/n$
a (Å)	9.882(2)
b (Å)	11.690(2)
c (Å)	27.481(6)
α(°)	90
β(°)	96.28(3)
γ(°)	90
Volume (Å^3)	3155.4(11)
Z/Z'	4/1
D calc density (g·cm^{-3})	1.330
θ range (°)	2.293-22.390
Reflections collected	41183
No. data I>2 σ (I)	7887
Final R Indices R_1, [I>2 σ (I)]	0.0466
Goodness-of-fit on F^2	1.010

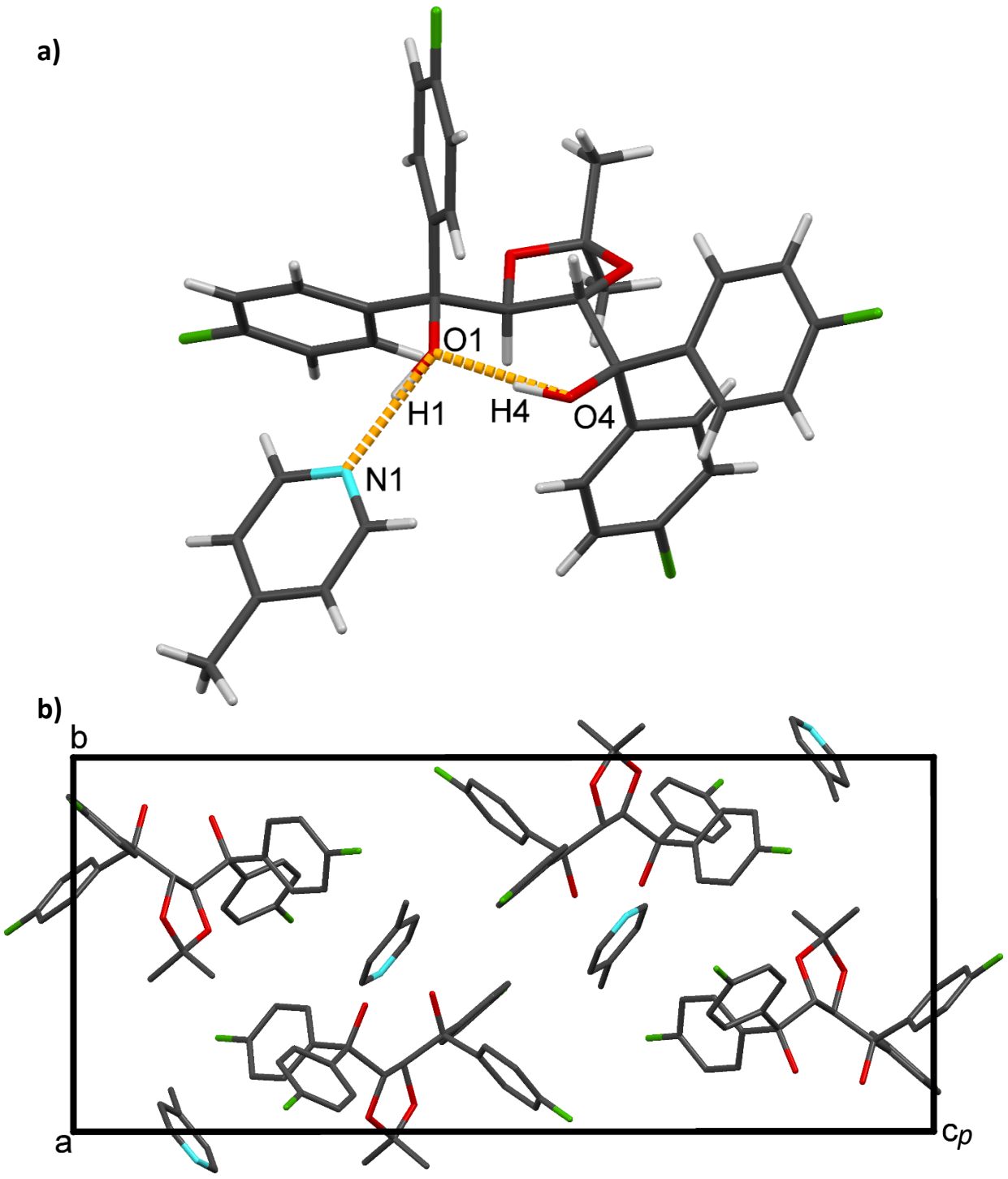

Figure 3.22: a) Asymmetric unit of **H2·4PIC** showing one host and one guest molecule connected with a hydrogen bond. b) The unit cell viewed down [100] of **H2·4PIC** including the four asymmetric units. Hydrogen atoms have been omitted for clarity.

H2·4PIC has the same 1:1 host:guest ratio present in **H1** and retains the intermolecular and intramolecular hydrogen bonds present in previous structures. The asymmetric unit is included in Figure 3.22a. The unit cell of **H2·4PIC** holds fours asymmetric units and shows two guests in the centre of cell with two on the edges. Figure 3.22b shows a view of the unit cell down [100] and the four guests are clearly visible. In Figure 3.23 the guests have been space-filled and coloured purple. The guests have a herringbone type pattern, where two guests are angled to the left and then another pair angled to the right. These guest pairs are arranged with the methyl group alternating, where one guest in the pair will have the methyl pointing one direction along [010], and the other guest with have it pointing in the opposite direction along [010]. This pattern is shown in Figure 3.23 with a view down [100].

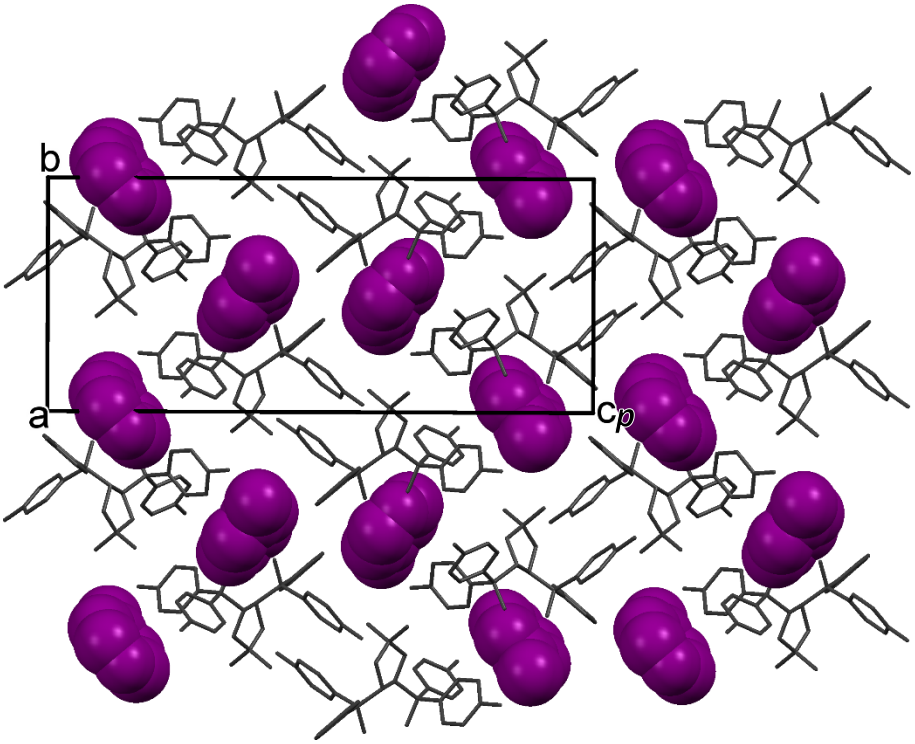

Figure 3.23: The packing of **H2·4PIC** showing the alternating herringbone pattern layers. View is down [100]. Hydrogen atoms have been omitted for clarity.

In Figure 3.24 the guests were removed and the voids were calculated with a probe radius of 1.2 Å and grid spacing of 0.7 Å. What is notable is the fact that the 4-picoline guests are enclosed in cavities. This is in contrast to the previous **H2** structures which displayed channels. Figure 3.24 shows the cavities and also highlights the alternating orientations of the methyl group in the 4-picoline guests.

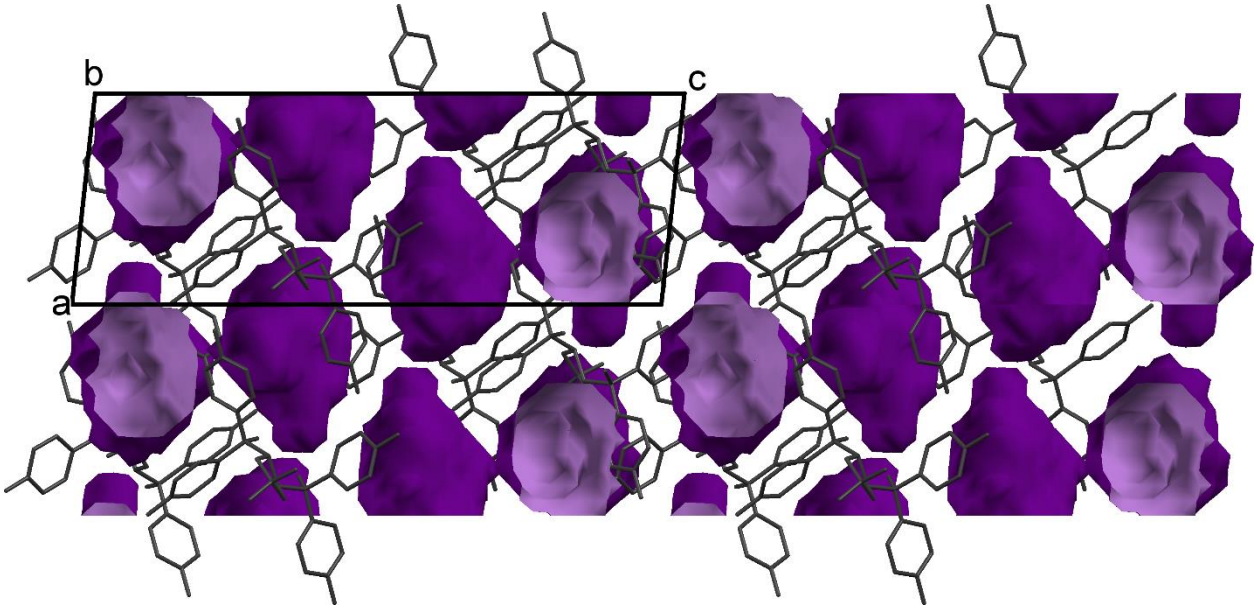

Figure 3.24: The void spaces of **H2·4PIC** showing the cavities in which the guests reside. Each guest is enclosed in a single cavity. Hydrogen atoms have been omitted for clarity.

3.8.2 Hirshfeld Surface Analysis

The non-bonded interactions of the **H2·4PIC** host-guest system were analysed using the programme CrystalExplorer. The Hirshfeld surface was generated around the guest molecule and points were mapped. A fingerprint plot was generated for the guest and the interactions catalogued. There was only one guest present in this host:guest system and the fingerprint for 4-picoline guest is shown below in Figure 3.25a. The interactions are summarised in Figure 3.25b, which shows the percentage composition of the intermolecular interactions.

As expected, the majority of interactions are H···H and C···H/H···C in nature. There are also significant N-H and H-F interactions, which are present in approximately the same quantity. Weaker interactions are grouped and make up approximately 8% of all interactions with the remainder being C···C.

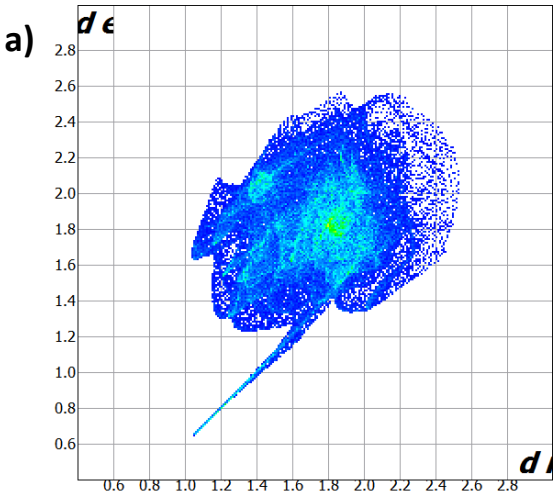

Figure 3.25: a) The Hirshfeld surface fingerprint plot of **H2·4PIC** showing the sharp peak of the hydrogen bond.

b) The breakdown of host- guest interactions present in the Hirshfeld fingerprint. Namely, H-H, H-C/C-H, H-F, C-C and other smaller interactions.

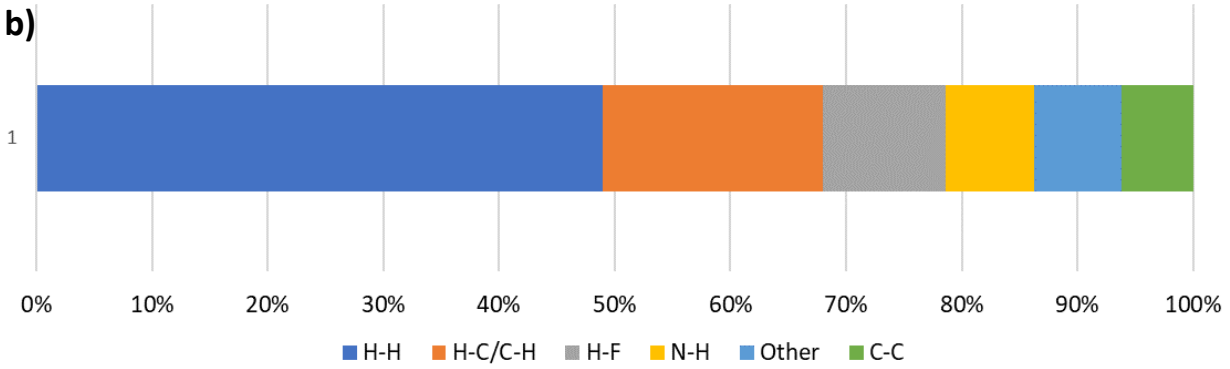

3.8.3 Intra- and Intermolecular Interactions

The classic hydrogen bonds, one intermolecular and one intramolecular, are noted in Table 3.27. The PLATON programme was used to generate further intermolecular interactions and, since the asymmetric unit contains only one host:guest pair, there are only six centroids. These centroids and their constituent atoms are listed in Table 3.28. The first five correspond to the host molecule with the final one being the 4-picoline guest. Table 3.29 includes X-H···Cg (H···Cg < 3 Å) and Y-X···Cg (X···Cg < 4 Å) interactions. The only two C-H···Cg are inter-host and there is a single C-F···Cg interaction, which lies within the asymmetric unit between host and guest. All notable π··· π interactions are between host and guest with multiple symmetry operators and are noted in Table 3.30.

Table 3.31 lists the short contacts present in **H2·4PIC**. These were included when the distance between the atoms was less than the sum of their respective van der Waals radii (outlined by Bondi). As with the previous **H2** structures, there is a diversity of interactions that include H···O, F···H, C···H etc. There is a mixture of host-host and host-guest interactions, including two H···C interactions which run from **H2** to the two carbon atoms on either side of the nitrogen atom on the 4-picoline guest. One of the host phenyl rings has two interactions with two of the guest hydrogen atoms, which also contributes to the stabilisation of the asymmetric unit. There are also multiple fluorine interactions that are host-host in nature.

Table 3.27: Hydrogen-bonding interactions in **H2·4PIC**.

Donor (D)	Acceptor (A)	D···A (Å)	D-H(Å)	H···A (Å)	<D-H···A (°)
O1	N1	2.765(3)	0.972(5)	1.794(6)	177(3)
O4	O1	2.705(2)	0.974(5)	1.758(9)	163(2)

Table 3.28: The centroids generated for **H2·4PIC** and their corresponding atoms.

Centroid	Nature	Atom 1	Atom 2	Atom 3	Atom 4	Atom 5	Atom 6
Cg 1	Host	O2	C2	C3	O3	C29	-
Cg 2	Host	C5	C6	C7	C8	C9	C10
Cg 3	Host	C11	C12	C13	C14	C15	C16
Cg 4	Host	C17	C18	C19	C20	C21	C22
Cg 5	Host	C23	C24	C25	C26	C27	C28
Cg 6	Guest	N1	C32	C33	C34	C35	C36

Table 3.29: Y-X···π interactions in **H2·4PIC**.

Nature	Y(I)-X(J) ··· Cg(k)	Symmetry Operator	X···Cg (Å)	Angle (°)
Host- Host	C(31)-H(31A) ··· Cg(3)	$\frac{3}{2}$-x, -$\frac{1}{2}$+y, $\frac{1}{2}$ -z	2.80	163
Host- Host	C(36)-H(36) ··· Cg(2)	x, y, z	2.71	146
Host- Guest	C(8)-F(1) ··· Cg(6)	$\frac{1}{2}$-x, -$\frac{1}{2}$+y, $\frac{1}{2}$ -z	3.50	94.82

Table 3.30: π···π interactions in **H2·4PIC** less than 5 Å.

Nature	Cg(I)-Cg(J)	Symmetry operator	Cg-Cg (Å)
Host- Guest	Cg(2)-Cg(6)	x, y, z	4.778(2)
Host- Guest	Cg(2)-Cg(6)	$\frac{1}{2}$ -x, -$\frac{1}{2}$+y, $\frac{1}{2}$ -z	4.606(2)
Host- Guest	Cg(5)-Cg(6)	1+x, y, z	3.691(2)

Table 3.31: Summary of shortest intermolecular contacts in **H2·4PIC**.

Nature	Contact	C(I)-H(J) ··· Cg(k)	Symmetry Operator	Length (Å)
Host- Guest	H···C	H(1) ··· C(32)	x, y, z	2.56
Host- Guest	H···C	H(1) ··· C(36)	x, y, z	2.63
Host- Host	F···H	F(3) ··· H(6)	1-x, -y, 1-z	2.49
Host- Host	O···H	O(3) ··· H(21)	2-x, -y, 1-z	2.54
Host- Host	F···H	F(4) ··· H(19)	1+x, y, z	2.53
Host- Host	O···H	O(4) ··· H(25)	2-x, 1-y, 1-z	2.59
Host- Guest	C···H	C(9) ···H(36)	x, y, z	2.77
Host- Guest	C···H	C(10) ··· H(36)	x, y, z	2.79
Host- Host	F···C	F(1) ··· C(15)	1+x, y, z	3.1
Host- Host	F···C	F(1) ··· C(14)	1+x, y, z	3.11
Host- Host	F···C	F(4) ··· C(19)	1+x, y, z	3.14

3.8.4 Powder X-ray Diffraction Analysis

A PXRD trace was generated from the single crystal data and was compared to the trace obtained experimentally. The two traces were compared to ensure the single crystal data was representative of the bulk sample. This was also done to ensure the integrity of the thermal and NMR analyses. These traces are shown in Figure 3.26 and share many common peaks, which indicates that the single crystal used for data collection is representative.

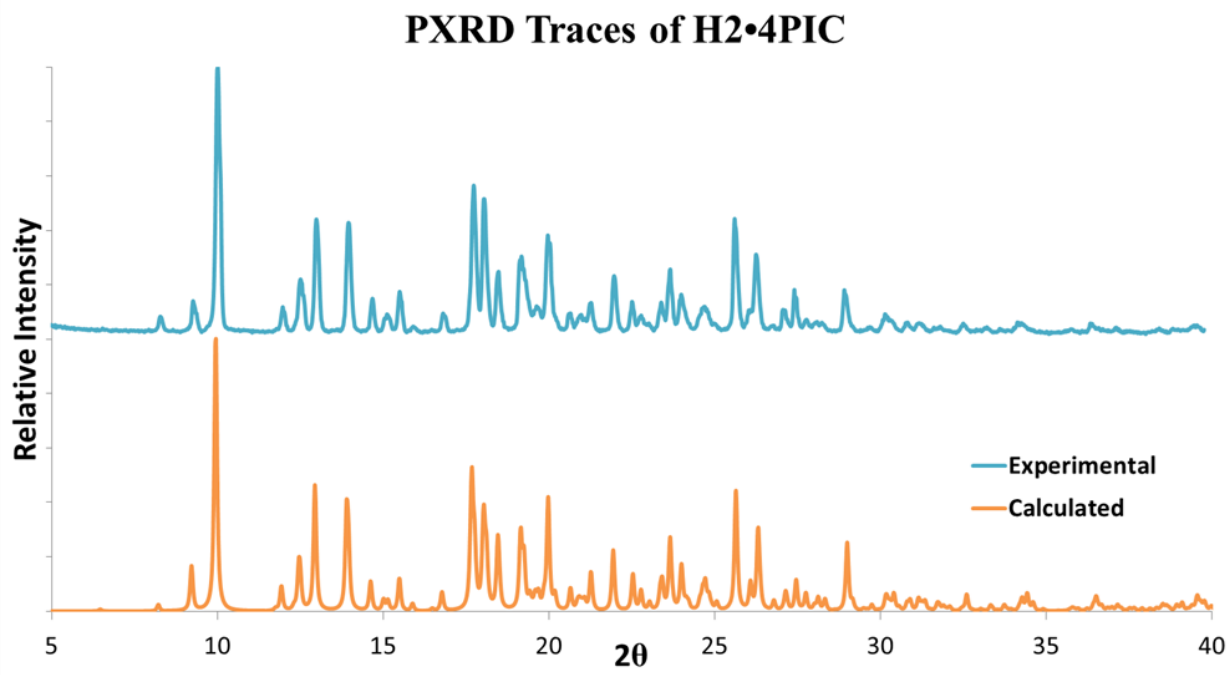

Figure 3.26: Calculated (orange) and experimental (blue) PXRD traces for **H2·4PIC**.

3.9 Structural Analysis of H2·PYR

3. 9.1 Single Crystal X-ray Diffraction Analysis

A colourless block-shaped crystal, with dimensions of 0.29 x 0.38 x 0.43 mm^3, was selected for single crystal X-ray diffraction analysis. The data were collected on a Bruker DUO APEX II^2 diffractometer at -100 °C. **H2·PYR** crystallises in the triclinic crystal system with the space group $P\bar{1}$.

The resulting structure was refined to R_1 = 0.0482 and wR_2 = 0.1231 with the asymmetric unit containing one host and one guest molecule. There are two of these units within the unit cell. This shows a host:guest ratio of 1:1, which was subsequently confirmed using thermal and ^1H NMR spectroscopic methods. The crystal data and refinement details are shown in Table 3.32.

The asymmetric unit contains one host and one guest and is shown in Figure 3.27. The ubiquitous intermolecular and intramolecular hydrogen bonds are, once again, present in **H2·PYR**. The unit cell contains two asymmetric units with the two guests stacked at a similar angle in the centre of the unit cell. This is shown in Figure 3.28a. This positioning of the two

Table 32: Crystal Data for **H2·PYR**.

Compound	H2·PYR
CCDC	1881569
Structural formula	$C_{36}H_{31}F_4NO_4$
Molecular mass ($g \cdot mol^{-1}$)	617.62
Data collection temp. (K)	173
Crystal system	Triclinic
Space group	$P\bar{1}$
a (Å)	9.751(2)
b (Å)	9.754(2)
c (Å)	18.339(4)
α(°)	88.32(3)
β(°)	74.76(3)
γ(°)	63.78(3)
Volume ($Å^3$)	1502.1(7)
Z/Z'	2/1
D calc density ($g \cdot cm^{-3}$)	1.365
θ range (°)	2.3235-31.955
Reflections collected	32995
No. data I>2 σ (I)	10448
Final R Indices R_1, [I>2 σ (I)]	0.0482
Goodness-of-fit on F^2	1.030

guests results in layers of guests. In Figure 3.28b, the guests have been coloured green and depicted in the space-filled style in order to show the layers from the view down [010].

These layers form the basis of the channels, which run along [100] and are generated when the guests have been removed and the void spaces mapped. The voids were generated with a probe radius of 1.2 Å and grid spacing of 0.7 Å. The channels are visible when looking down [100] and the host molecules form a rectangular lattice surrounding the guest channels. This is illustrated in Figure 3.29.

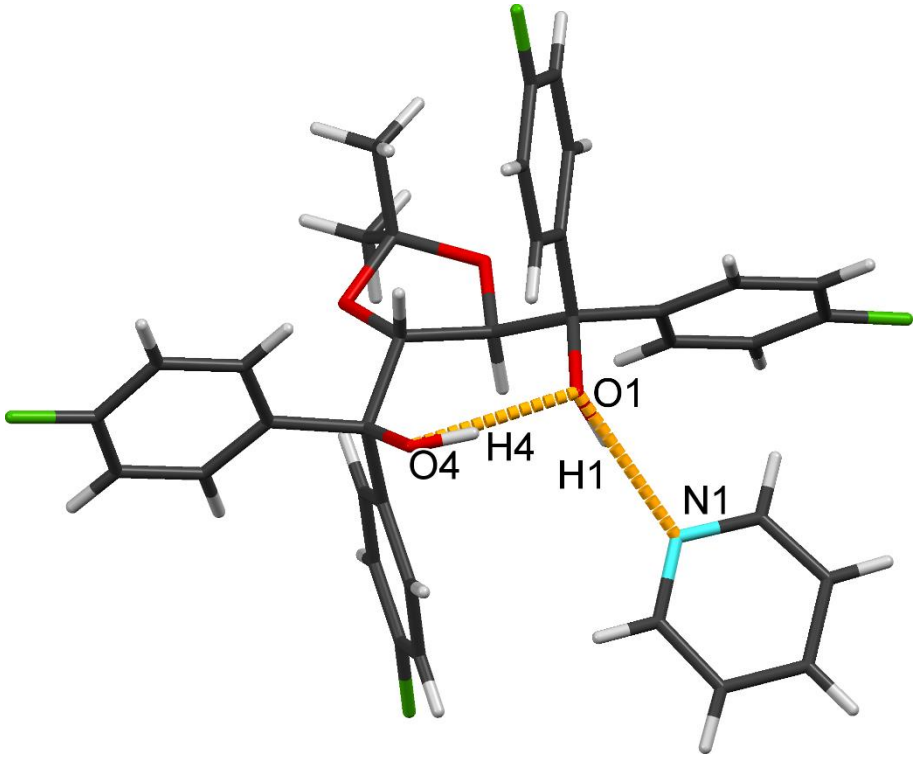

Figure 3.27: The asymmetric unit of **H2·PYR** showing the hydrogen bonds in orange along with the 1:1 host:guest ratio.

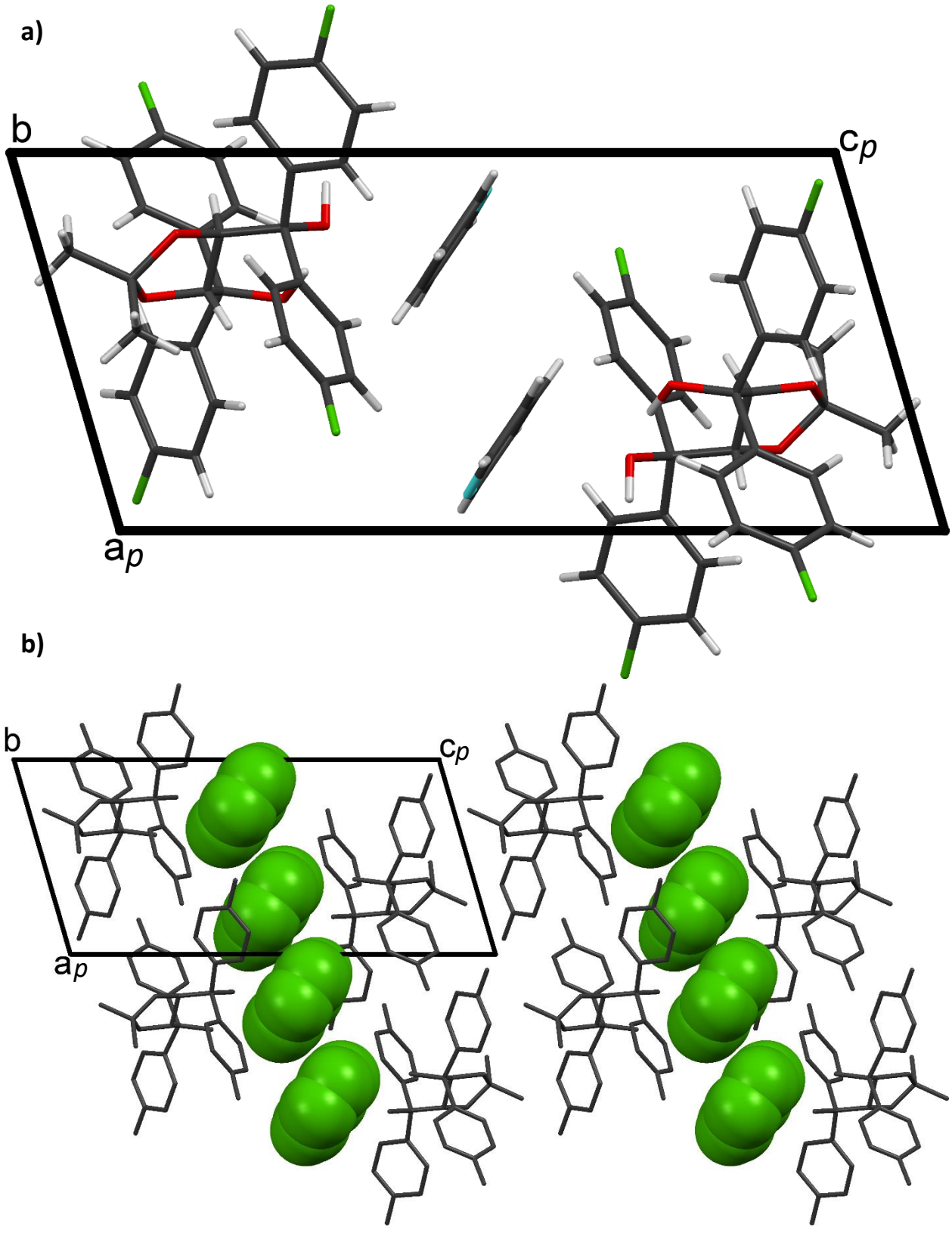

Figure 3.28: a) The unit cell of **H2·PYR** showing the position of the guests in the centre at a similar angle. b) The packing diagram with the guests in green showing the uniform layers. The view shown in this diagram is down [010] and hydrogen atoms have been omitted.

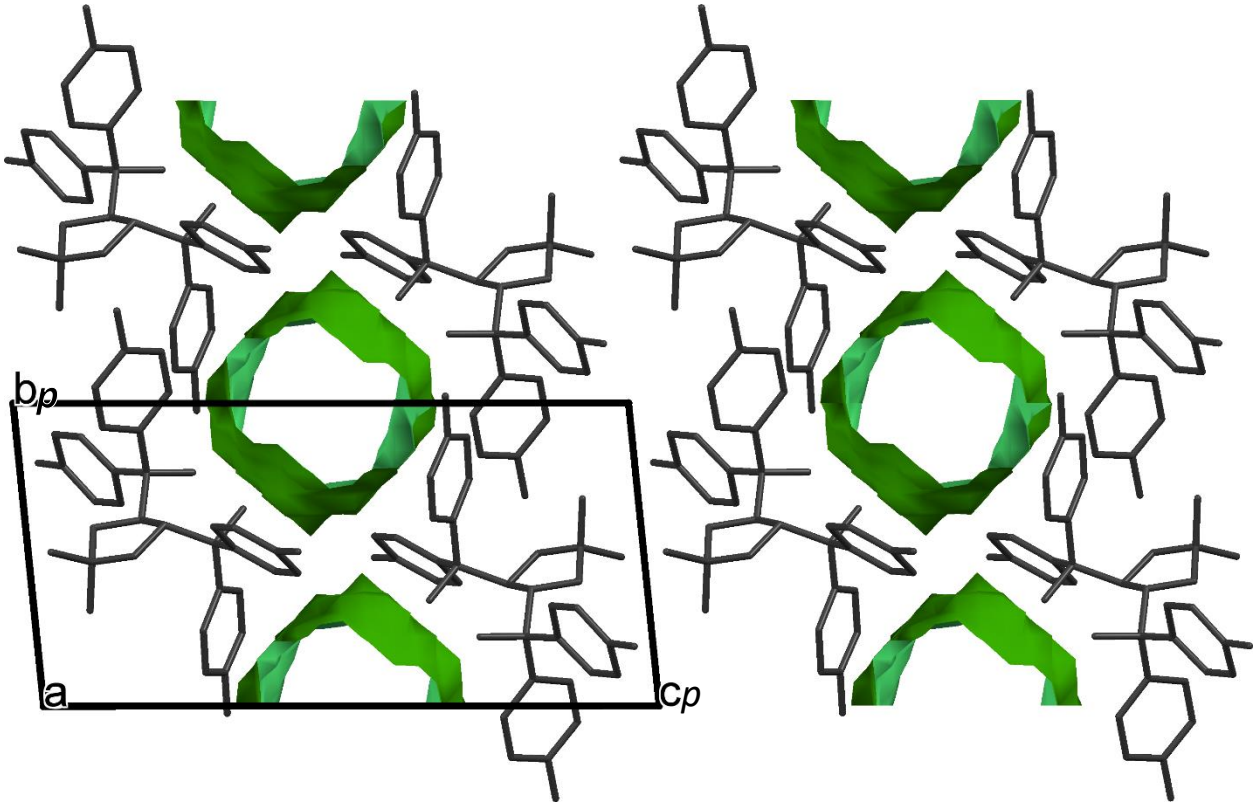

Figure 3.29: The guest channels present in **H2·PYR** once the guests have been removed. These channels run down [100] and hydrogen atoms have been omitted for clarity.

3.9.2 Hirshfeld Surface Analysis

The non-bonded interactions of the **H2·PYR** host-guest system were analysed using the programme CrystalExplorer. The Hirshfeld surface was generated around the guest molecule and points were mapped. A fingerprint plot was generated for the guest and the interactions catalogued. There is only one unique guest present in this host:guest system and the fingerprint for the pyridine guest is shown below in Figure 3.30a. The interactions are summarised in Figure 3.30b which shows the breakdown of the interactions present on the Hirshfeld surface.

The majority of interactions in this host:guest complex are H-H and C-H/H-C in nature. There are also significant N-H and H-F interactions, which are present in approximately the same quantity. Weaker interactions are grouped together and make up around 8% of the total interactions.

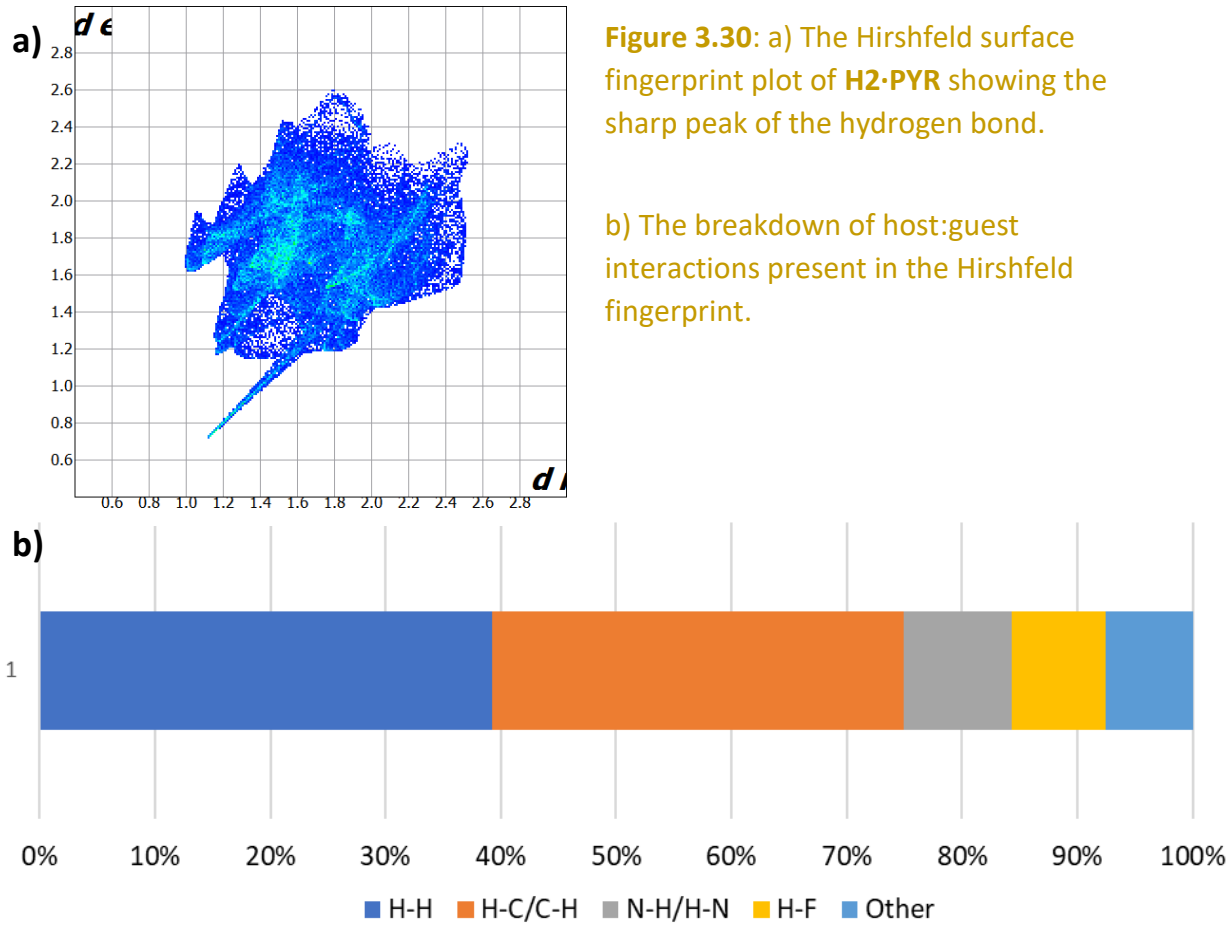

Figure 3.30: a) The Hirshfeld surface fingerprint plot of **H2·PYR** showing the sharp peak of the hydrogen bond.

b) The breakdown of host:guest interactions present in the Hirshfeld fingerprint.

3.9.3 Intra- and Intermolecular Interactions

As with the previous structures, **H2·PYR** displays two hydrogen bonds; their metrics are listed in Table 3.33. The programme PLATON was, once again, used to generate further intermolecular interactions and, like **H2·4PIC**, this structure contains one host and one guest within the asymmetric unit. These centroids and their constiuent atoms are listed in Table 3.34. The first five correspond to the host molecule, with the final one being the pyridine guest. Table 3.35 includes X-H···Cg (H···Cg < 3 Å) and Y-X···Cg (X···Cg < 4 Å) interactions. There are three C-H···Cg interactions, two of which are host:guest. There are two C-F···Cg interactions which both involve C14-F2. π··· π interactions have been listed in Table 3.36 and notably one of the interactions is inter-guest. This is the interaction which can be seen in the unit cell with the stacking of the pyridine guests.

Table 3.37 lists the short contacts present in **H2·PYR**; these were included when the distance between the atoms was less than the sum of their respective van der Waals radii (outlined by Bondi). There are numerous host-guest interactions, which contribute to stabilisation of the host-guest complex. There is also a F-F interaction involving F1 of one host interacting with F1 of a second host outside of the asymmetric unit.

Table 3.33: Hydrogen-bonding interactions in **H2·PYR**.

Donor (D)	Acceptor (A)	D···A (Å)	D-H(Å)	H···A (Å)	<D-H···A (°)
O1	N1	2.758(7)	0.971(5)	1.834(9)	158(2)
O4	O1	2.710(2)	0.970(5)	1.757(7)	167(2)

Table 3.34: The centroids generated for **H2·PYR** and their corresponding atoms.

Centroid	Nature	Atom 1	Atom 2	Atom 3	Atom 4	Atom 5	Atom 6
Cg 1	Host	O2	C2	C3	O3	C29	-
Cg 2	Host	C5	C6	C7	C8	C9	C10
Cg 3	Host	C11	C12	C13	C14	C15	C16
Cg 4	Host	C17	C18	C19	C20	C21	C22
Cg 5	Host	C23	C24	C25	C26	C27	C28
Cg 6	Guest	N1	C32	C33	C34	C35	C36

Table 3.35: C-X···π interactions in **H2·PYR**.

Nature	C(I)-X(J) ··· Cg(k)	Symmetry Operator	X···Cg (Å)	Angle (°)
Host- Host	C(21)-H(21) ··· Cg(2)	x, 1+y, z	2.73	165
Guest- Host	C(35)-H(35) ··· Cg(3)	-x, 1-y, 1-z	2.88	145
Guest- Host	C(36)-H(36) ··· Cg(2)	x, y, z	2.50	151
Host- Host	C(14)-F(2) ··· Cg(4)	1+x, -1+y, z	3.70	105
Host- Guest	C(14)-F(2) ··· Cg(6)	1+x, -1+y, z	3.69	103

Table 3.36: π···π interactions in **H2·PYR** less than 5 Å.

Nature	Cg(I)-Cg(J)	Symmetry operator	Cg-Cg (Å)
Host-Guest	Cg(2)-Cg(6)	x, y, z	4.626(2)
Host-Guest	Cg(3)-Cg(6)	-x, 1-y,1-z	4.966(2)
Host-Host	Cg(4)-Cg(5)	x, y, z	4.807(2)
Guest-Guest	Cg(6)-Cg(6)	-x, 2-y, 1-z	4.660(2)

Table 3.37: Summary of shortest intermolecular contacts in **H2·PYR**.

Nature	Contact	C(I)-H(J) ··· Cg(k)	Symmetry Operator	Length (Å)
Host-Host	F···H	F(4) ··· H(30A)	1+x, y, z	2.44
Host-Guest	H···C	H(1) ··· C(36)	x, y, z	2.66
Host-Host	F···H	F(3) ··· H(24)	1+x, 1+y, z	2.49
Host-Guest	C···H	C(9) ··· H(36)	x, y, z	2.73
Host-Guest	C···H	C(10) ··· H(36)	x, y, z	2.73
Host-Host	O···H	O(3) ··· H(30C)	1-x, 1-y, -z	2.59
Host-Host	F···F	F(1) ···F(1)	1-x,1-y, 1-z	2.85
Host-Guest	C···H	C(14) ··· H(35)	-x, 1-y, 1-z	2.83
Host-Host	F···H	F(1) ··· H(16)	1+x, y, z	2.61
Host-Guest	C···H	C(8) ··· H(36)	x, y, z	2.84
Host-Guest	C···H	C(5) ··· H(36)	x, y, z	2.86
Host-Guest	H···C	H(1) ··· C(32)	x, y, z	2.86

3.9.4 Powder X-ray Diffraction Analysis

A PXRD trace was generated from the single crystal data and compared to the trace obtained experimentally from the bulk sample. The two traces were compared to ensure the single crystal was representative of the bulk sample. These traces are shown in Figure 3.31.

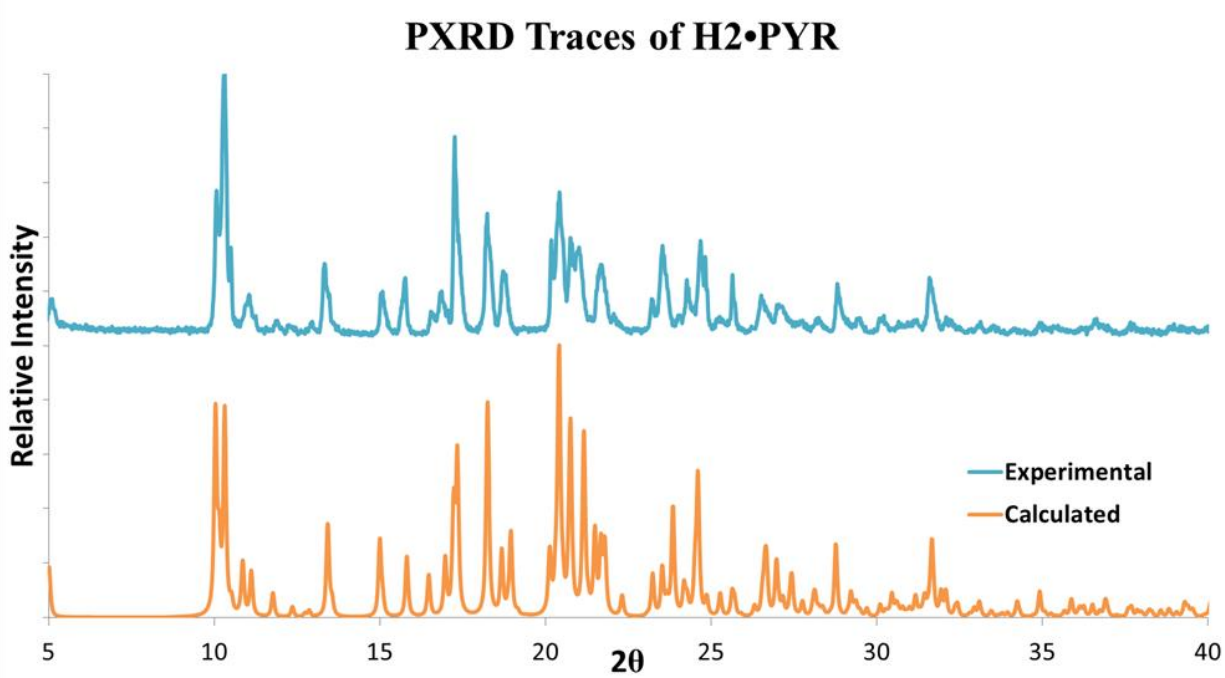

Figure 3.31: The PXRD traces obtained from the data collected from the SXRD analysis of **H2·PYR** (orange) compared to the experimental trace (blue).

3.10 Structural Analysis of H3·2PIC

3.10.1 Single Crystal X-ray Diffraction Analysis

A previous investigation conducted by Barton et al. dealt with **H3** and its associated inclusion compounds with picolines and pyridine.[1] The authors synthesised inclusion compounds using **H3** with all three picolines and pyridine and conducted SCXD and thermal analyses. However, the authors were not able to elucidate a structure of **H3·2PIC** using SCXD, due to poor crystal quality. Fortunately, during the course of this investigation, this inclusion compound was synthesised and the structure characterised, thus completing the series and allowing for full comparison between the **H1**, **H2** and **H3** systems.

A colourless needle-shaped crystal, with dimensions of 0.14 x 0.21 x 0.38 mm^3, was selected for single crystal X-ray diffraction analysis. The data were collected on a Bruker DUO APEX II[2] diffractometer at -100 °C. **H3·2PIC** crystallises in the monoclinic crystal system with the space group $P2_1/n$. This is notably different from the reported structures for **H3·3PIC**, **3H3·(4)4PIC·H_2O** and **H3·PYR** which crystallises in the triclinic crystal system with space group $P\bar{1}$, similar to the crystals obtained for **H1**.

The resulting structure was refined to R_1 = 0.0422 and wR_2 = 0.0997 and the asymmetric unit contains one **H3** molecule and one 2-picoline guest. This shows a host:guest ratio of 1:1, which was subsequently confirmed using thermal and ^{1}H NMR spectroscopic methods. The unit cell contains four of these host-guest pairs. The crystal data are summarised in Table 3.38 and the crystal data for **H3** inclusion compounds reported by Barton et al. are included in the Supplementary Information for comparison purposes.[1]

Table 3.38: Crystal Data for **H3·2PIC**.

Compound	H3·2PIC
CCDC	1881577
Structural formula	C_{37} H_{37} NO_4
Molecular mass (g·mol^{-1})	559.67
Data collection temp. (K)	173
Crystal system	Monoclinic
Space group	$P2_1/n$
a (Å)	9.900(2)
b (Å)	29.412(6)
c (Å)	11.321(2)
α(°)	90
β(°)	112.45(3)
γ(°)	90
Volume (Å^3)	3046.9(12)
Z/Z'	4
D calc density (g·cm^{-3})	1.220
θ range (°)	2.331-28.830
Reflections collected	70688
No. data I>2 σ (I)	7608
Final R Indices R_1, [I>2 σ (I)]	0.0422
Goodness-of-fit on F^2	1.025

The hydrogen bonding in **H3·2PIC** displays the same intramolecular O—H···O bond within the host molecule and the O—H···N connecting host and guest. The asymmetric unit of **H3·2PIC** is shown in Figure 3.32a along with the unit cell in Figure 3.32b. The unit cell shows four host-guest pairs viewed down [100] with two hosts forming a dimer centred within the cell. The packing is shown in Figure 3.33a, with the guests coloured pink and in space-filled style, and with the hosts shown in grey. The guests and hosts pack in alternating layers with the guests stacking down [100]. The guests are stacked at alternating angles and the layers along [010] are arranged (guest):(two hosts):(guest) etc.

The void spaces within **H3·2PIC** (Figure 3.33b) show that the guests reside in constricted channels running along [101] with a minimum cross section of 3.6 Å x 4.2 Å. Overall, the structure of **H3·2PIC** is divergent from that of the reported structures for **H3·3PIC** and **3H3·(4)4PIC·H_2O**. The main differences are crystal system (monoclinic vs triclinic), space group ($P2_1/n$ vs $P\bar{1}$) and having a Z= 4 (compared with Z = 2 for both the 3-picoline and 4-picoline inclusion compounds). **H3·2PIC** does retain the channels characteristic of the other **H3** compounds.

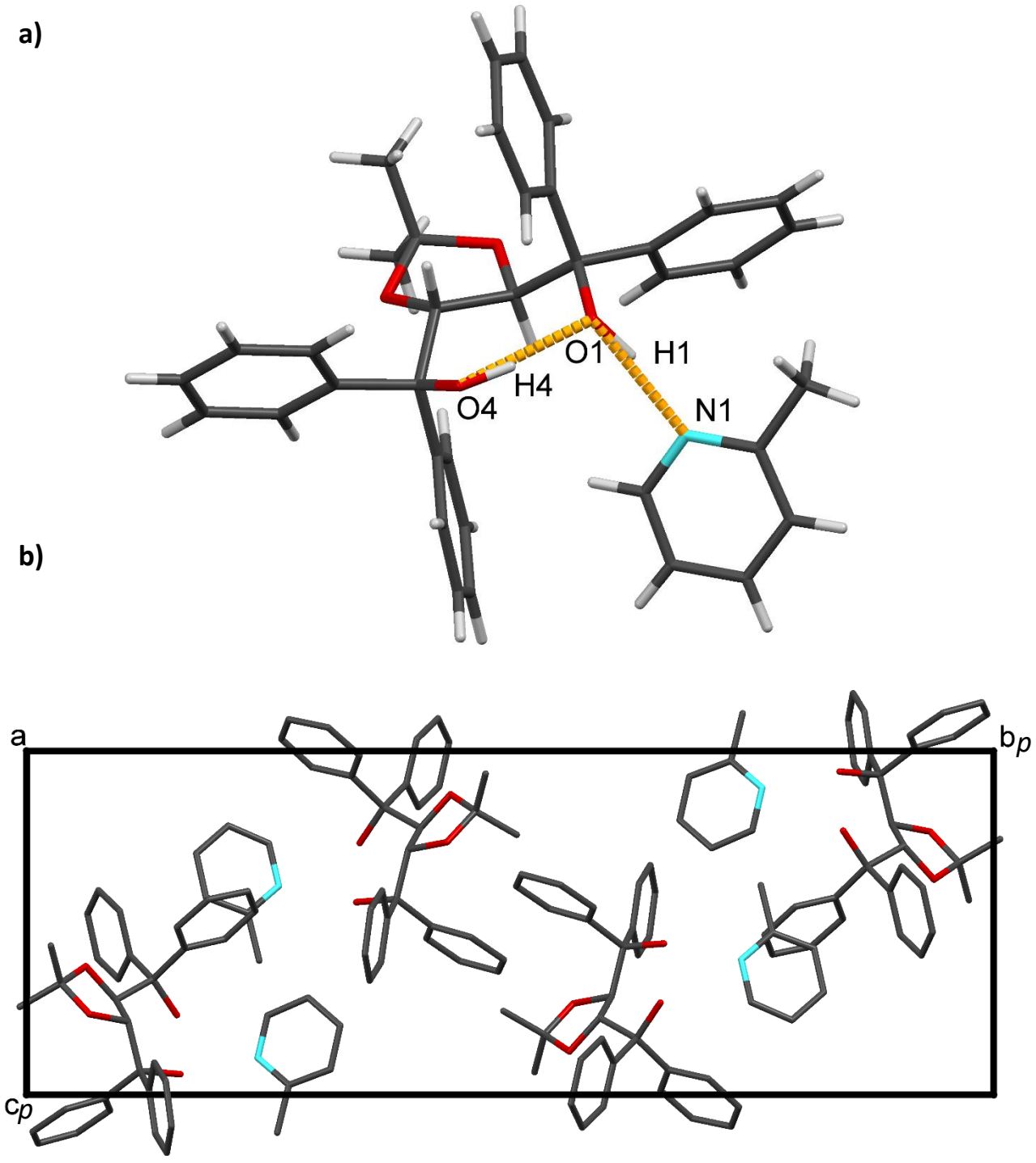

Figure 3.32: a) The asymmetric unit of **H3·2PIC** with the hydrogen bonds shown in orange. b) The unit cell of **H3·2PIC** showing the four host-guest units and the central dimer consisting of two hosts.

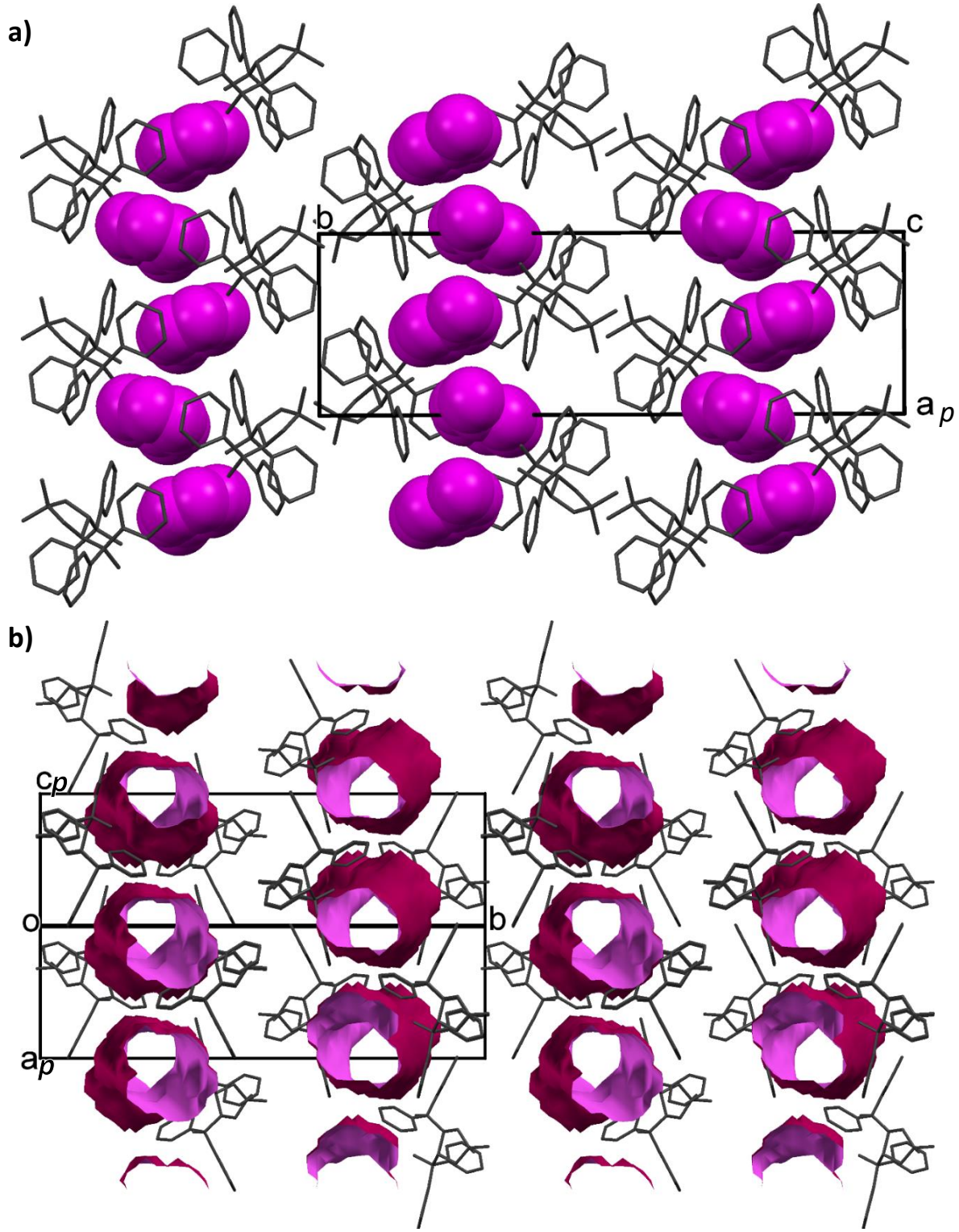

Figure 3.33: a) The packing diagram of **H3·2PIC** viewed down [001] showing the stacked pink guest layers – the hydrogen atoms have been omitted for clarity. b) The restricted channels revealed when the guests are removed and the void spaces mapped. The channels run down [101] and have a minimum cross section of 3.6 Å x 4.2 Å. The hydrogen atoms have been omitted for clarity.

3.10.2 Hirshfeld Surface Analysis

Once again, a Hirshfeld surface was generated around the 2-picoline guest molecule and the intermolecular interactions calculated. The fingerprint plot for **H3·2PIC** is shown in Figure 3.34a, with Figure 3.34b showing the composition of the interactions. The majority of interactions are H···H in nature followed by C···H/H···C and N···H/H···N. Weaker interactions make up the remaining 7% of the overall interactions. As in previous structures, the strongest interaction is the hydrogen bond O-H···N, which is the most prominent spike in the fingerprint plot. Since **H3** lacks the fluorine groups present in **H2**, there are no F interactions. When compared to **H1,** which had methyl groups in the para position on the host phenyl rings (compared to only H in **H3**), the percentage of C···C and O···H interactions decreases in **H3·2PIC.**

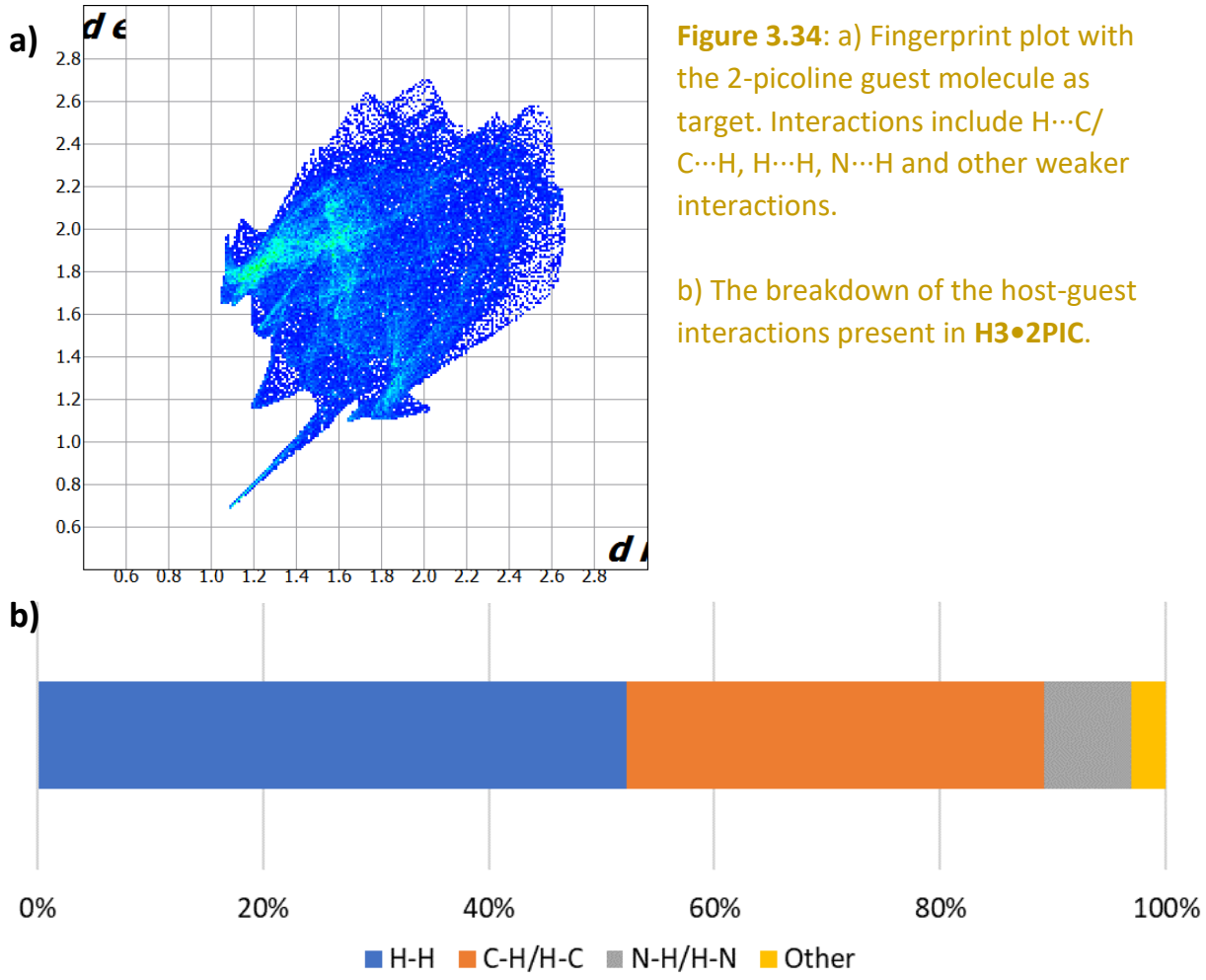

Figure 3.34: a) Fingerprint plot with the 2-picoline guest molecule as target. Interactions include H···C/ C···H, H···H, N···H and other weaker interactions.

b) The breakdown of the host-guest interactions present in **H3•2PIC**.

3.10.3 Intra- and Intermolecular Interactions

This structure has a host:guest ratio of 1:1. There are two hydrogen bonds present in this structure, the intramolecular O-H···O and the intermolecular host-guest bond O-H···N. The specifics of those bonds are captured in Table 3.39. The atoms comprising the generated centroids have been listed in Table 3.40 with six host rings and one guest centroid. Table 3.41 shows X-H···Cg (H···Cg < 3Å) interactions with two host-host interactions and three associated with host-guest. Table 3.42 lists the strongest π··· π interactions present within the complex. Two of these interactions lie within the asymmetric unit: one host-host and one host-guest. The third, and strongest, connects the host to a guest outside of the asymmetric unit. Table 3.43 includes the intermolecular short contacts, which comprise interactions whose intermolecular distances were less than the sum of the van der Waals radii given by Bondi.

These include C···H, H···H and O···H interactions and are interhost and interguest. There are five host-guest interactions that lie within the asymmetric unit, including two H···C contacts which lie on either side of the host-guest hydrogen bond. There is also a contact from the guest methyl hydrogen atom to a host carbon atom and two contacts from two host carbon atoms to a single guest hydrogen atom. This last guest hydrogen atom is the same one involved in the host-guest C-H··· π contact and indicates multiple interactions stemming to and from this particular hydrogen atom.

Table 3.39: Hydrogen bonding interactions in **H3·2PIC**.

Donor (D)	Acceptor (A)	D···A (Å)	D-H(Å)	H···A (Å)	<D-H···A (°)
O4	N1	2.716 (1)	0.922(5)	1.823(8)	163 (2)
O1	O4	2.707 (1)	0.949(5)	1.767(6)	173 (2)

Table 3.40: The centroids generated for **H3·2PIC** and their corresponding atoms.

Centroid	Nature	Atom 1	Atom 2	Atom 3	Atom 4	Atom 5	Atom 6
Cg 1	Host	O2	C2	C3	O3	C29	-
Cg 2	Host	C5	C6	C7	C8	C9	C10
Cg 3	Host	C11	C12	C13	C14	C15	C16
Cg 4	Host	C17	C18	C19	C20	C21	C22
Cg 5	Host	C23	C24	C25	C26	C27	C28
Cg 6	Guest	N1	C32	C33	C34	C35	C36

Table 3.41: CH···π interactions in **H3·2PIC**.

Nature	C(I)-H(J) ··· Cg(k)	Symmetry Operator	H···Cg (Å)	Angle (°)
Host-Host	C(15)-H(15) ··· Cg(5)	x, y, -1+z	2.85	158
Host-Host	C(21)-H(21) ··· Cg(2)	x, y, 1+z	2.95	148
Host-Guest	C(27)-H(27) ··· Cg(6)	$\frac{1}{2}$ +x, $\frac{3}{2}$ -y, $\frac{1}{2}$ +z	2.73	144
Guest-Host	C(33)-H(33) ··· Cg(4)	$\frac{1}{2}$ +x, $\frac{3}{2}$ -y, -$\frac{1}{2}$ +z	2.58	153
Guest-Host	C(36)-H(36) ··· Cg(5)	x, y, z	2.68	153

Table 3.42: π···π interactions in **H3·2PIC** < 5 Å.

Nature	Cg(I)-Cg(J)	Symmetry Operator	Cg-Cg (Å)
Host-Guest	Cg(4)-Cg(6)	-$\frac{1}{2}$ +x, $\frac{3}{2}$ -y, -$\frac{1}{2}$ +z	4.771(2)
Host-Host	Cg(5)-Cg(4)	x, y, z	4.817(2)
Host-Guest	Cg(5)-Cg(6)	x, y, z	4.821(2)

Table 3.43: Summary of shortest intermolecular contacts in **H3·2PIC**.

Nature	Contact	C(I)-H(J) ··· Cg(k)	Symmetry Operator	Length (Å)
Host-Guest	H···C	H(1) ··· C(36)	x, y, z	2.56
Host-Host	C···H	C(21) ··· H(31B)	1-x, 1-y, 2-z	2.75
Host-Host	H···H	H(13) ··· H(18)	1+x, y, z	2.27
Host-Host	C···H	C(27) ··· H(15)	x, y, 1+z	2.78
Host-Host	O···H	O(3) ··· H(31C)	1-x, 1-y, 2-z	2.62
Host-Guest	C···H	C(23) ··· H(36)	x, y, z	2.80
Host-Guest	H···C	H(1) ··· C(32)	x, y, z	2.81
Host-Guest	C···H	C(24) ··· H(36)	x, y, z	2.85
Host-Guest	H···H	H(19) ··· H(31B)	-1+x, y, z	2.35
Host-Host	C···H	C(31) ··· H(19)	1+x, y, z	2.86
Host-Guest	C···H	C(15) ··· H(37A)	x, y, z	2.88
Host-Host	H···H	H(15) ··· H(22)	x, y, 1+z	2.39

3.10.4 Powder X-ray Diffraction Analysis

A PXRD trace was generated from the **H3·2PIC** single crystal data and compared to the trace obtained experimentally to ensure the single crystal was representative of the bulk sample. These traces are shown in Figure 3.35 and exhibit the same peaks.

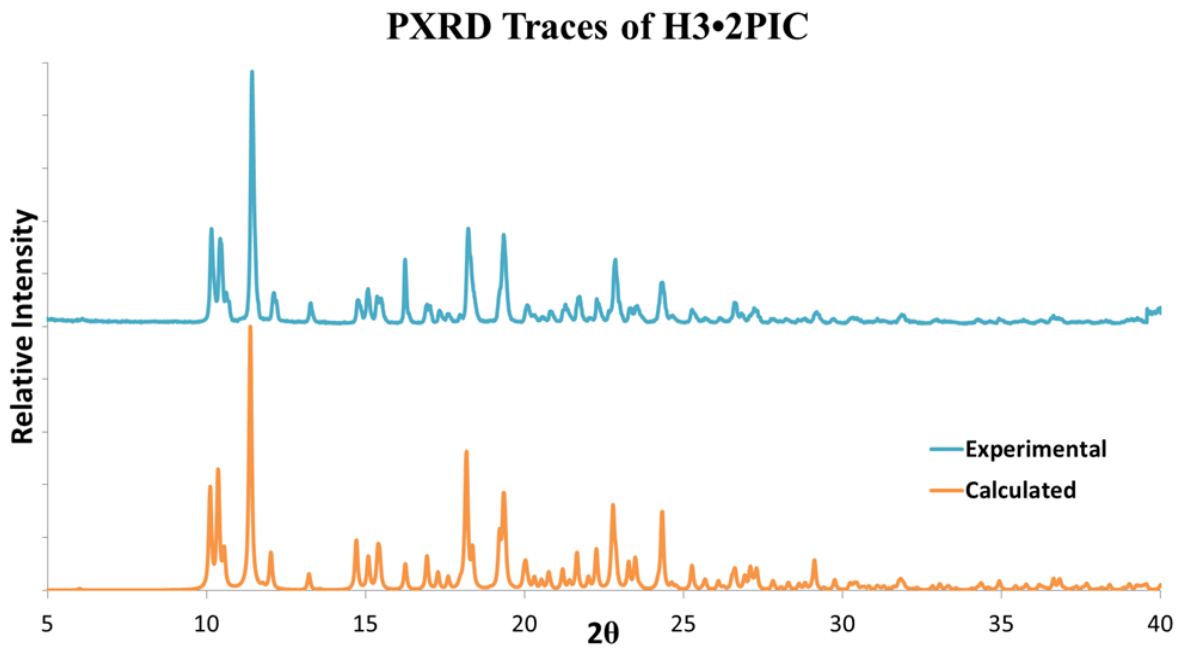

Figure 3.35: The calculated (orange) and experimental (orange) PXRD traces of **H3·2PIC**.

3.11 Structural Analysis of H3·(1.5)4PIC

3.11.1 Single Crystal X-ray Diffraction Analysis

In a previous investigation, conducted by Barton et al. a **3H3·(4)4PIC·H_2O** complex was synthesised and analysed.[1] The presence of waters of crystallisation made it difficult to compare to the other **H3** structures and, therefore, in this investigation we endeavoured to synthesise a crystal structure involving **H3** and 4-picoline without the water included. This was achieved by distilling the 4-picoline guest to remove all traces of water from the reagent and growing the crystals via slow evaporation in a supersaturated solution in a desiccator.

A colourless block-shaped crystal, with dimensions of 0.21 x 0.29 x 0.38 mm^3, was selected for single crystal X-ray diffraction analysis. The data were collected on a Bruker DUO APEX II[2] diffractometer at -100 °C. **H3·(1.5)4PIC** crystallises in the triclinic crystal system with the space group $P\bar{1}$. The resulting structure was refined to R_1 = 0.0488 and wR_2 = 0.1159 and the asymmetric unit contains one **H1** molecule and 1.5 4-picoline guests and the unit cell contains two of this units giving a Z = 2.

One 4-picoline guest lies in a general position and contains a hydrogen bond which binds it to the host molecule. The second guest is located on a centre of inversion at Wykoff position *b*. This shows a host:guest ratio of 1:1.5, which was subsequently confirmed using thermal and ^{1}H NMR spectroscopic methods. The crystal data and refinement details are shown in Table 3.44. Figure 3.36a shows the asymmetric unit of **H3·(1.5)4PIC** with the host molecule hydrogen-bonded to the 4-picoline guest, which lies in a general position. The second disordered guest is shown and it has an occupancy of 0.5. The unit cell is depicted in Figure 3.36b where the two host molecules and two 'full' guests are seen. The value of *Z* for **H3·(1.5)4PIC** is two as there are 2 asymmetric units present in the unit cell.

Table 3.44: Crystal Data for **H3·4PIC** with **3H3· (4)4PIC·H_2O** included for comparison.

Compound	H3·1.5·4PIC	3·H3·3·4PIC·H_2O
CCDC	1881568	1519653
Structural formula	C_{31} H_{30} O_4·1.5C_6H_7N	3C_{31} H_{30} O_4 ·4C_6H_7N·0.877· H_2O
Molecular mass (g·mol^{-1})	606.24	1787.95
Data collection temp. (K)	172	200
Crystal system	Triclinic	Triclinic
Space group	$P\bar{1}$	$P\bar{1}$
a (Å)	9.473(1)	12.112(1)
b (Å)	9.882(1)	18.852(2)
c (Å)	18.363(2)	22.890(2)
α(°)	92.21(1)	72.83(1)
β(°)	102.58(1)	77.44(1)
γ(°)	101.77(1)	82.96(1)
Volume (Å^3)	1636.3(3)	4866.3(7)
Z/Z'	2	2
D calc density (g·cm^{-3})	1.230	-
θ range (°)	2.281-28.270	-
Reflections collected	24298	-
No. data I>2 σ (I)	8162	-
Final R Indices R_1, [I>2 σ (I)]	0.0488	-
Goodness-of-fit on F^2	0.992	-

The packing of **H3·(1.5)4PIC** is shown in Figure 3.37a and the guests are packed in layers. The layers are formed when two of the general position guests are sandwiched by the disordered guest on each side. This pattern is repeated down [010] forming a stacked column of guests which results in layers, which are clearly seen when viewed down [100]. The guests were removed and void spaces mapped. The channels down [010] are shown in Figure 3.37b and the segments forming the channels are evident. Each segment corresponds to four guests and they merge to create the channels.

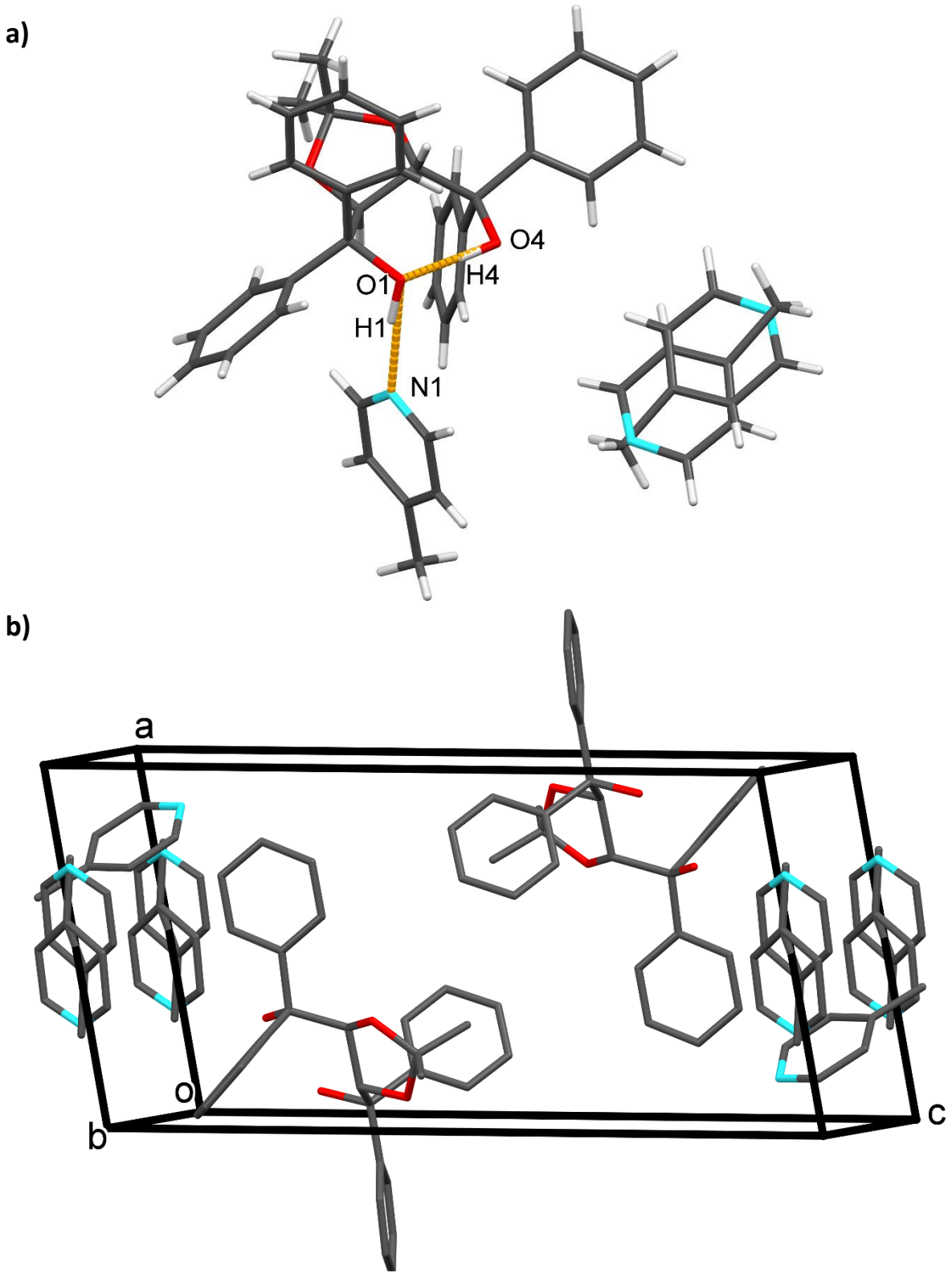

Figure 3.36: a) The asymmetric unit of **H3·(1.5)4PIC** showing the guest hydrogen bonded to the host and the other disordered guest. b) The unit cell of **H3·(1.5)4PIC** showing the two host-guest pairs along with four of the disordered guests in Wykoff position *b*.

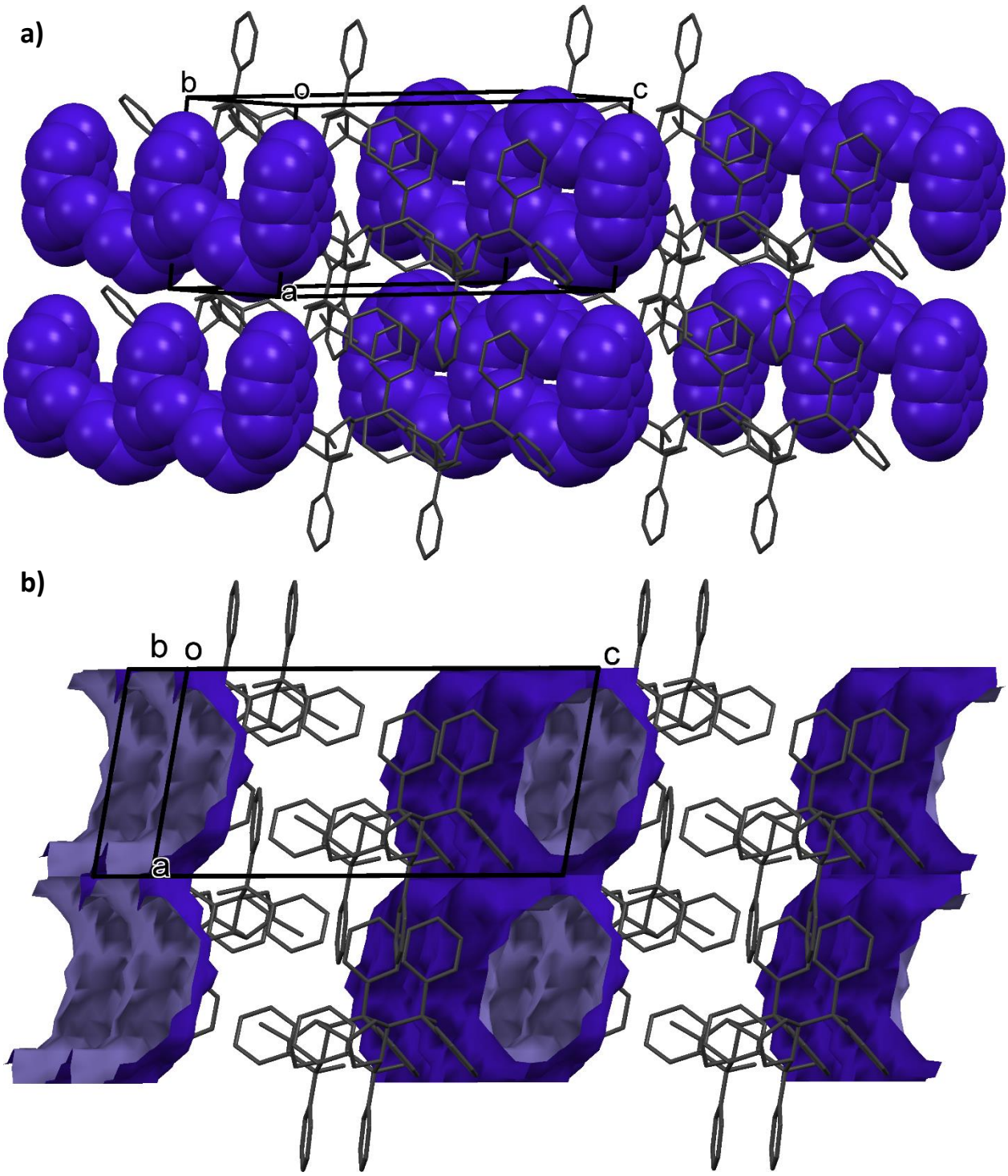

Figure 3.37: a) The packing of **H3·(1.5)4PIC** with the guests in indigo. b) The voids of **H3·(1.5)4PIC** running down [010] revealed once the guests are removed. Hydrogen atoms have been omitted for clarity.

3.11.2 Hirshfeld Surface Analysis

The non-bonded interactions of the **H3·(1.5)4PIC** host-guest system were analysed using the programme CrystalExplorer. The Hirshfeld surface was generated around the guest molecule and points were mapped. Due to the disorder in the second guest, only the first guest, which lies in a general position, was subjected to this Hirshfeld analysis. The fingerprint plot and interaction breakdowns for the guests of **H3·(1.5)4PIC** are shown in Figure 3.38. The majority of interactions are H···H in nature with C···H/H···C, N···H/H···N and other weaker interactions making up the rest. There is a small peak labelled ①, which corresponds to a H···O interaction: H35···O4. This is one of the stronger short contact interactions in the host:guest complex.

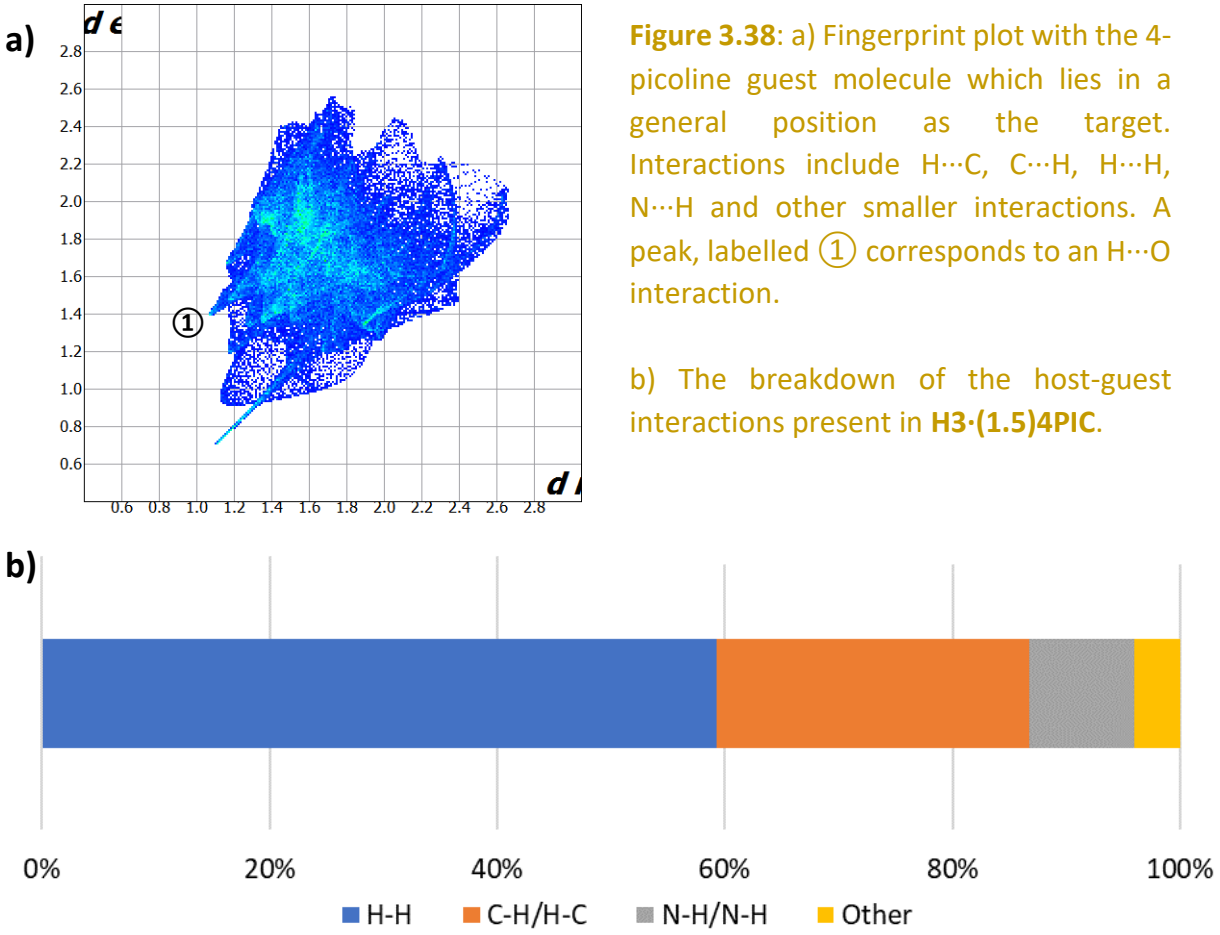

Figure 3.38: a) Fingerprint plot with the 4-picoline guest molecule which lies in a general position as the target. Interactions include H···C, C···H, H···H, N···H and other smaller interactions. A peak, labelled ① corresponds to an H···O interaction.

b) The breakdown of the host-guest interactions present in **H3·(1.5)4PIC**.

3.11.3 Intra- and Intermolecular Interactions

As in all the previous **H1**, **H2** and **H3** complexes, **H3·(1.5)4PIC** contains two hydrogen bonds. One connects the host molecule to the 4-picoline guest in a general position and the other is the classic host intramolecular O-H···H hydrogen bond. However, the disorder of the second guest means that this one does not have any hydrogen bond interactions. This is unusual for these complexes since in all the previous compounds described in this investigation, each guest is connected to a host via a N···H-O hydrogen bond.

The asymmetric unit contains one host and 1.5 guests. Guest A lies in a general position and is connected to the host via the two hydrogen bonds described in Table 3.45. Guest B is disordered. The centroids were calculated and are named, along with their constituent atoms, in Table 3.46.

The C-H·· π interactions shorter than 3.0 Å were calculated and are included in Table 3.47. There are three of these interactions with two being host-host and one which connects the host to the disordered guest. Table 3.48 lists the π··· π interactions shorter than 5.0 Å and there is a Host-Guest A interaction which lies within the asymmetric unit. There is also a π··· π interaction between two Guest B molecules.

Table 3.49 lists the intermolecular short contacts, which include interactions whose intermolecular distances are less than the sum of the van der Waals radii given by Bondi. The vast majority of these short contacts are host-guest in nature, which is interesting. The O···H peak present in the Hirshfeld fingerprint corresponds to a Host-Guest A interaction H35···O4.

Table 3.45: Hydrogen-bonding interactions in **H3·(1.5)4PIC**.

Donor (D)	Acceptor (A)	D···A (Å)	D-H(Å)	H···A (Å)	<D-H···A (°)
O1	N1	2.579(2)	0.976(5)	1.798(7)	168(2)
O4	O1	2.637(1)	0.984(5)	1.653(5)	177(2)

Table 3.46: The centroids generated for **H3·(1.5)4PIC** and their corresponding atoms.

Centroid	Nature	Atom 1	Atom 2	Atom 3	Atom 4	Atom 5	Atom 6
Cg 1	Host	O2	C2	C3	O3	C29	-
Cg 2	Host	C5	C6	C7	C8	C9	C10
Cg 3	Host	C11	C12	C13	C14	C15	C16
Cg 4	Host	C17	C18	C19	C20	C21	C22
Cg 5	Host	C23	C24	C25	C26	C27	C28
Cg 6	Guest A	N1	C32	C33	C34	C35	C36
Cg 7	Guest B	N2	C38	C39	C40	C41	C42

Table 3.47: C-H···π interactions in **H3· (1.5)4PIC**.

Nature	C(I)-H(J) ··· Cg(k)	Symmetry Operator	H···Cg (Å)	Angle (°)
Host-Host	C(13)-H(13) ··· Cg(4)	-1+x, -1+y, z	2.80	157
Host-Host	C(30)-H(30A) ··· Cg(2)	x, y, z	2.94	148
Guest B-Host	C(38)-H(38) ··· Cg(5)	x, -1+y, z	2.88	139

Table 3.48: π···π interactions in **H3·(1.5)4PIC**.

Nature	Cg(I)-Cg(J)	Symmetry Operator	Cg-Cg (Å)
Host-Guest A	Cg(3)-Cg(6)	x, y, z	4.736(2)
Host-Host	Cg(4)-Cg(3)	1+x, y, z	4.996(2)
Guest B-Guest B	Cg(6)-Cg(6)	-x, 1-y, -z	4.898(2)

Table 3.49: Summary of shortest intermolecular contacts **H3·(1.5)4PIC**.

Nature	Contact	C(I)-H(J) ··· Cg(k)	Symmetry Operator	Length (Å)
Host-Guest B	H···H	H(26) ··· H(43A)	-1+x, 1+y, z	2.17
Host-Guest B	H···H	H(25) ··· H(43C)	-1+x, 1+y, z	2.23
Host-Guest A	H···C	H(1) ··· C(36)	x, y, z	2.70
Host-Guest A	O···H	O(4) ··· H(35)	-x, 1-y, -z	2.55
Host-Guest B	H···C	H(26) ··· C(43)	-1+x, 1+y, z	2.76
Host-Guest A	H···C	H(1) ··· C(32)	x, y, z	2.77
Host-Guest B	C···H	C(25) ··· H(38)	x, 1+y, z	2.80
Host-Guest B	C···H	C(26) ··· H(43A)	-1+x, 1+y, z	2.84
Host-Guest A	O···H	O(4) ··· H(37C)	-x, 1-y, -z	2.68
Host-Host	C···H	C(6) ··· H(27)	x, -1+y, z	2.86
Host-Guest B	H···C	H(19) ··· C(42)	1-x, 1-y, -z	2.86
Host-Host	H···C	H(27) ··· C(6)	x, -1+y, z	2.86
Host-Guest A	C···H	C(16) ··· H(32)	x, y, z	2.87
Host-Guest B	C···C	C(19) ··· C(42)	1-x, 1-y, -z	3.38

3.11.4 Powder X-ray Diffraction Analysis

A PXRD trace was generated from the **H3·(1.5)4PIC** single crystal data and compared to the traces obtained experimentally. The powder was obtained by removing the crystals from the mother liquor and lightly crushing to produce a uniform powder. The two traces were compared to ensure that the single crystal was representative of the bulk sample. These traces are shown in Figure 3.39 and includes the calculated traces from the novel crystal structure **H3·(1.5)4PIC** and the previously reported **3H3·(4)4PIC·H_2O**. It is clear that the calculated powder patterns for each structure are very similar. It is difficult to determine which compound makes up the majority of the experimental sample, or even if there is a mixture at all. Therefore, the powder pattern does not provide the diagnostic confirmation of whether the hydrate or the new **H3·(1.5)4PIC** is the main component of the experimental sample.

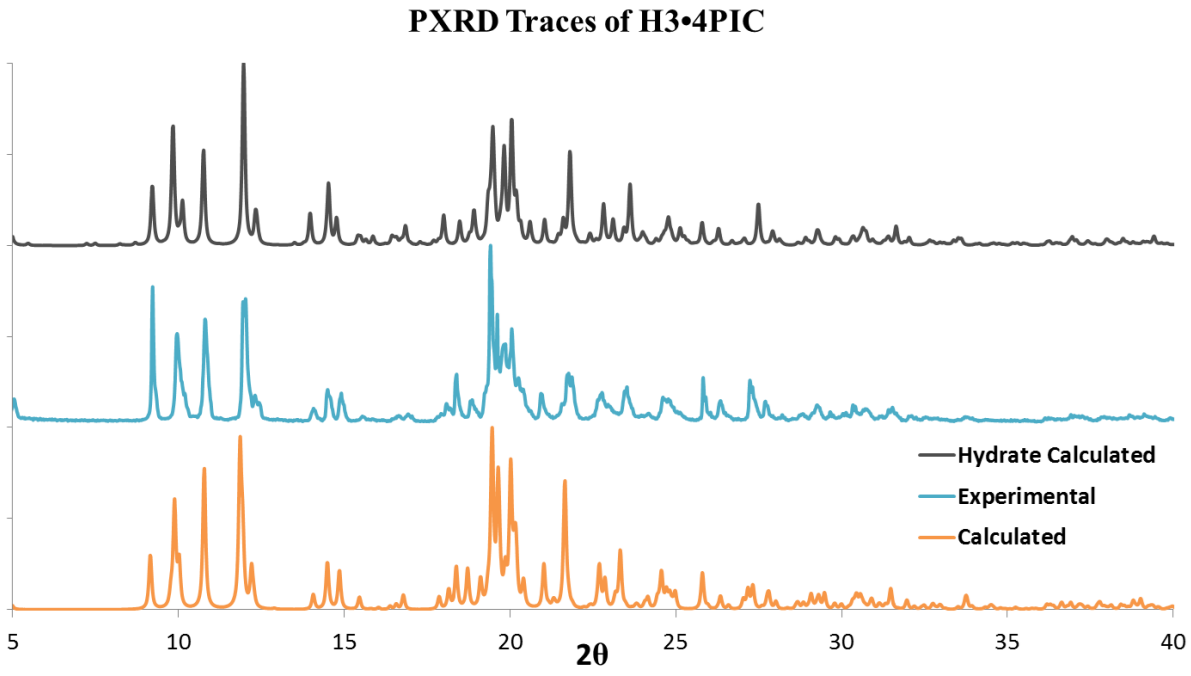

Figure 3.39: The PXRD traces for the **H3·4PIC** compounds. The orange corresponds to the trace obtained from the **H3·(1.5)4PIC** structure. The blue to the experimental traces performed on the sample. The grey reflects the calculated trace from the hydrate **3H3· (4)4PIC·H_2O**.

3.11.5 Structural Comparison of H3·(1.5)4PIC and 3H3·(4)4PIC·H_2O

Unfortunately, due to the similarity of the powder X-ray diffraction analysis, it was unclear whether the crystals grown were entirely **H3·(1.5)4PIC** or a mixture of **H3·(1.5)4PIC** and the previously reported hydrate, **3H3·(4)4PIC·H_2O**. It is clear that **H3·(1.5)4PIC** was formed to some degree since the selected single crystal yielded a novel structure. It is possible that other crystals within the vial were the hydrate crystals and were simply not selected for analysis. In ordinary cases, the powder patterns would give insight as to the composition of the mixture. However these patterns are so similar, to the point of being indistinguishable, when compared to an experimental trace.

The reason for this similarity in PXRD traces is due to the fact that both **H3·(1.5)4PIC** and the hydrate have very similar structures. This is evident when the two structures are overlaid in Figure 3.40. The water included in the hydrate is represented by a single, spaced-filled blue oxygen atom as the hydrogen atoms have been omitted for clarity. The primary similarity is that the host molecules are almost identically packed in both structures, with the difference lying in the guest packing. It can be seen that the non-disordered guest present in **H3·(1.5)4PIC** (orange) lies in the same position as a guest from the hydrate structure.

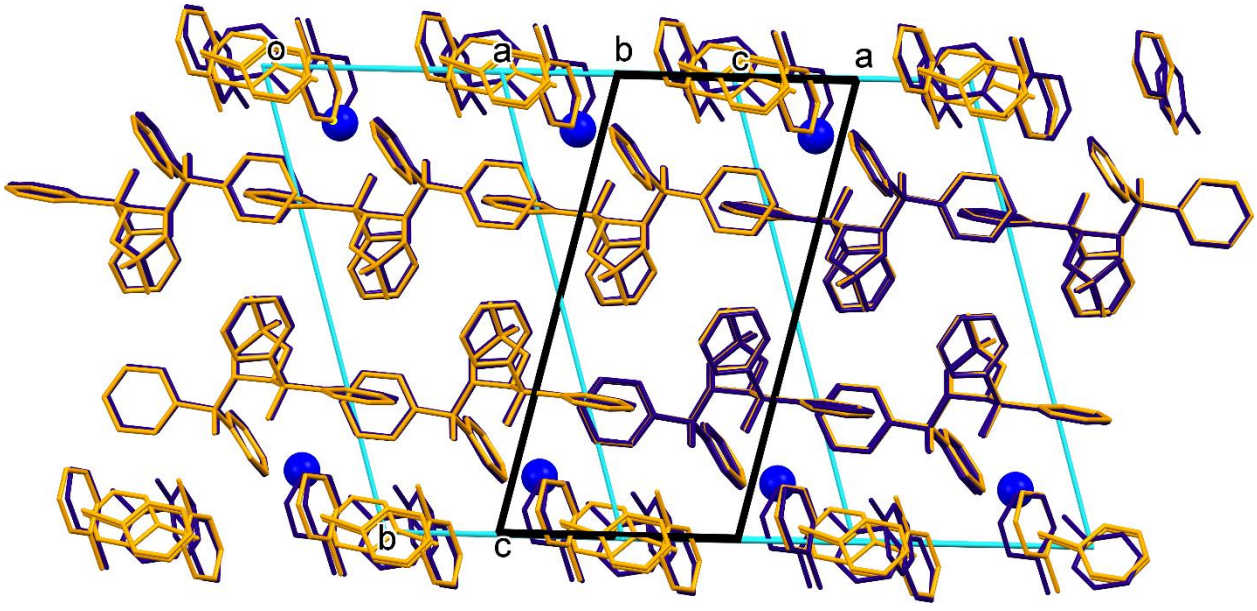

Figure 3.40: The overlay of the structures of **H3·(1.5)4PIC** (orange) with black unit cell axes and **3H3·(4)4PIC·H_2O** (purple) with blue unit cell axes. The host molecules are almost perfectly overlaid. Hydrogen atoms have been omitted for clarity but the water molecule present in the hydrate has been space-filled and coloured blue.

In **H3·(1.5)4PIC** the guests lie down the edge of the unit cell with two hosts present in the centre. Similarly, in **3H3·(4)4PIC·H_2O** the guests run in the same channels with the same layer consisting of two host molecules sandwiched between the guest layers on the edge of the unit cell.

These structural similarities result in the PXRD traces being almost identical, since the only differences are in the orientation of some of the guest molecules and the inclusion of water in the hydrate structure. The difference in the position of the guest molecules and the presence of water are not enough to notably change the PXRD trace. Further thermal analysis would be required to determine whether a mixture of the **H3** 4-picoline compounds was formed.

3.12 Thermal Analysis of H1, H2 and H3 Inclusion Compounds

Samples of each inclusion compound were subjected to Host Stage Microscopy (HSM), Thermogravimetric Analysis (TGA) and Differential Scanning Calorimetry (DSC). HSM was used to obtain an indication of the thermal profile of the sample when heated. DSC and TGA analysis were performed to determine the nature of guest release and obtain the melting information. Host-to-guest ratio was also confirmed using TGA by noting the weight loss resulting from the guest release. An example of the profile obtained from each sample is included in Figure 3.41. This shows the TGA and DSC traces of **H1·2PIC**. The TGA trace shows a mass loss of 15.1% in a single step across a broad temperature range from 72 °C to 170 °C, which corresponds to the release of the 2-picoline guest from the inclusion compound. The calculated host:guest ratio from this mass loss is 1:1, which confirms the ratio evident in the obtained **H1·2PIC** crystal structure. The DSC trace shows two endotherms, the first of which (T_{peak} = 155.0 °C) is attributed to the loss of the 2-picoline guest in a single step, followed by the melting of the host at T_{peak} = 211.8 °C.

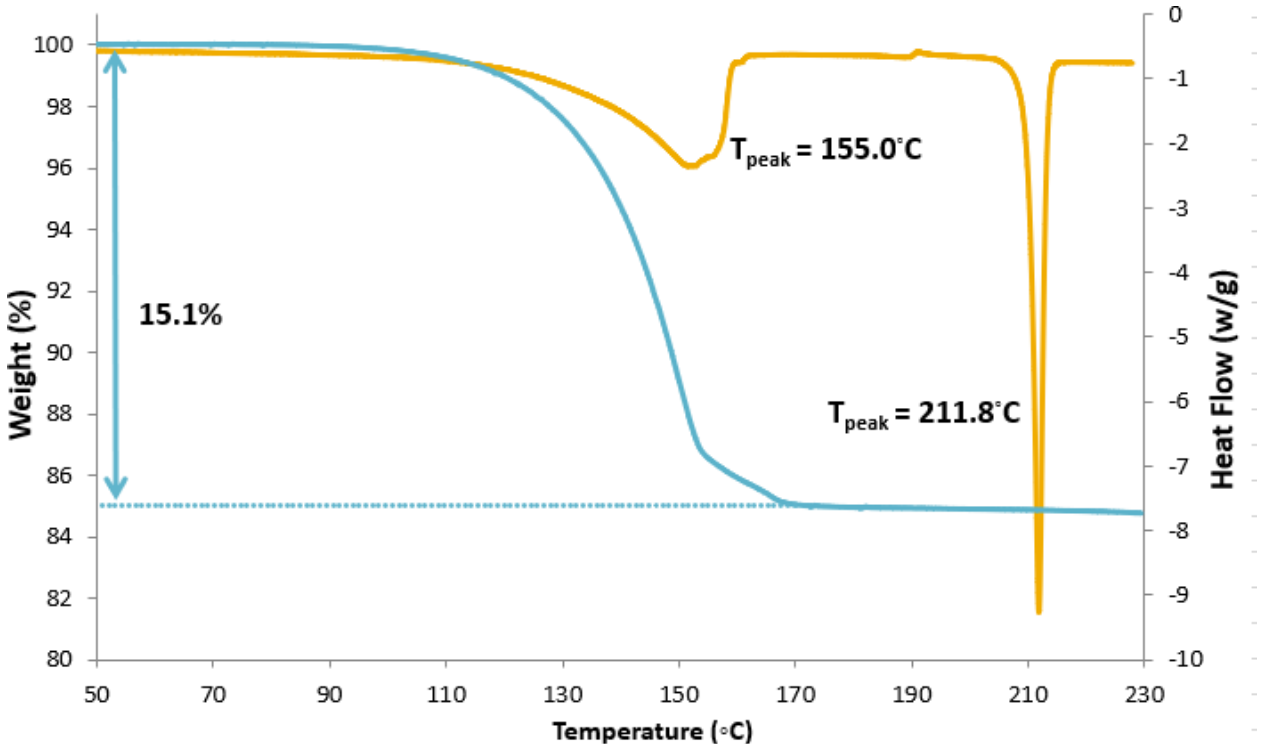

Figure 3.41: The TGA (blue) and DSC (orange) traces of **H1·2PIC** with the notable peaks labelled.

These thermal experiments were repeated for all of the **H1** inclusion compounds. The experimental guest mass loss is consistent with that calculated and all compounds showed a host melting point around 211.8 °C. The DSC showed a variation in the T_{peak} values with **H1·3PIC** having a guest loss peak at 142.8 °C, **H1·4PIC** at 138.4 °C and **H1·PYR** at 137.6 °C. These have been included in the Supplementary Information.

The **H2** inclusion compounds were also subjected to these analyses. All the TGA traces showed a mass loss that comports with their calculated values. Each DSC trace displayed two endotherms which correspond to the guest loss and the host melt, respectively. The **H2·3PIC** TGA trace in Figure 3.42 shows a two-step mass loss, which is congruent with the structure of the crystal. The **H2·3PIC** structure contains two guests, one of which is enclosed in the host dimer. This may explain the steps, since one guest is more tightly held within the crystal. The **H2** values are included in Table 3.50, which summarises all the thermal results across the host-guest compounds.

All compounds were subjected to thermal analysis, including the ones reported by Barton el al. These compounds, **H3·3PIC** and **H3·4PIC·H_2O** were resynthesised and the PXRD traces compared to those calculated from the reported structures to ensure the correct structures

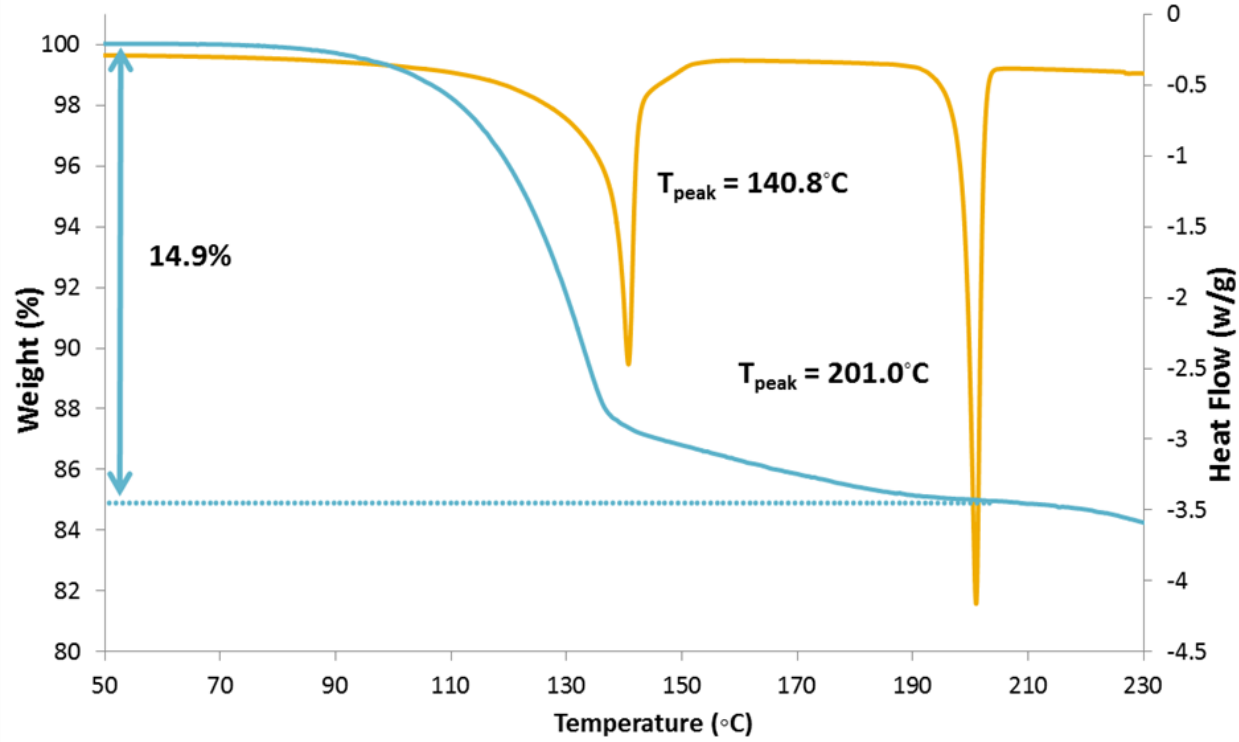

Figure 3.42: The TGA (blue) and DSC (orange) traces of **H2·3PIC** with the notable peaks labelled. Note the two-step mass loss in the TGA curve.

were synthesised and subjected to thermal analysis. An interesting phenomenon was discovered when running DSC analysis on **H3·2PIC**. This compound displays a definitive double melt, which is associated with polymorphic changes of the host. The TGA and DSC traces of **H3·2PIC** are shown in Figure 3.43, which shows a guest loss of 16.5% and the double melt. The TGA trace shows a definitive two step guest lost, which suggests that a rearrangement occurs after the first series of guest release. This corresponds to the peaks present in the DSC profile where the first broad peak is due to the first release of the 2-picoline guests and the second peak matches the second 'step' in the TGA trace. The primary T_{peak} was determined by taking the derivative of the DSC curve, which improved accuracy.

Figure 3.44 shows the TGA and DSC results from the **H3·(1.5)4PIC** sample. There is a single guest loss in the TGA, which corresponds to the calculated mass loss of 22.4%. There is one main endotherm present at 102.4 °C and there does not seem to be any water released in either trace. There is, once again, a double melt present in this host.

TGA and DSC were used to confirm the host:guest ratio and as a measure of the stability of guest included in the compound. The results of the TGA and DSC experiments of all the inclusion compounds are shown in Table 3.50. The inclusion compounds originally described by Barton et al. have also been included for comparison purpose. These compounds were resynthesised and subjected to thermal analysis – these traces have been included in the Supplementary Information. Overall, the observed mass loss agrees with the expected mass loss displayed in the TGA traces. The melting point values has been included to show the consistency of the thermal traces. All the DSC and TGA traces can be found in the supplementary data.

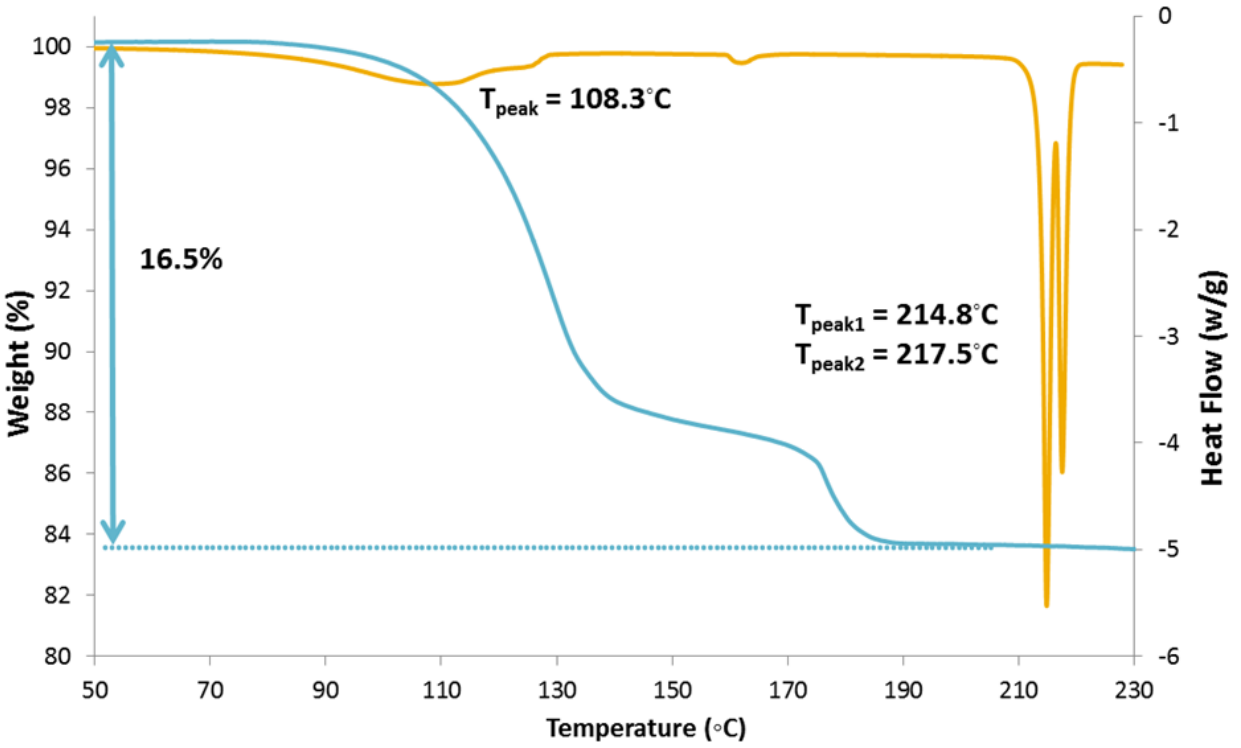

Figure 3.43: The TGA (blue) and DSC (orange) traces of **H3·2PIC** with the notable peaks labelled. There is an obvious double melt present in the DSC.

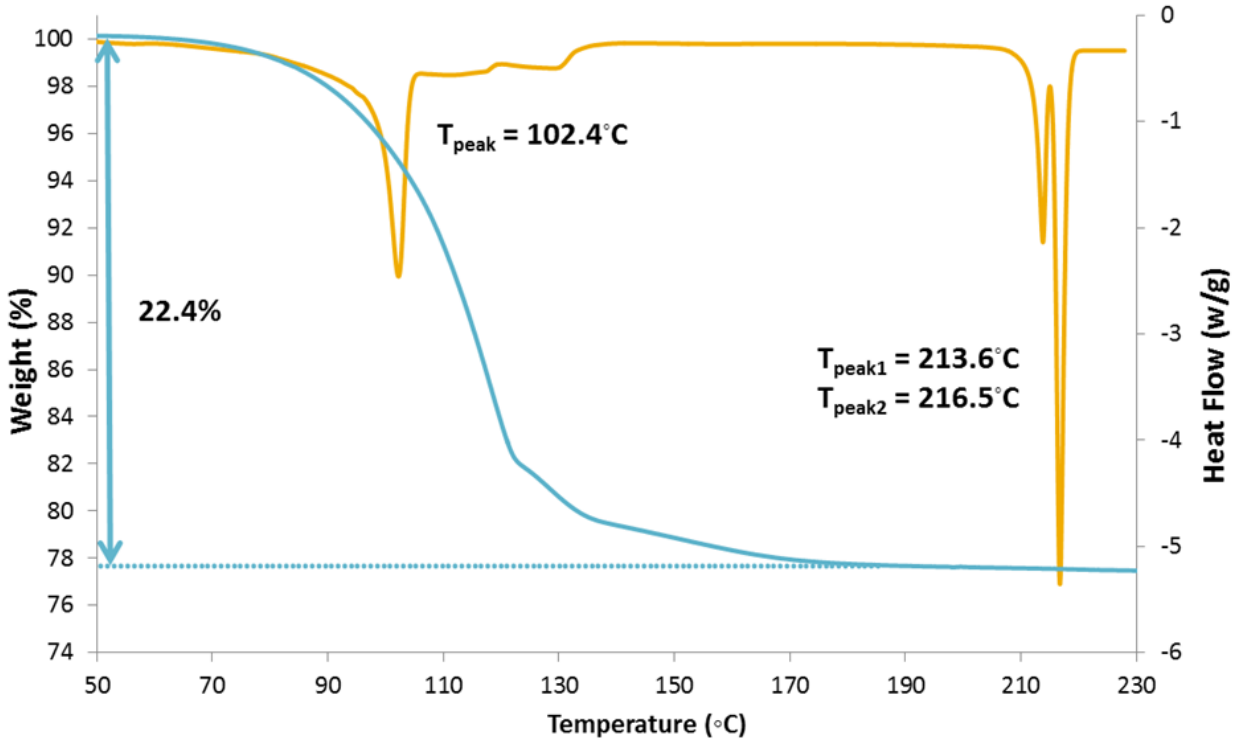

Figure 3.44: The TGA (blue) and DSC (orange) traces of **H3· (1.5)4PIC** with the notable peaks labelled.

Table 3.50: The thermal data for the pyridyl host-guest complexes of **H1**, **H2** and **H3**.

Compound	TGA		DSC	
	Mass Loss		Guest Endo	Host
	Expt %	Calc %	T_{peak} (°C)	T_{melt} (°C)
H1•2PIC	15.1	15.1	155.0	211.8
H1•3PIC	15.2	15.1	142.8	211.9
H1•4PIC	15.1	15.1	138.4	211.7
H1•PYR	13.8	12.8	137.6	211.0
H2•2PIC	13.5	14.7	117.2	198.5
H2•3PIC	14.9	14.7	140.8	201.0
H2•4PIC	14.9	14.7	148.3	200.5
H2•PYR	12.9	12.5	127.5	200.8
H3•2PIC	16.5	16.6	108.3	214.8 / 217.5
H3•3PIC	16.4	16.6	140.9	217.3
H3•(1.5)4PIC	22.4	22.4	102.4	213.6/216.7
3H3•(4)4PIC•H_2O	21.4	21.7	133.2	217.5
H3•PYR	14.5	14.1	116.8	214.9/217.5

3.13 Nuclear Magnetic Resonance Spectra of Inclusion Compounds

^{1}H-NMR spectroscopy was useful in confirming inclusion and the host:guest ratios. These spectra would also serve as templates when comparing crystals that were obtained from mixed-guest experiments. The ^{1}H-NMR spectra for **H1·2PIC** are included in Figure 3.45 as an example and show the regions where guest and host peaks overlap, as well as the peaks used for identification. The spectra for the other **H1** structures are included in the Supplementary Information. This allows for direct comparisons and to confirm that inclusion has occurred. Table 3.51 lists the peaks present in the picoline guests, and the corresponding chemical shifts.

The samples were prepared by removing the crystals from the mother liquor, patting them dry and crushing into powder. A sample of approximately 10 mg was dissolved in deuterated dimethyl sulfoxide (D_6-DMSO) and subjected to ^{1}H-NMR to generate a 1D spectrum. The methyl peaks of the guests were particularly useful for confirming the host-to-guest ratio, as it was known that this particular peak corresponds to three host hydrogen atoms. Slight deshielding of all guest peaks was observed. This suggests that there is an association of host and guest solution and did not affect identification as all guest peaks shifted to the same degree. All spectra were referenced to the solvent peak at 2.50 ppm.

Table 3.51: Proton chemical shift assignments for the pure picolines in D_6-DMSO in ppm

	2-picoline	**3-picoline**	**4-picoline**
	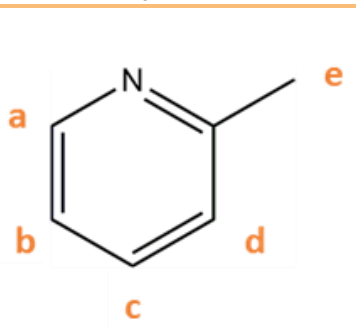	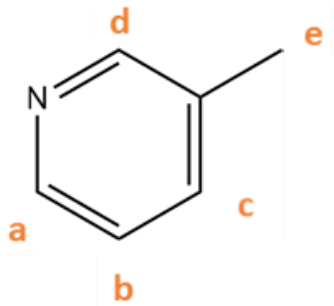	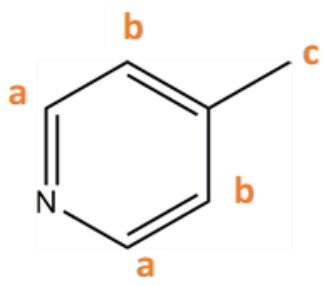
a	8.44	8.37	8.42
b	7.12	7.22	7.16
c	7.61	7.54	2.27
d	7.18	8.40	n/a
e	2.44	2.25	n/a

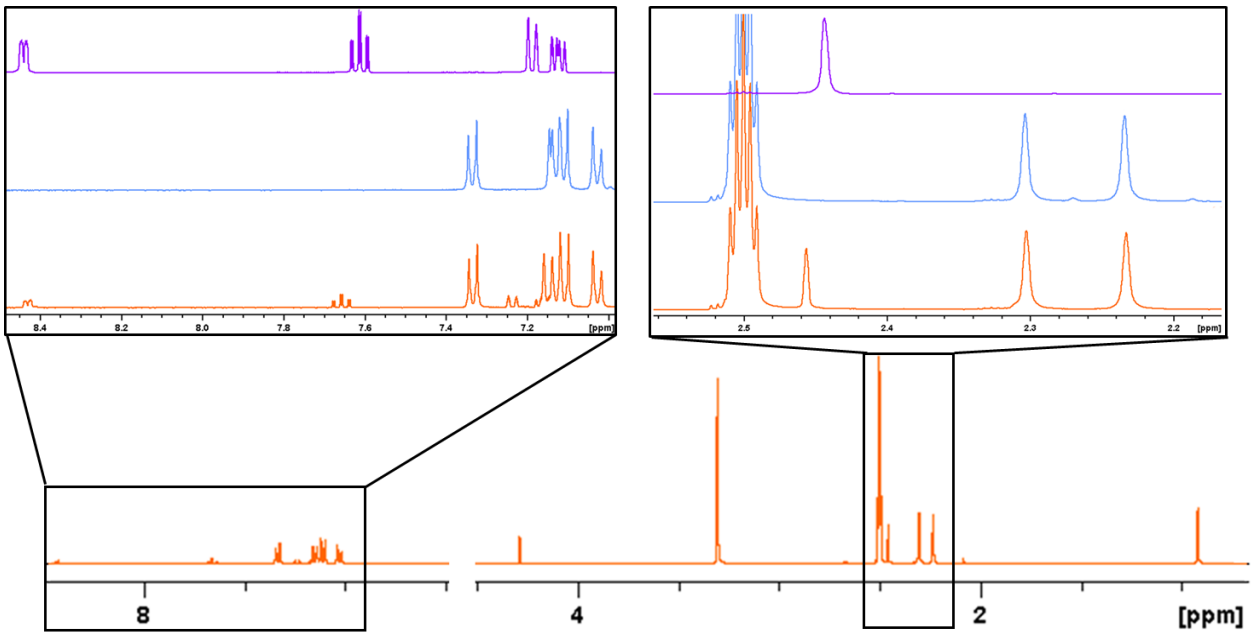

Figure 3.45: ^{1}H-NMR spectra of **H1·2PIC** (orange) showing exploded views of the relevant guest peaks. The blue is the H1 host and the purple 2-picoline. The midsection of the ^{1}H-NMR trace has been omitted for brevity. The solvent used was D_6-DMSO and the spectrum referenced to the D_6-DMSO solvent peak at 2.50 ppm. Spectra not to scale.

Figure 3.45 shows the ^{1}H-NMR spectra of **H1·2PIC.** The main peak used for identification of the guest was the 2-methyl peak at 2.44 ppm. There are two host peaks at approximately 2.22 and 2.30, which correspond to each set of para-methyl groups. The primary host peak used for integration was the one at approximately 0.87 ppm and integrates to six hydrogen atoms, which correspond to the two methyl groups on the five-membered host ring. This host peak was calibrated to integrate for six hydrogen atoms and then the guest methyl peak integrated. If the host:guest ratio is 1:1 then the methyl peak should produce an integral of approximately 3. This ratio was present in all **H1** compounds and their spectra have been included in the Supplementary Information. Inclusion could also be confirmed by inspecting the aromatic region as peaks corresponding to the picoline guests would be present. The host:guest ratio can also be confirmed using these peaks as, for example, in 2-picoline each peak in the aromatic region would integrate for one hydrogen atom. This method of confirming inclusion and host:guest ratio was repeated with all compounds.

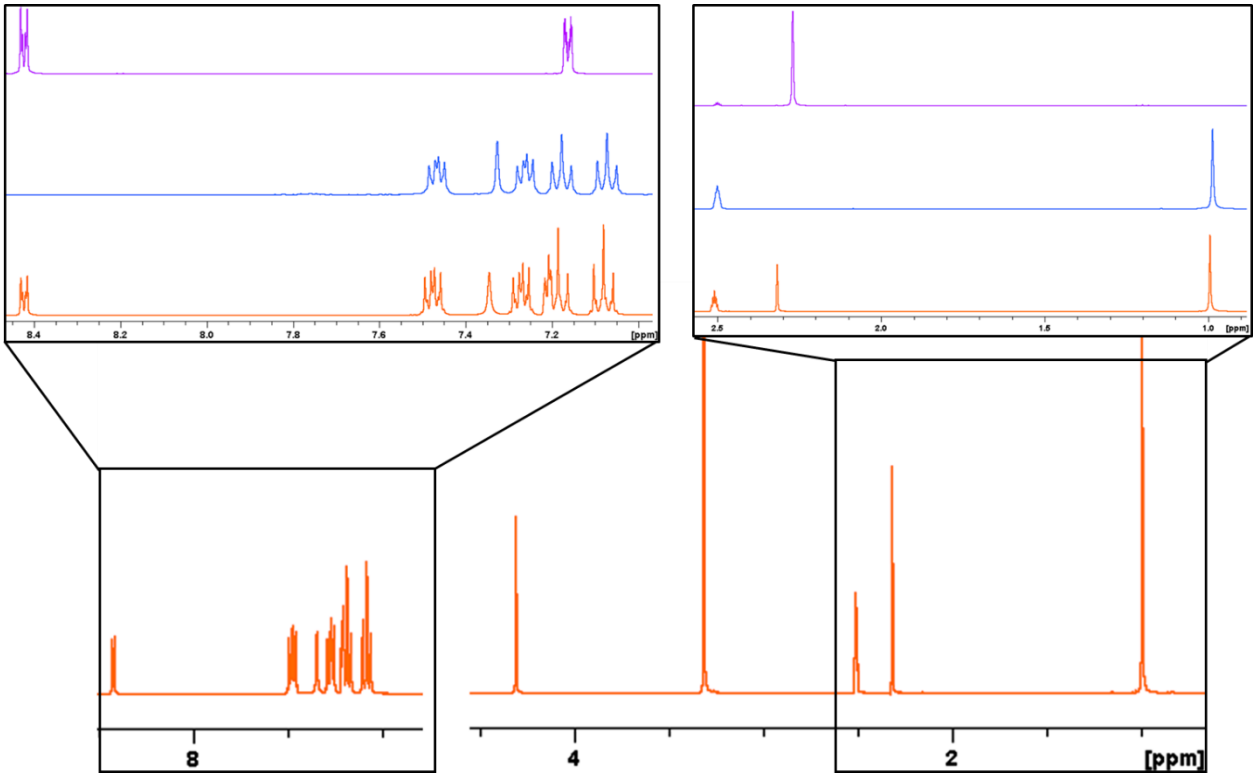

Figure 3.46: ^{1}H-NMR spectra of **H2·4PIC** (orange) showing exploded views of the relevant guest peaks. The blue is the H3 host and the purple 2-picoline. The midsection of the ^{1}H-NMR trace has been omitted for brevity. The solvent used was D_6-DMSO and the spectrum referenced to the DMSO solvent peak at 2.50 ppm. Spectra not to scale.

The same method was used for the inclusion compounds with **H2**. Figure 3.46 shows the spectra for **H2·4PIC**. The host peaks are different as the para-methyl groups of **H1** are absent. The 6-hydrogen peak corresponding to the two methyl groups on the 5-membered host ring is still present and was used for calibration. The guest methyl group is clear and once again was used to confirm inclusion and the host:guest ratio. The aromatic region was once again useful for confirming the ratio as one of the two peaks corresponding to the guest aromatic hydrogen atoms is clear for integration. This peak at approximately 8.41 corresponds to two hydrogen atoms, due to the symmetry of the molecule resulting in two equivalent environments.

Figure 3.47 shows the spectra of **H3·2PIC** and is similar to that of **H2** in that the absence of the four para methyl groups results in a clear picture of the guest methyl peak. The guest methyl group was used to determine the host to guest ratio, with further confirmation using

the aromatic region being possible. The most upfield 2-picoline guest peaks are clear and are not overlapped by host peaks.

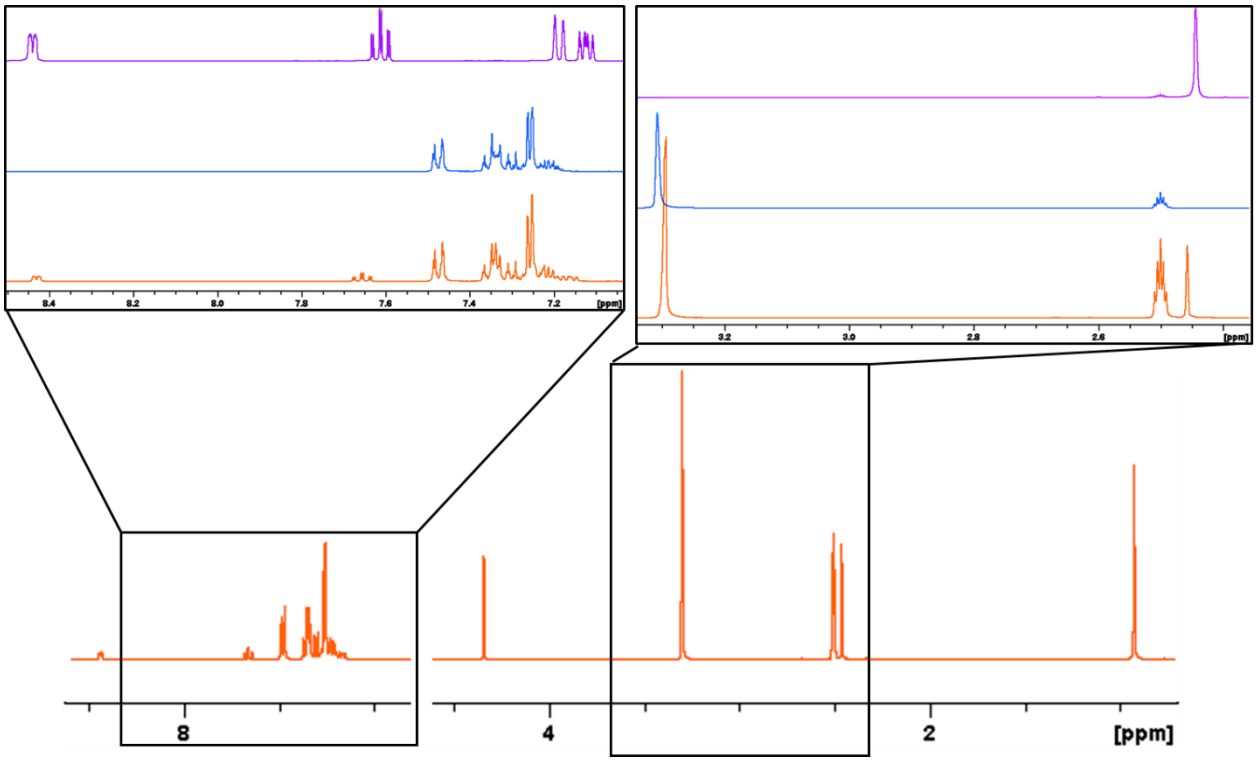

Figure 3.47: ^{1}H-NMR spectra of **H3·2PIC** (orange) showing exploded views of the relevant guest peaks. The blue is the **H3** host and the purple 2-picoline. The midsection of the ^{1}H-NMR trace has been omitted for brevity. The solvent used was D_6-DMSO and the spectrum referenced to the DMSO solvent peak at 2.50 ppm. Spectra not to scale.

3.14 References

1. Barton B., Hosten E. C., Jooste D. V., Comparative investigation of the inclusion preferences of optically pure versus racemic TADDOL hosts for pyridine and isomeric methylpyridine guests, *Tetrahedron*, 2017, **73**, 2662, DOI: https://doi.org/10.1016/j.tet.2017.03.049.

2. Lusi M., Barbour L. J., Determining Hydrogen Atom Positions for Hydrogen Bonded Interactions: A Distance-Dependent Neutron-Normalized Method, *Cryst. Growth Des.*, 2011, **11** (12), 5515–5521, DOI: https://doi.org/10.1021/cg201087s.

3. McKinnon J. J., Spackman M. A., Mitchell A. S. Novel tools for visualizing and exploring intermolecular interactions in molecular crystals, *Acta Crystallogr.*, 2004, **B60**, 627-668, DOI: https://doi.org/10.1107/S0108768104020300.

4. 11. Speck A. L., PLATON, A multipurpose crystallographic tool, 1980-2000.

5. Bondi A., Van der Waals Volumes and Radii, *J. Phys. Chem.*, 1964, 68(3), 441-451, DOI: https://pubs.acs.org/doi/pdf/10.1021/j100785a001.

Chapter 4. Selectivity Experiments with H1, H2 and H3

4.1 Introduction

H1, **H2** and **H3** form inclusion compounds with all three picoline isomers and pyridine. The **H1** and **H2** compounds are novel and, therefore, there is scope for selectivity experiments to determine whether the host shows any preference for one guest over another. Once again, the guests were 2-picoline, 3-picoline, 4-picoline and, to a limited extent, pyridine. The selectivity experiments for **H3** were repeated, as the reported literature only gave the results for 50/50 compositions and, therefore, 75/25 and 25/75 compositions were useful in outlining a more accurate curve. This would give more insight into the selectivity of **H3**.

4.2 Preparation of Inclusion Complexes

50 mg of the host material was weighed out and mixed with 1.5 ml of binary guest mixtures. The mole fractions of each guest were varied in order to obtain an accurate determination of the host selectivity. The solutions were stirred briefly until the liquid was clear and were left open on the benchtop to facilitate slow evaporation. The evaporation occurred at room temperature and was monitored each day for crystal growth.

It was noted that **H1** is less soluble in 2-picoline, but dissolved easily in 3-and 4-picoline. This difference in behaviour is strange, considering the guests are isomers and there is no functionality argument that can explain why **H1** would dissolve in the others but not 2-picoline. This effect was noticed during the synthesis of the inclusion compound **H1·2PIC**. However, large amounts of the 2-picoline guest were not required for the selectivity experiments, as when 2-picoline was mixed with 3- and 4-picoline there were no solubility issues. Colourless crystals appeared over the course of one day to two weeks.

4.3 ^{1}H-NMR Analysis of Inclusion Compounds

Crystals were removed from the mother liquor, patted dry and dissolved in deuterated dimethyl sulfoxide (D_6-DMSO), and then analysed using ^{1}H-NMR spectroscopy. The spectra were compared with the host and guest reference spectra and the proton signals assigned. In the case of mixtures, the integrals of certain peaks corresponding to each guest were compared to determine the composition of the crystals.

4.3.1 ^{1}H-NMR Analysis of Guest Peaks

In order to determine the composition of the inclusion compounds, it is necessary to differentiate the guests. As they are isomers, they have similar spectra. However, there are enough differences to allow for the quantification of the amount of each respective guest within the sample of inclusion compounds. The proton assignments and chemical shifts for the pure picoline guests are shown in Table 4.1.

The chemical shifts of the methyl (CH_3) peaks are different for the three guests, notably the peak for 2-picoline is around 0.2 ppm further downfield from 3- and 4-picoline. This methyl peak is convenient to distinguish 2-picoline from 3- and 4-picoline as it is a large, readily identifiable, and distinct peak. The methyl peaks of the 3-picoline and 4-picoline are very close

Table 4.1: Proton chemical shift assignments for the pure picolines in D_6-DMSO in ppm

	2-picoline	**3-picoline**	**4-picoline**
	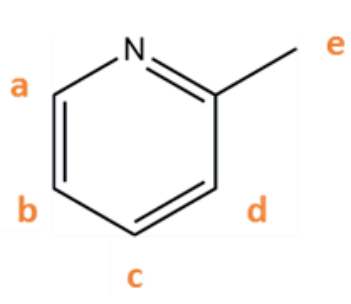	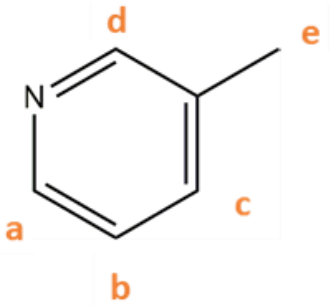	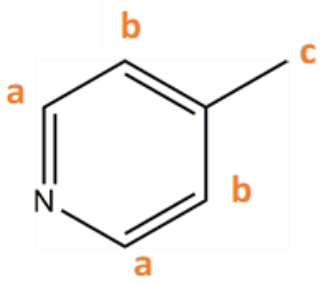
a	8.44	8.37	8.42
b	7.12	7.22	7.16
c	7.61	7.54	2.27
d	7.18	8.40	n/a
e	2.44	2.25	n/a

but are still able to be identified, as the 3-picoline peak is slightly upfield of the 4-picoline peak. However, the proximity can present issues when quantifying those peaks as the overlap in integrals distorts the results.

An overlay of the spectra obtained from each of the three guests is shown in Figure 4.1. In addition to the methyl peaks described above, the aromatic regions of the 2- and 4-picoline overlap. This is not an issue, though, as the methyl peaks are at a reasonable distance apart, allowing for easy integration and quantification. As described above, the methyl peaks of 3- and 4-picoline are in close proximity, meaning that the aromatic region becomes more important when determining the composition of a mixture of these two guests. The doublet of 3-picoline at 7.54 ppm is distinct from the two aromatic peaks of 4-picoline, allowing integration and comparison in the case of that particular mixture. 4-picoline has only two peaks that fall within the aromatic region, as the symmetry of the molecule results in two equivalent aromatic environments. The spectra of all three guests with the important regions highlighted are shown in Figure 4.1.

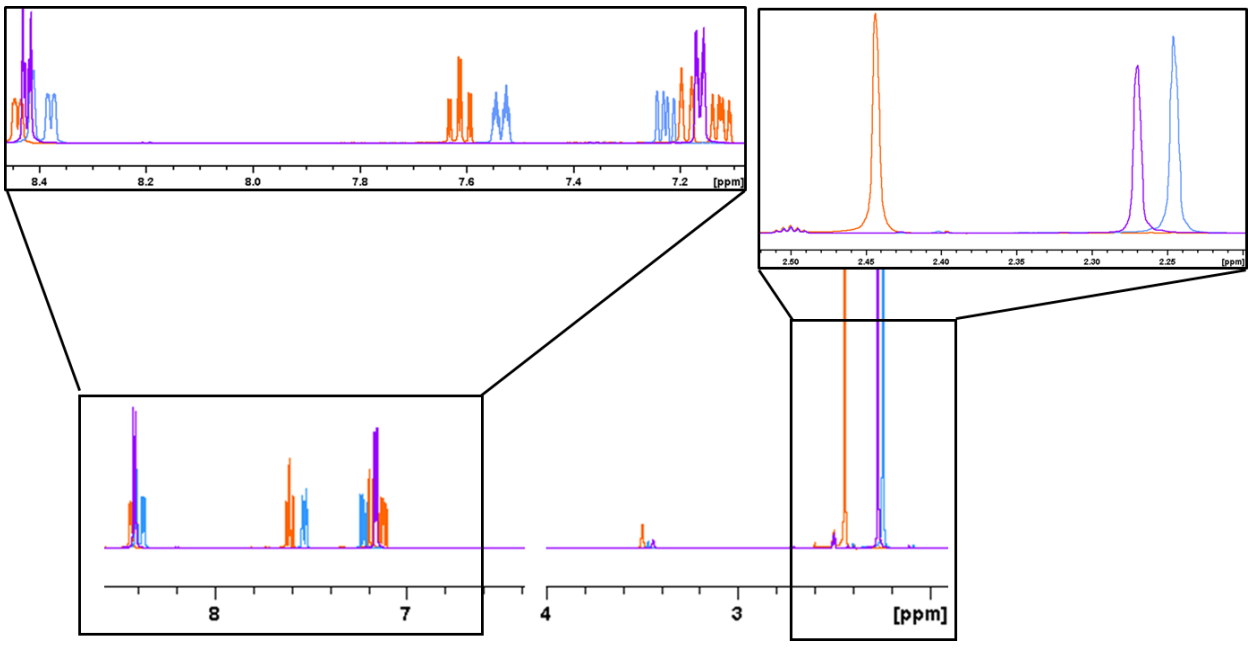

Figure 4.1: ^{1}H-NMR spectrum showing the overlays of three picoline guests; 2-picoline (orange), 3-picoline (blue) and 4-picoline (purple) in D_6-DMSO. The solvent peak was fixed to 2.50 ppm.

4.3.2 Analysis of the H1 Inclusion Compounds.

When ^{1}H-NMR analysis is performed and the spectra of the **H1** inclusion compounds obtained, there are both host and guest peaks present. There are two host peaks corresponding to the four methyl (CH_3) groups on the phenyl rings, which fall into the same region as the guest methyl groups. The methyl peak from 2-picoline is distinct as it is slightly more downfield than the 3-/4-picoline, which both become obscured by a host peak. This issue can be overcome as it is known that the host:guest ratio is 1:1 (via SCXD and thermal analysis) and, therefore, the host peak would integrate for six hydrogen atoms. The combined peak, featuring a host peak and a 3-/4-picoline methyl peak, can be integrated and the 6 corresponding to the host hydrogen atoms can be subtracted. This gives the integral of the guest methyl group only.

The spectrum pictured in Figure 4.2 shows the results of the competition experiment between 2-/3-picoline, which were present in a 50:50 ratio in the initial solution. This serves as an example of how all the 2-/3-picoline mixed spectra were analysed. The method of integration

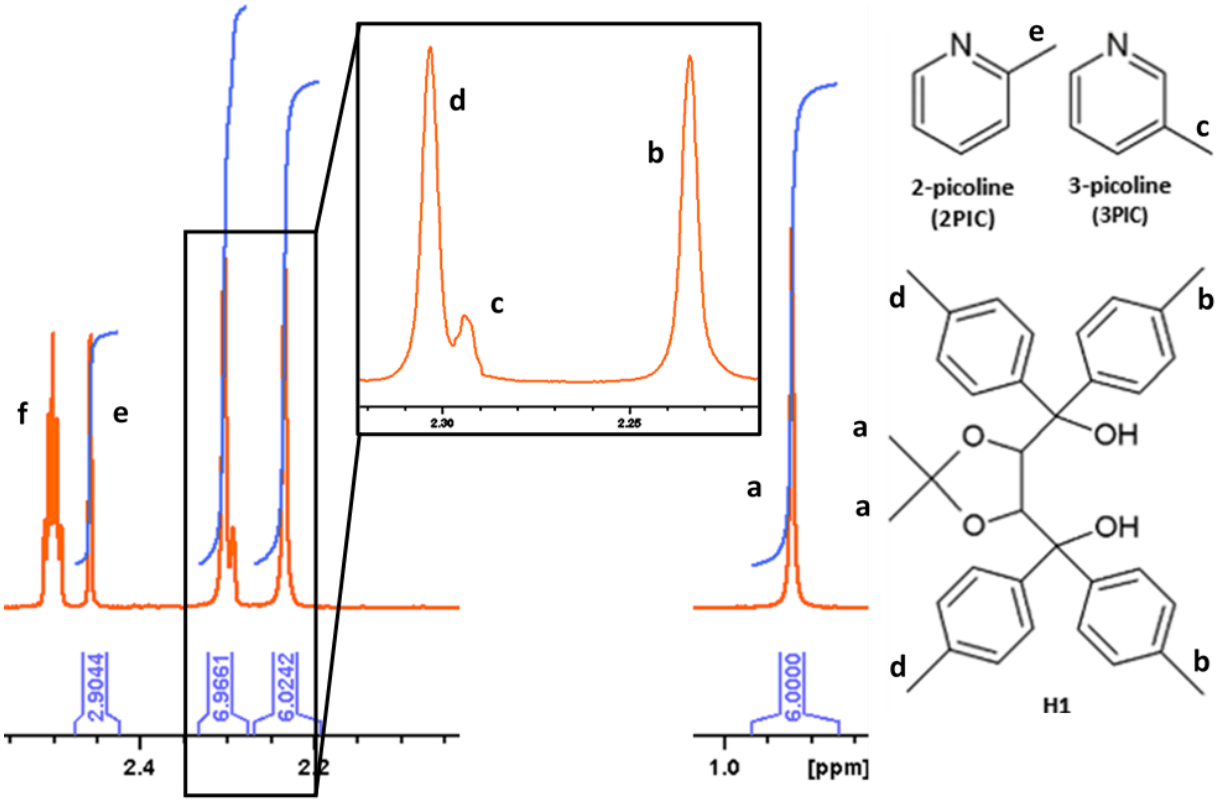

Figure 4.2: ^{1}H-NMR spectrum showing the spectrum of **H1** exposed to a binary mixture of 2-picoline and 3-picoline. Inset shows the corresponding environments on the guests and hosts. Mid-section of the spectrum is omitted for clarity. Spectra not to scale.

is shown below in Figure 4.2. First the peak labelled *a* is calibrated to 6, which corresponds to the two methyl groups on the dioxolane ring in host compound. The peak labelled *e*

$$\text{\% inclusion of 2-picoline: } \frac{2.9044}{[2.9044+0.9661]} \times 100 = 75\% \text{ (using peaks } a \text{ and } b\text{)}$$

corresponds to the methyl group of the 2-picoline, while the peaks *d* and *c* are a blend of host and 4-picoline methyl group with *b* also a host peak. The overall integral is measured and the 6 simply subtracted from the result.

This gives a result of 75% of 2-picoline and 25% 3-picoline and this method was employed whenever a sample contained a mixture of 2- and 3-picoline or a mix of 2- and 4-picoline.

However, in the case of a 3-/4-picoline mixture, the above method is no longer useful. As can be seen, once inclusion occurs, the host peaks described above overlap with the methyl peaks of 3- *and* 4-picoline, leading to issues with integration. Therefore, the aromatic region has to be used to determine the ratios of the relevant guests. This is illustrated in Figure 4.3, where peak *b* shows an overlap of 3- and 4-picoline CH_3 peaks across a host peak, making it impossible to discern the ratio. The peak labelled *a* corresponds to a host peak. Therefore, the 3-picoline peak at 7.60 ppm (labelled *e*) or at 7.26 ppm (*d*) is utilised and compared to that at 7.20 ppm of 4-picoline (*c*).

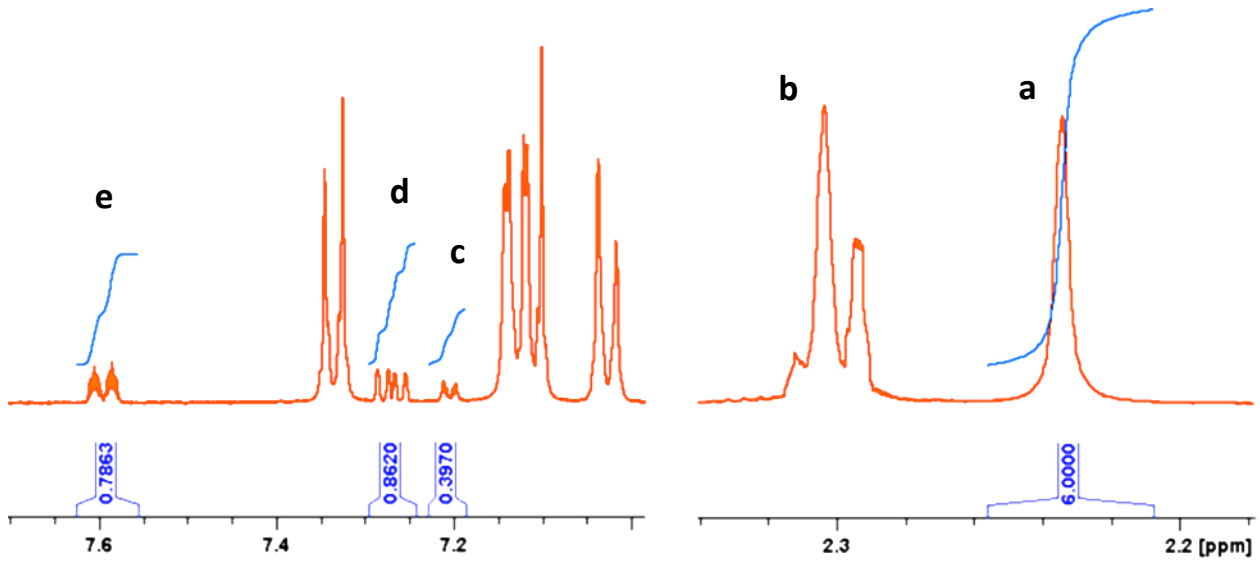

Figure 4.3: ^{1}H-NMR spectrum of the sample which contains a mixture of 3-picoline and 4-picoline and **H1**, the mid-section has been omitted for clarity. Spectra not to scale.

The selectivity percentage is calculated below, noting that peak *c* corresponds to two protons as 4-picoline is symmetrical and, therefore, there are two equivalent aromatic proton environments.

$$\text{\% inclusion of 3-picoline: } \frac{0.7863}{[0.7863+(0.3970\div 2)]} \times 100 = 80\% \text{ (using peaks } e \text{ and } c\text{)}$$

$$\text{\% inclusion of 3-picoline: } \frac{0.8620}{[0.8620+(0.3970\div 2)]} \times 100 = 81\% \text{ (using peaks d and } c\text{)}$$

The percentage inclusion for the above spectra would be 80-81% 3-picoline, depending on whether peak *e* or *d* was used in the calculation. The average, in this case 80%, is reported in all cases. This was the method used to analyse all samples which contained a mixture of 3- and 4-picoline with **H1**.

4.3.3 Analysis of the H2 Inclusion Compounds.

The method of determining the guest composition of the **H2** inclusion compounds is similar to that of **H1**. The lack of para-methyl groups on the phenyl rings removes the two host peaks which were present in the **H1** inclusion compound spectra. This means that all the guest methyl peaks are unobstructed and can be used to determine guest inclusion ratios. The peaks are well apart in the case of a mixture of 2-picoline and 3-/4-picoline and have been illustrated in Figure 4.4.

Figure 4.4 is an example where there is a mixture of 2-picoline and 4-picoline in the resulting inclusion compounds. The original mother liquor contained 75% 2-picoline and 25% 4-picoline. The peak at approximately 1.00 ppm corresponds to the two methyl groups on the host dioxolane and corresponds to six hydrogens. This is used as the calibration peak. The 2-picoline peak is further downfield and integrates to 0.1975 and the 4-picoline peak integrates to 2.6967.

$$\text{\% inclusion of 4-picoline: } \frac{2.6967}{[2.6967+0.1975]} \times 100 = 93\%$$

Despite 4-picoline making up only 25% of the initial starting solution, it constitutes 93% of the guests included in the resulting crystals. This gives great insight into the selectivity of **H2** and

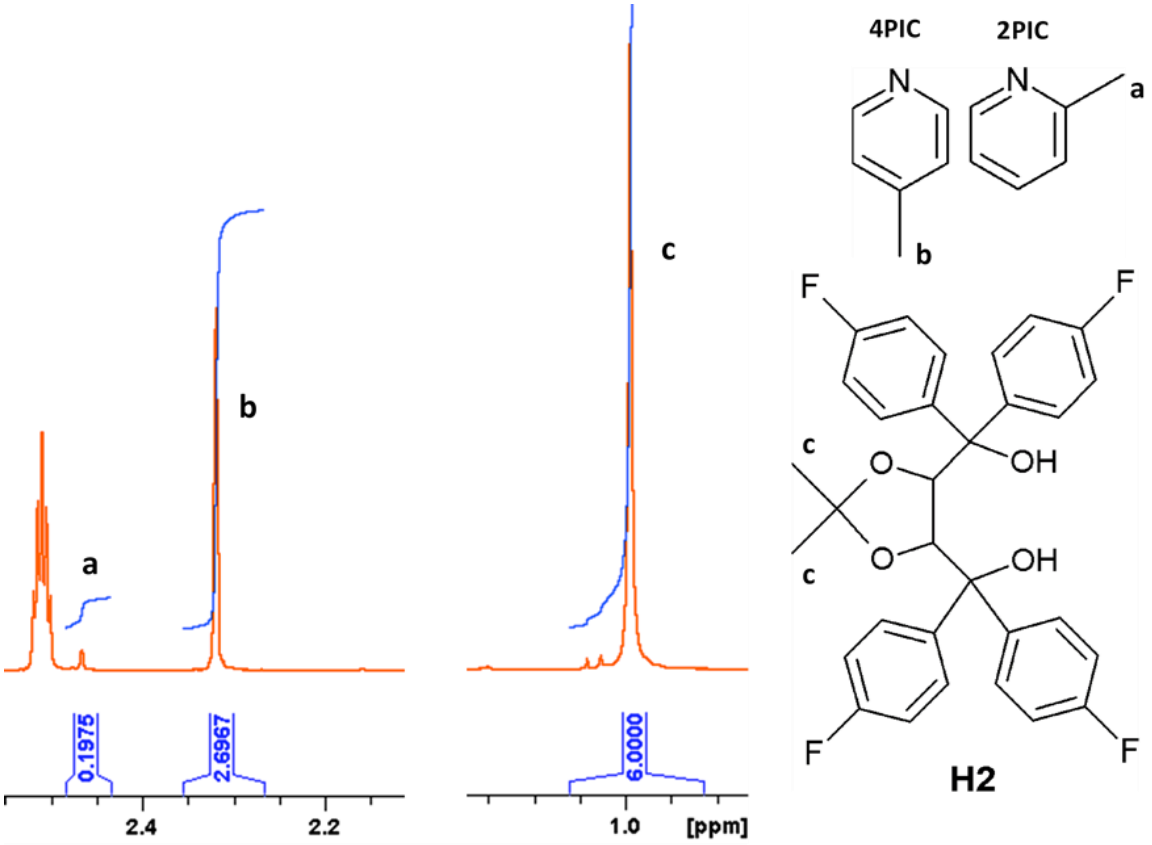

Figure 4.4: ^{1}H-NMR spectrum showing the result of H2 exposed to a mother liquor of 75% 2-picoline and 25% 4-picoline. The peaks used to determine the overall guest composition have been indicated along with the corresponding environments on the host and guest moecules. The mid-section has been omitted for clarity. Spectra not to scale.

the fact that 4-picoline is so favoured is interesting. This method of determining the guest components was used for identifying mixtures of 2-picoline and 3-picoline as well.

The methyl peaks of 3-picoline and 4-picoline are relatively close on the ^{1}H-NMR spectrum, as seen in the case of mixtures with **H1**. The absence of the para methyl peaks in **H2** allow for the methyl peaks of 3- and 4-picoline to be integrated accurately and, therefore, samples which include a mixture of these guests can have their compositions quantified using these peaks. This process is shown in Figure 4.5 where the **H2** host was exposed to a mixture of 50/50 3-picoline and 4-picoline in the starting solution. The resulting sample comprised a mixture of the two guests and, while the peaks were close, it is possible to integrate each peak separately in order to determine the amount of each guest present in the sample. The peaks were once again calibrated to the six-hydrogen host peak at 1.0 ppm. The 4-picoline

$$\text{\% inclusion of 4-picoline: } \frac{2.3507}{[2.3507+0.5958]} \times 100 = 80\%$$

peak is slightly more downfield of the 3-picoline peak and therefore the peaks can be identified. The results of this selectivity experiment are as follows.

H2 shows a preference for 4-picoline over 3-picoline in this case.

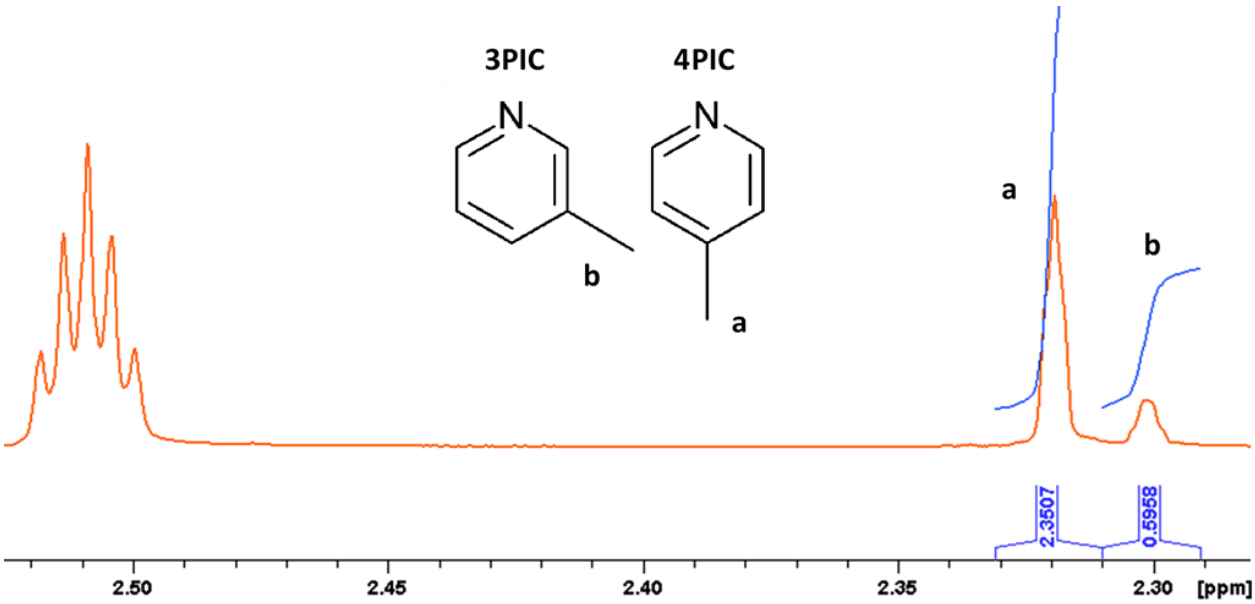

Figure 4.5: ^{1}H-NMR spectrum showing the result of H2 exposed to a starting solution of 50% 2-picoline and 50% 4-picoline. The peaks used to determine the overall guest composition have been indicated.

4.3.4 Analysis of the H3 Inclusion Compounds.

The inclusion compounds with **H3** were analysed in much the same way as **H2**, with the lack of host peaks in the methyl region allowing for unobstructed integration of the methyl peaks. Once again, the 2-picoline methyl peak was notably downfield of the ones associated with the methyl groups of 3-picolines and 4-picoline. The 3- and 4-picoline peaks were also far enough apart to allow for accurate integration and it was possible to analyse these mixtures. Since the method of determining the guest composition within the sample was identical to that of **H2** example spectra have not been included.

The spectra are included in the Supplementary Information and the resulting selectivities are outlined in the Supplementary Information.

4.4 Results of the H1, H2 and H3 Competition Experiments

Competition experiments were set up by weighing out 50 mg of host and adding 1.5 ml of binary picoline guest mixtures. The molar fractions of each guest were varied in order to obtain a series of results which would be used to generate a selectivity profile. The resulting crystals were collected and subjected to ^{1}H-HMR analysis. The spectra were analysed as described above in section 4.3 and the results plotted to generate selectivity curves. These selectivity curves are obtained by plotting the percentage of a given guest present (Z) in the resulting crystals against the amount of that guest present in the starting mixture (X).

The first series was that of **H1** and a comprehensive profile was generated for all three binary competition series. The selectivity profiles for 4PIC vs 2PIC, 3PIC vs 2PIC and 4PIC vs 3PIC are included in Figure 4.6. All three selectivity profiles are sigmoidal in nature (refer to Figure 1.9). The red square markers show the results of each spectrum and the grey line shows no selectivity and acts as a reference. In Figure 4.6a, **H1** shows a slight preference towards 2-picoline over 4-picoline, with the starting mixture containing a 50/50 mixture yielding crystals containing only 2-picoline. Figure 4.6b once again has 2-picoline as the more favoured guest, with the selectivity profile notably skewed towards 2-picoline. The preference for 2-picoline over 3-picoline is slightly stronger than that for 2-picoline over 4-picoline. The final profile in Figure 4.6c has the host subjected to binary mixtures of 4-picoline and 3-picoline. In this profile it can be seen that 4-picoline is definitely preferred over 3-picoline as when 4-picoline only makes up 40% of the initial solution it is expressed in all of the crystals sampled.

These results allow for the preference of **H1** to be established and a selectivity order generated. It can be said that **H1** prefers 2-picoline over both 3-picoline and 4-picoline, and 4-picoline over 3-picoline. This gives a selectivity order of 2-picoline > 4-picoline > 3-picoline. This order is also confirmed when looking at the area under the curve where a greater area corresponds to a higher preference.

The selectivity profiles for the second host **H2** are included in Figure 4.7. These profiles were generated in the same way those for **H1.**

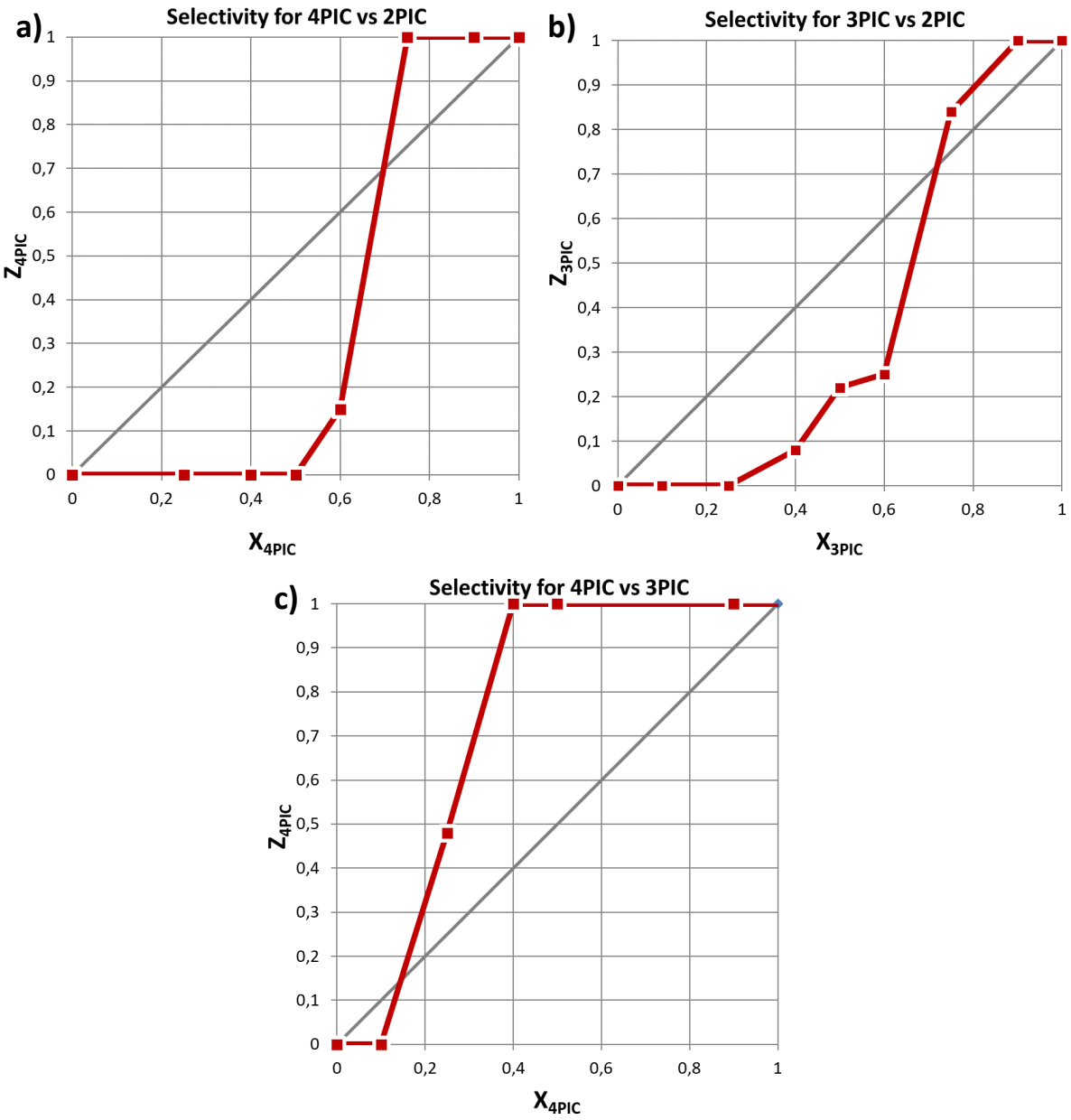

Figure 4.6: Results of the **H1** binary competition experiments with a) 4PIC/2PIC b) 3PIC/2PIC and c) 4PIC/3PIC for **H1**. X_A is the mole fraction of guest A in the starting solution and Z_A the amount of that guest in the resulting crystal mixture.

In Figure 4.7a, **H2** is exposed to varying mole fractions of 4-picoline and 2-picoline. This host has a strong preference for 4-picoline over 2-picoline, with 4-picoline making up 95% of the included guest when present at just 25% in the starting solution. There is a slight dip in the profile when going from a 25/75 mixture of 4-picoline/2-picoline to a 50/50 mixture but this can be attributed to the error associated with using ^{1}H-NMR to determine the ratios. The overall result of 4-picoline being preferred over 2-picoline is clear.

In Figure 4.7b, the selectivity profile for 3-picoline vs 2-picoline is shown. The preference is clearly skewed towards 3-picoline, with 3-picoline making up the majority of the included crystals at only 25% concentration. The profile for the 4-picoline versus 3-picoline competition experiment is shown in Figure 4.7c. There is a preference for 4-picoline over 3-picoline although not as pronounced as the preference for 4-picoline over 2-picoline. This gives the overall selectivity preference for **H2** as 4-picoline favoured over 3-picoline favoured over 2-picoline. This is different from **H1** in that 2-picoline does not seem to be favoured at all by **H2**.

The final set of selectivity profiles is given in Figure 4.8, which shows the results of competition experiments involving the picolines and **H3**. The selectivities of **H3** have been previously studied by Barton et al. However, Barton's investigation studied the ^{1}H-NMR results for **H3** exposed to binary 50/50 solutions of the picolines and pyridine. In this investigation the 50/50 experiments were repeated and further competition experiments with varied mole fractions of guests in the initial solution were conducted. This led to the generation of a selectivity profile for each binary pair of guests which would give more insight into the nature of the selectivity of **H3**. In Figure 4.8a the selectivity profile for 4-picoline versus 2-picoline is shown. It is clear that **H3** favours 4-picoline over 2-picoline with the former making up 95% of the included guest in the crystals generated from a 50/50 solution. Figure 4.8b shows that 3-picoline is markedly favoured over 2-picoline with 3-picoline being preferentially included even when making up as little as 25% of the starting solution. Finally, Figure 4.8c depicts the selectivity profile for 4-picoline vs 3-picoline. In this case the selectivity is less pronounced than those exhibited in the previous profiles. However, 3-picoline is preferred to 4-picoline. For example, in a 50/50 binary mixture of 4-picoline and 3-picoline, 3-picoline makes up 13% of the included guest. This gives a selectivity preference for **H3** as 3-picoline > 4-picoline > 2-picoline, which is in line with the study conducted by Barton et al.[1]

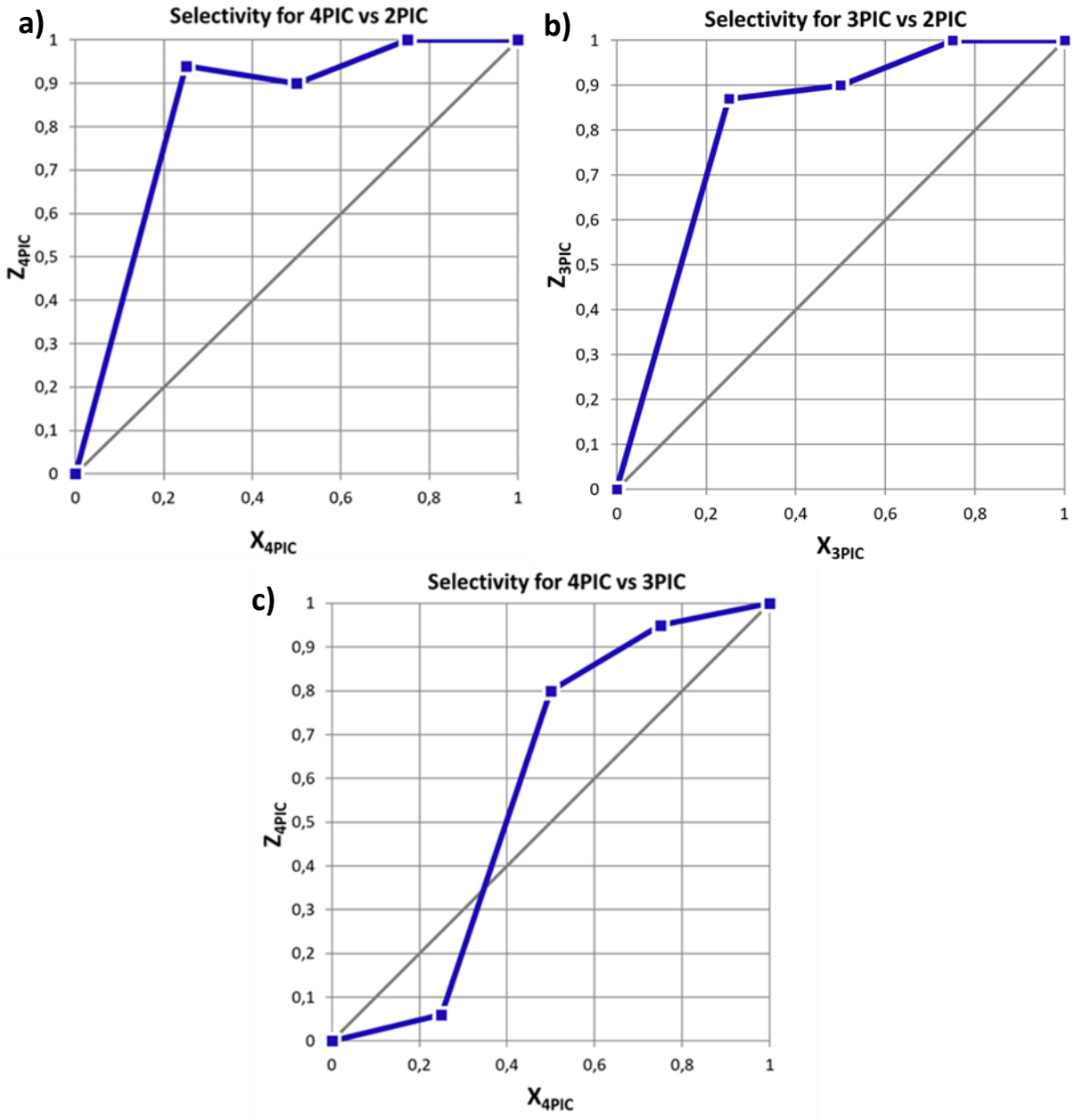

Figure 4.7: Results of the **H2** binary competition experiments with a) 4PIC/2PIC b) 3PIC/2PIC and c) 4PIC/3PIC for **H1**. X_A is the mole fraction of guest A in the starting solution and Z_A the amount of that guest in the resulting crystal mixture.

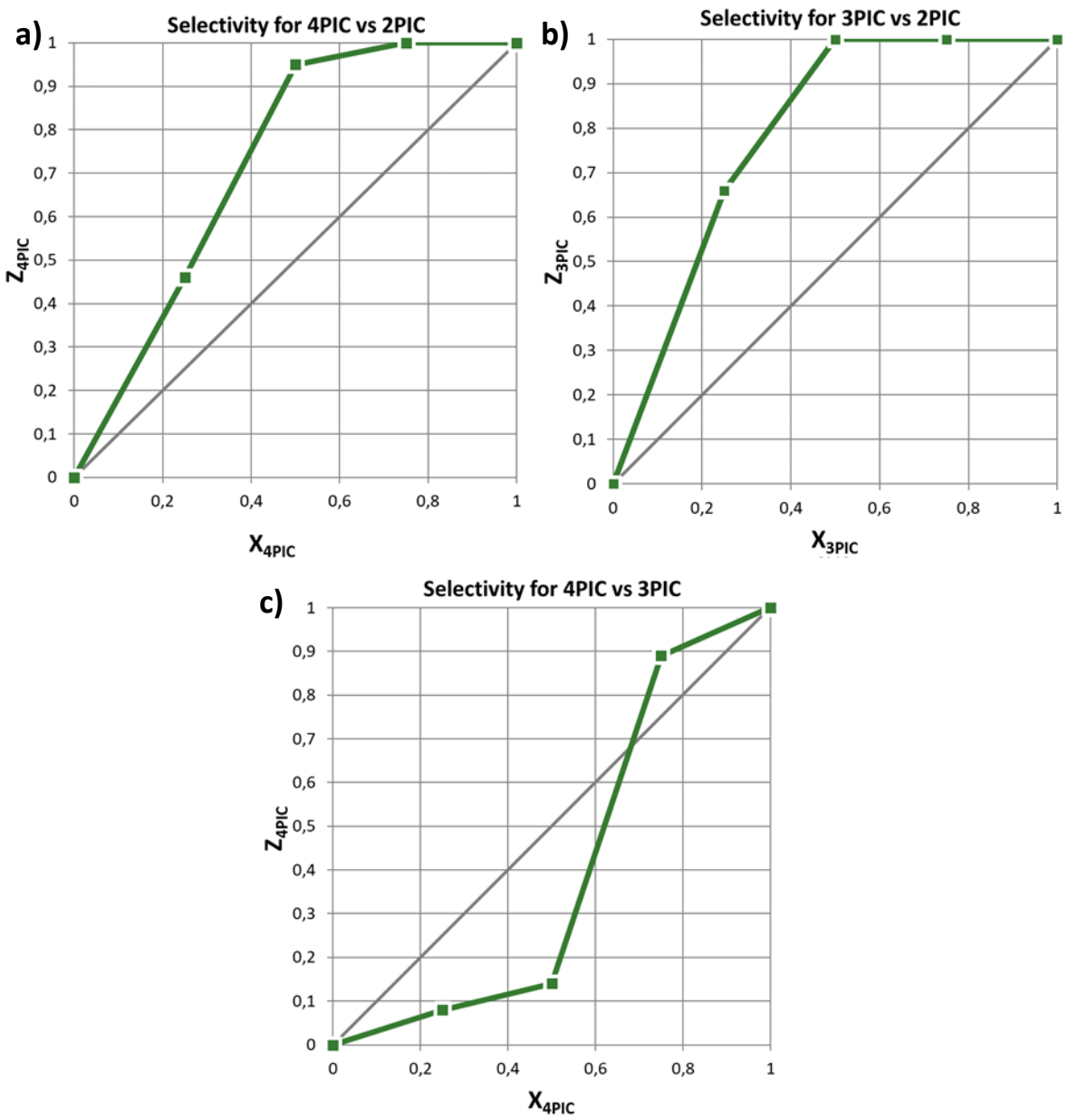

Figure 4.8: Results of the **H3** binary competition experiments with a) 4PIC/2PIC b) 3PIC/2PIC and c) 4PIC/3PIC for **H1**. X_A is the mole fraction of guest A in the starting solution and Z_A the amount of that guest in the resulting crystal mixture.

Overall, the three hosts show different selectivity preferences towards the three picoline isomers:

H1 has a preference for 2-picoline > 4-picoline > 3-picoline

H2 has a preference for 4-picoline > 3-picoline > 2-picoline

H3 has a preference for 3-picoline > 4-picoline > 2-picoline

These results show the impact of substituting one group or moiety for another. For example, the removal of the para-methyl groups on the phenyl rings of **H1** results in reversing the selectivity order. The most notable difference is that the 2-picoline guest, which is highly favoured by **H1**, is not at all preferred by **H2** and **H3**. Also, the preference of **H3** for 3-picoline is unlike that of either of the two other hosts. It is to be noted that the majority of **H3·4PIC** sample collected in these competition experiments is the hydrate form which was elucidated by Barton et al. in a previous investigation. It is also clear from the attempts to synthesise the non-hydrate form that the hydrated form is formed preferentially in typical conditions. These typical conditions are the use of the non-distilled 4-picoline guest and the growth of these compounds on the bench (as opposed to the desiccator required for the growth non-hydrate compound).

4.5 Discussion of Selectivity Results

There are a few potential reasons for the change in selectivity preferences and these will be further explored. The preferences may be related to the stability of the resulting inclusion compounds as the more stable a compound the more likely that it will be the one formed. A way to examine the stability of an inclusion compound is to consider the thermal results. DSC results can be used to determine the thermal stability of a compound by comparing the temperature of guest release to the boiling point of said guest.[2]

One can take the temperature of the guest release endotherm peak (T_{peak}) and subtract the guest's boiling point (T_{boil}) and the resulting difference indicates thermal stability. The larger the $T_{peak} - T_{boil}$ value the more stable the compound. This is due to the inclusion compound 'holding onto the guest' for longer, and therefore being more stable. Therefore, when looking at competition experiments, if Guest A is preferred to Guest B then it could be expected that the $(T_{peak} - T_{boil})_A$ would be greater than $(T_{peak}-T_{boil})_B$. The usual procedure is to establish T_{on}

(the onset temperature of an endotherm). However, if the endothermic peak is strongly skewed, giving an asymmetric profile, T_{on} is difficult to measure. We therefore employed T_{peak} throughout, because it can be measured consistently.

Table 4.2: The thermal data for the pyridyl host-guest complexes of **H1**, **H2** and **H3**.

Compound	TGA		DSC			
	Mass Loss		Guest Endo T_{peak} (°C)	Guest BP (°C)	Guest $T_{peak} - T_{bp}$ (°C)	Host T_{melt} (°C)
	Expt %	Calc %				
H1•2PIC	15.1	15.1	155.0	128.5	+26.0	211.8
H1•3PIC	15.2	15.1	142.8	144.0	-1.2	211.9
H1•4PIC	15.1	15.1	138.4	145.0	-6.6	211.7
H2•2PIC	13.5	14.7	117.2	128.5	-11.3	198.5
H2•3PIC	14.9	14.7	140.8	144.0	-3.2	201.0
H2•4PIC	14.9	14.7	148.3	145.0	+3.3	200.5
H3•2PIC	16.5	16.6	108.3	128.5	-20.2	214.8 / 217.5
H3•3PIC	16.4	16.6	140.9	144.0	-3.1	217.3
H3•4PIC	21.4	22.7	133.2	145.0	-11.8	217.5

These values for the inclusion compounds involved in the competition experiments are given in Table 4.2. Overall most of these values fall in line with the selectivity preferences exhibited by the hosts. For **H1** the most preferred guest, 2-picoline, has a T_{peak}-T_{boil} value of +26.0 °C which indicates it is a very thermally stable compound, especially in comparison to 3-picoline and 4-picoline which have values of -1.2 °C and -6.6 °C, respectively. It is noted that according to the selectivity profile 4-picoline is preferred over 3-picoline but the T_{peak}-T_{boil} values are not in that order. There is only a difference of approximately 5 °C and this is within the expected error but there may be other causes for the selectivity. This does however indicate that the selectivity for 4-picoline over 3-picoline may be close. **H1·2PIC** also has the structural feature of having the 2-picoline guests enclosed in lacunae which may improve stability as the crystal would naturally hold onto the guest for longer. It is the only **H1** structure to house guests in lacunae as the other structures have channels running through the crystal.

The **H2** compounds have the T_{peak}-T_{boil} values in line with the selectivity preference order. **H2·4PIC** is the most thermally stable with a +3.3 °C difference in peak and boiling temperature. It is also the most preferred guest and like **H1·2PIC** has its guests encased in lacunae. This is in contrast to **H2·2PIC** and **H2·3PIC** which have their guests arranged in channels. The 2-picoline inclusion compound is the least favoured and has the most negative T_{peak}-T_{boil} value.

The inclusion compounds formed with **H3** also show T_{peak}-T_{boil} values which are in line with the selectivity order determined from the competition experiments. The most positive value is -3.1 °C which is ascribed to **H3·3PIC** and is also the most favoured compound. The least positive is **H3·2PIC** which has the most negative value of all at -20.2 °C. While all the values for the **H3** inclusion compounds are negative the differences between them are significant. All three of these **H3** compounds have their guests arranged in channels, which may explain why all the values are negative.

Overall it seems that the fact that **H1·2PIC** and **H2·4PIC** have their guests enclosed in lacunae may increase their T_{peak} values and therefore their T_{peak}-T_{boil} values. These structures have positive values and are the most thermally stable. They are also the most preferred structures in their respective competition experiments. Overall it seems that DSC analysis can be extremely valuable in determining thermal stability and it is likely that thermal stability plays a large part in which inclusion compounds are preferentially formed as this trend holds true across all three competition studies.

There is another interesting aspect which may have an impact on the selectivity preferences of the host. The host compounds have varying solubility in each of the picoline isomers and the order of solubility seems to be in the same order of the selectivity preferences. The number of grams of liquid picoline required to dissolve a gram of host compound has been captured in Table 4.3.

Table 4.3: Number of mg guest required to dissolve 1 mg of host.

Host	Guest	Amount of Guest Required (mg)
H1	2-picoline	52.0
H1	3-picoline	7.9
H1	4-picoline	14.7
H2	2-picoline	10.5
H2	3-picoline	13.9
H2	4-picoline	14.3
H3	2-picoline	16.7
H3	3-picoline	28.3
H3	4-picoline	13.3

Notably, the solubility of **H1** in 2-picoline is much lower than in either 3-picoline or 4-picoline. It is significantly less soluble, requiring approximately 52 g of 2-picoline to dissolve one gram of **H1**. As shown by the competition experiments **H1** has a much higher preference for 2-picoline over 4-picoline and 3-picoline, and then prefers 4-picoline over 3-picoline. Also, according to the solubility experiments, more 4-picoline was required to dissolve **H1** than 3-picoline.

The solubilities are relatively close with **H2** so the trend is not as definitive, but the solubilities do fall in line with the selectivity preference of the host. 4-picoline is the least soluble and 2-picoline the most soluble. Similarly, in the **H3** experiments, more 3-picoline is required to dissolve one gram of **H3** than either 2-picoline and 4-picoline. This is in line with the selectivity preference displayed in the competition experiments as 3-picoline is clearly the most favoured guest. The 4-picoline guest is slightly favoured over 2-picoline in the selectivity experiments. However the solubilities of **H2** in these guests are not that distinct, with 4-picoline being actually the most effective at dissolving **H3**.

Overall, the solubilities of the hosts in the various guests do not precisely correlate to the selectivity preferences. It is notable, however, that two of the most favoured guests are relatively poor at dissolving those respective hosts. **H1** undoubtably favours 2-picoline in the competition experiments and this guest is required in large volumes to adequately dissolve the host. The 3-picoline guest is the least effective at dissolving **H3** and is the most favoured guest in those selectivity experiments. This trend, while not entirely reliable, does pique some interest regarding whether solubility in fact contributes to the selectivity behaviour exhibited by these host compounds.

A way this could manifest is during the growth of inclusion complex crystals. The method employed during this investigation is slow evaporation. The host is dissolved in the guest and left to stand at room temperature, the liquid guest slowly evaporates and, as the solution becomes more concentrated, the crystals begin to grow. If the host is not very soluble in the guest, then it stands to reason that the solution would reach the required concentration for crystallisation sooner than perhaps one with a higher solubility. This rationalisation of the selectivity seems straightforward; however the interplay of the guests within the binary solution is complex. For instance, if the host dissolves differently in each of the liquid guests then it stands to reason that when these guests are combined the solubility of the host would

change. It is difficult to quantify the nature or degree of this change and therefore dilutes the effect that the degree of solubility may have on the selectivities.

The amount of time for a crystal to form may also factor into the outcome of a selectivity experiment. If one crystal forms in solution much faster than another, then it may be over represented when the sample is collected for analysis. The time of crystallisation for each crystal is listed in Table 4.4. Note that is for the crystals to precipitate out of solutions which include only one guest. These experiments utilised 30 mg of host compound dissolved in 1.5 ml of each liquid guest. These were left at room temperature to evaporate and the time elapsed was noted as soon as crystals appeared.

Table 4.4: The time that it takes for each crystal to appear (days).

Compound	Time for Crystallisation (days)
H1•2PIC	1
H1•3PIC	15
H1•4PIC	6
H2•2PIC	9
H2•3PIC	11
H2•4PIC	11
H3•2PIC	5
H3•3PIC	3
H3•4PIC•H_2O	9

These results indicate that there may be a correlation between the solubility and the time in which the crystals precipitate out of the solution. If we look at the results of **H1**, the preferred guest 2-picoline produces crystals after only one day. This falls in line with the solubility experiments as the lower the solubility of the solid in solution the quicker the solution reaches the saturation threshold required to trigger crystallisation. This time of crystallisation order continues to line up with the results of the selectivity experiments for the remaining **H1** compounds. The least preferred guest, 3-picoline, takes over two weeks to crystallise out in the pure guest, well beyond both 2-picoline and 4-picoline.

With the **H2** compounds there is less of a distinction in the number of days for the crystals to be formed. All three compounds show crystallisation times from 9 to 11 days and this mirrors their solubilities, which are not significantly different. This similarity does not reflect the extent of the selectivity which is observed during the competition experiments where 2-picoline is notably rejected in favour of both 3-picoline and 4-picoline, and where 4-picoline

is preferred over 3-picoline. In fact, the **H2·2PIC** inclusion compound crystallises sooner than both the 4-picoline and 3-picoline compounds.

In the **H3** experiments, we see the most favoured **H3·3PIC** compound forming after only 3 days and this is in line with the solubility of **H3** in this guest. The 2-picoline and 4-picoline **H3** compounds are only present after 5 and 9 days, respectively. 2-picoline is the least favoured guest but forms before **H3·4PIC·H_2O**. This may be a consequence of the small solubility difference of **H3** in these guests, where it is slightly less soluble in 2-picoline. However, these solubilities are similar and may not be correlated to the crystallisation times at all. There are multiple aspects to crystallisation times, including the temperature of the ambient environment and potential nucleation sites such as dust in the vials. It may be the case that in a mixed guest system, where one inclusion compound precipitates early, that this crystal growth may trigger the other inclusion compound to form. For example, the crystal structures of **H1·3PIC** and **H1·4PIC** are isomorphous, which may allow the formation of one compound to seed the other.

In order to determine whether crystallisation times play a role in the outcome of selectivity experiments future work is needed where samples of the resulting crystals are collected at multiple intervals. This could give further insight into whether there is a change in the composition of the crystal mixture over time.

Ultimately the process of how crystals are formed in a mixed guest solution is unclear and there are potentially many ways to look at this resulting selectivity. The thermal stability of the resulting inclusion compound is correlated to the selectivities and may be a contributing factor to the preference of a host towards certain guests. While these aspects of solubility, time of formation and thermal stability are distinct it is likely that they all play a role to some degree.

4.6 References

1. Barton B., Hosten E. C., Jooste D. V., Comparative investigation of the inclusion preferences of optically pure versus racemic TADDOL hosts for pyridine and isomeric methylpyridine guests, *Tetrahedron*, 2017, **73**, 2662, DOI: https://doi.org/10.1016/j.tet.2017.03.049.

2. Caira M.R., Nassimbeni L.R., Niven M.L., Schubert W.D., Weber E., Dörpinghaus N. Complexation with hydroxy host compounds. Part 1. Structures and thermal analysis of a suberol-derived host and its host–guest complexes with dioxane and acetone, *J. Chem. Soc. Perkin Trans.*, 1990, **2**, 2129-2133, DOI: https://doi.org/10.1039/P29900002129.

Chapter 5. Discussion, Conclusion and Future Work

5.1 Discussion of H1 Compounds

Four novel inclusion compounds with **H1** were synthesised during the course of this investigation; **H1·2PIC**, **H1·3PIC**, **H1·4PIC** and **H1·PYR**. The structures of these complexes were elucidated and their packing, bonding interactions and powder patterns analysed. This was in addition to the TGA and DSC analysis used to confirm their stoichiometric and thermal stability. These compounds were also analysed using ^{1}H-NMR spectroscopy and these spectra were used to determine the results of competition experiments. These competition experiments were used to glean the selectivity preferences of **H1** towards the picoline guests and these selectivity preferences are discussed in Chapter 4.

The thermal stabilities of the resulting inclusion compounds correlate to the order in which the host selects the guests. There are various structural properties of the inclusion compounds that would affect the thermal stability, including the topography of the host-guest compound and the various bonds which are present in the structure. The temperature of the endothermic peak corresponding to the guest release is compared to the boiling point temperature of the pure guest to give an indication of thermal stability. The more positive the difference when the boiling point temperature is subtracted from guest release endotherm the more thermally stable the compound.[1]

The most thermally stable compound is the **H1·2PIC** inclusion compound with a difference of +26.0 °C. This strong positive difference implies that the guest is tightly bound within the crystal structure, taking it well past its boiling point before decomposing. This is congruent with the crystal structure where the 2-picoline guests are held in cavities within the crystal lattice. These cavities make guest release more difficult since the guests have no easy way to exit the crystal structure. This makes the structure more thermally stable. This topology is the result of intra- and intermolecular bonds present within the crystal structure. **H1·2PIC** contains three CH···π bonds shorter than 3.00 Å and three π···π interactions which are shorter than 5.00 Å. These are in addition to the two hydrogen bonds present as intra-host and host-guest interactions.

The **H1·3PIC** and **H1·4PIC** inclusion compounds have similar thermal stability, being -1.2 °C and -6.6 °C respectively. These are relatively close in comparison with the **H1·2PIC**'s +26 °C difference. These two structures are isomorphous and therefore the bonding needs to be looked at carefully to ascertain what could be affecting the thermal stability. Both of these guests are housed in channels within their crystal structures and therefore they are more likely to escape when subjected to heating. This is because the guests have a clear way out of their crystal lattices simply moving through the channels present in the structures. When looking at the bonds present in each of these crystal structures it is noticeable that there is an extra peak in the Hirshfeld fingerprint plot of **H1·4PIC** which corresponds to a host-guest O··H short contact which is not present in **H1·3PIC**. This is a notable interaction which is of significant strength as it presents as a sharp peak in the fingerprint plot. It is also the strongest interaction to be noted in the short contact table. **H1·3PIC** has a notable guest-guest π···π interaction of 3.956 Å which is the strongest one in comparison to **H1·4PIC** which has its shortest π···π interaction at 4.681 Å.

It is difficult to determine how to weigh up these interactions as the presence of a strong interaction may not outweigh several weaker interactions. However, it is clear that these inclusion complexes are similar to each other and the closeness in thermal stability is likely a result of very similar interactions occurring within the structures of these isomorphous compounds. The deciding factor, with regard to **H1** preferring 4-picoline over 3-picoline, may be a consequence of solubility or the time of crystallisation, both of which favour 4-picoline.

The fact that **H1·3PIC** and **H1·4PIC** are isomorphous may mean that in a mixed guest solution; as soon as some crystalline material is formed it leads to the growth of further crystals. This 'self-seeding' of a saturated solution may trigger the growth of inclusion compounds in a way that cannot be predicted in terms of thermal stability. This would muddy the selectivity preferences and would warrant further investigation. **H1·PYR** has been somewhat neglected due to not being involved in the selectivity experiments. It is isomorphous to **H1·3PIC** and **H1·4PIC**. It has a much lower boiling point than all of the picolines at only 115.2 °C and the DSC traces shows a guest release occurring at 137.6 °C. Therefore, when calculating thermal stability this results in a +22.4 °C difference. This is more stable than either **H1·3PIC** or **H1·4PIC** but less so than **H1·2PIC**. There are some intermolecular interactions which may contribute to this increase in thermal stability, including a guest-host C-H···π short contact which is

noticeably stronger than any present in the picoline compounds at 2.52 Å. There are also some weaker host-guest π···π interactions which may have an impact on the thermal stability. However, these interactions do not necessarily explain the large increase in thermal stability and more investigation would be necessary. It would be interesting to conduct competition experiments and generate selectivity profiles comparing the pyridine guest to the picoline. The thermal stability predicts that **H1** may favour pyridine over 3- and 4-picoline.

Overall, the structural analysis suggests that thermal stability ascribed to inclusion compounds may be linked to how the guests are contained in the crystal. The 2-picoline compound is the most thermally stable picoline inclusion compound and is also the one which has its guests enclosed in cavities within the crystal. This was linked back to the interactions present in the crystal structure and is correlated to the outcome of the selectivity experiments where 2-picoline is greatly favoured. The 4-picoline inclusion compound has several favourable interactions which distinguish it from the 3-picoline compound. This may explain why the thermal stabilities are close but 4-picoline is more favoured in competition experiments. The pyridine guest with **H1** needs further study but seems to have high thermal stability resulting from some several favourable interactions.

5.2 Discussion of H2 Compounds

Four novel inclusion compounds utilising **H2** were synthesised during the course of this investigation; **H2·2PIC**, **H2·3PIC**, **H2·4PIC** and **H2·PYR**. These inclusion complexes were further characterised with their structures being determined and their parameters, packings, interactions and powder patterns analysed. They were also subjected to thermal analysis and the **H2** host utilised in competition experiments with the picolines to generate selectivity profiles.

The first inclusion compound, **H2·2PIC**, was the least thermally stable compound, with a difference of -11.3 °C between the guest release endotherm on the DSC trace and the boiling point of 2-picoline. This suggests that there is some structural reason for the lack of stability and therefore the structural information needs to be examined. It is notable that this inclusion compound has a host:guest ratio of 2:2 and contains four asymmetric units within the unit cell. This leads to the guest forming large channels through the crystal lattice, with one channel forming a wide, kinked layer encompassing many guests. This may be the reason why

the inclusion compound is so poor at retaining the guest molecules when subjected to thermal stress. These wide channels which hold many guests would allow for easy escape and would lead to rapid decomposition of the crystal structure.

When examining the interactions within the inclusion compound the Hirshfeld surface does not indicate any particularly strong peaks aside from the hydrogen bonds. The π···π interactions are noticeably weaker than those noted in the **H1** inclusion compounds with all being 4.70 Å and longer. There is a F···F contact within the asymmetric unit which is unique in the **H2** series of inclusion compounds. As above, it is difficult to quantify the contributions of all the weak and strong interactions. However, no interaction really stands out as a factor in stabilising this inclusion compound. This lack of thermal stability may contribute to why it is the least favoured guest in the **H2** series. The 2-picoline guest is also the best at dissolving **H2** which may also contribute to the selectivity preferences.

The **H2·3PIC** inclusion compound is the second most thermally stable of the **H2**-picoline inclusion compounds. The $T_{peak} - T_{boil}$ value is -3.2 °C, which indicates that the inclusion compound holds on to the guest until close to its boiling point. This suggests that the **H2·3PIC** structure is more stable than that of **H2·2PIC**, which is much less thermally stable. The structure once again has a host:guest ratio of 2:2 and notably one of the 3-picoline guests is enclosed within a dimer consisting of two hosts. The topology shows that the guests are held in channels which are one guest in width (as opposed to two in **H2·2PIC**), which suggests that the channels are perhaps more constricted. This could inhibit the release of guests during thermal experiments but would still allow for the guests to move out of the crystal lattice. There are three strong π···π bonds which are less than 4.5 Å and two these occur between a host molecule and the entrapped 3-picoline guest. The third is an interaction between the two hosts in the asymmetric unit. The non-entrapped guest still experiences a number of host-guest F···H interactions and these make up a large percentage of the Hirshfeld fingerprint plot. These interactions may contribute to the stability of the **H2·3PIC** inclusion compound. The 3-picoline has easily dissolves the **H2** host compound but is not significantly better than 2-picoline. 3-picoline is significantly more preferred by **H2** in the competition experiments than 2-picoline and this may be related to the thermal stability of the resulting inclusion compound.

H2·4PIC shows the greatest thermal stability of the **H2** picoline inclusion compounds. The host-guest compound holds on to the guests +3.3 °C past 4-picoline's boiling point. This suggests that there is a good fit between host and guest and that there is some structural reason for why it is slightly more stable than **H2·3PIC** and significantly more stable than **H2·2PIC**. This **H2·4PIC** inclusion compound has a host:guest ratio of 1:1 and the guests are housed in cavities. These cavities hold on to the 4-picoline guest and would make it more difficult for the guests to exit the crystal when exposed to heat. Cavities indicate that there is a better fit of host and guest and suggest that there are significant interactions which result in this topology. When analysing the interactions present in the crystal structure there are fewer than those present in both previous **H2** structures. This is due to the diminished host-guest ratio. There is a host-guest π···π interaction which is 3.691 Å in length, which is the shortest so far described in the **H2** series, implying that it is a strong interaction. The two strongest short contacts are H···C in nature and run from host to the two carbon atoms on either side of the nitrogen atom in the guest. This may enhance the total interaction and stabilise the hydrogen bond, which is the primary interaction between host and guest. These additional interactions may contribute to the snug fit of guest within **H2**, leading to the enclosed cavity topography. This may explain why 4-picoline is significantly favoured over 2-picoline in the competition experiments. However, it is only slightly more favoured than 3-picoline. The fact that the 4-picoline inclusion compound is somewhat more thermally stable may explain this selectivity preference.

The **H2·PYR** inclusion compound suffers from the same lack of information as **H1·PYR** as pyridine was not included in the **H2** competition experiments. The results of the DSC show that **H2·PYR** retains its guests well beyond the pyridine boiling point with a T_{peak}- T_{boil} value of +12.3 °C. This is significantly more stable than any of the previous **H2** inclusion compounds. This compound has a host-guest ratio of 1:1, like the 4-picoline compound, and the guests are housed in channels. The intermolecular interactions show some relatively strong F···H and one F···F but overall there is not a singular or set of interactions which distinguish themselves from the previous **H2** structures. This would require further investigation as to why this inclusion shows much higher thermal stability. It would be likely that this **H2·PYR** is favoured in selectivity experiments but further analysis regarding solubility may be useful.

Overall, these compounds show thermal stability which can be explained by their topology and intra-/intermolecular interactions. The most thermally unstable inclusion compound is the one with 2-picoline and this may be due to the nature of the guests forming large channels within the crystal lattice. **H2·3PIC** and **H2·4PIC** have similar thermal stabilities. However the main difference is that the 4-picoline guests are housed in cavities with the inclusion compound and 3-picoline in channels (but smaller channels than **H2·2PIC**). These structural features and thermal stabilities can be compared to the interactions present in the inclusion compounds. These factors may play a role in the selectivity preferences of **H2** but further investigation is required. The pyridine inclusion compound presents some questions regarding how thermal stability arises, and further analysis of the interactions present in the structure may be warranted. Since pyridine is not isomeric with the picolines the degree to which one can compare these may be called into question.

5.3 Discussion of H3 Compounds

This investigation produced two novel inclusion compounds with **H3**; **H3·2PIC** and **H3·(1.5)4PIC**. The 2-picoline inclusion compound completed the series studied by Barton et al., who were not able to elucidate the structure of **H3·2PIC**. The initial 4-picoline and **H3** inclusion compound reported by Barton et al. contained waters of crystallisation and this made comparison difficult since the inclusion of water makes it difficult to study structural and thermal features of inclusion compounds. A new **H3·(1.5)4PIC** inclusion compound was synthesised and further studied in this project.

Since two novel structures were synthesised in this series the discussion will centre around these inclusion compounds. The additional three **H3** structures with 3-picoline, 4-picoline and pyridine have been previously described by Barton et al. However, further analysis of these compounds may be valuable when looking at the thermal profiles in order to determine the relationship between thermal stability and structural features.

H3·2PIC is the least thermally stable with the difference between guest release and the 2-picoline boiling point being -20.5 °C. These guests are held in channels with slight restrictions across the channel face. There are multiple intermolecular interactions present in this inclusion compound, with a large mix of host-host and host-guest short contacts. There are no particularly strong π···π interactions present and no notable spikes in the Hirshfeld

fingerprint. Thermal analysis shows a two-step guest loss and there is clearly a rearrangement after the first guest loss. This may mean there is a second inclusion compound formed during the heating process. In the competition experiments the 2-picoline is the least favoured guest and this may be related to the thermal stability of this compound.

H3·(1.5)4PIC was synthesised by drying the 4-picoline liquid guest and growing the crystals in a desiccator. This resulted in an inclusion compound which did not contain water but was disordered. The thermal analysis showed a $T_{peak} - T_{boil}$ of -42.6 °C which is very thermally unstable. The guests are held in wide channels which take up a large part of the unit cell due to the disordered nature of one of the guests.

The PLATON programme was used to calculate some contacts and these gave limited insight into the interactions within this crystal structure.[2] One guest is hydrogen bonded to the host molecule but the disordered guest is not. This most likely contributes to the thermal instability as the hydrogen bond between host and guest has been the strongest bond throughout these inclusion compounds. The two **H3** and 4-picoline compounds have very similar structures in terms of host alignment, with the major differences being the placement of the guests. These structures are so similar that the PXRD patterns are almost identical, requiring the use of thermal analyses to determine which crystal is formed. The hydrate structure is more thermally stable than the non-hydrate, which correlates to the fact that when **H3** is grown exposed to the atmosphere it always prefers to form the hydrate. This shows that the more thermally stable product is the one produced.

Thermal analyses of **H3·3PIC** and **3H3·(4)4PIC·H_2O** were conducted and the thermal stabilities calculated. This showed that the 3-picoline structure was the most thermally stable with a $T_{peak} - T_{boil}$ of -3.1 °C. Further structural analysis would need to be conducted in order to determine the reason behind this stability. It is notable that 3-picoline is the guest most preferred by **H3** and this may be correlated to the thermal stability of the resulting inclusion compound. 3-picoline is also the least effective at dissolving **H3**, which is also factor worth considering. **3H3·(4)4PIC·H_2O** is the second most thermally stable but the release of water at 93.9 °C may cause breakdown of the crystal structure, which would cast doubt on the accuracy of the guest release. This means that the $T_{peak} - T_{boil}$ value for this compound may not in fact be able to give insight into the thermal stability of the host-guest compound.

What is notable about the **H3** series is that the most preferred guest is the one which is the worst at dissolving the host. This may be an avenue to explore when looking at the selectivity preferences.

5.4 Conclusion

In summary, ten novel inclusion compounds were synthesised and characterised during the course of this investigation. The TADDOL-derived hosts **H1**, **H2** and **H3** were able to act as hosts towards all three isomers of picoline and pyridine, showing that the properties associated with these specialist molecules make them valuable host compounds.

These hosts exhibited some notable selectivity preferences towards different guests and these selectivities were compared to the stability of the inclusion compounds, their structural attributes and how they were dissolved by the liquid guests. Crystallisations in mixed guest systems are complex with the interplay between guests affecting the crystallisations in unknown ways. Further work on these types of systems would be encouraged.

The degree of selectivity is, in some cases, quite high which makes industrial applications possible. Even if industrial applications are not explored further, the insight gained into how hosts behave towards different targets is valuable for future work in host-guest chemistry.

5.5 Future Work

Future work into the crystallisation times of mixed guest systems would give insight as to whether the time of formation of the crystals determines the overall selectivity. Taking samples of crystals grown from mixed guest systems at different intervals of crystal growth to determine whether there is a change in crystal composition over time. The **H3** 3-picoline and 4-picoline hydrate compounds could be subjected to further in-depth structural analyses in order to account for the thermal stabilities obtained from the DSC traces. Different TADDOL-derived hosts could be used with the picolines to explore further discriminatory behaviour. The degree to which the solubility of the host compounds in the various guests affects the selectivities could be expanded upon. This could be achieved by employing co-solvents or determining the solubilities of hosts in mixed guest compounds.

5.6 References

1. Caira M.R., Nassimbeni L.R., Niven M.L., Schubert W.D., Weber E., Dörpinghaus N. Complexation with hydroxy host compounds. Part 1. Structures and thermal analysis of a suberol-derived host and its host–guest complexes with dioxane and acetone, *J. Chem. Soc. Perkin Trans.*, 1990, **2**, 2129-2133, DOI: https://doi.org/10.1039/P29900002129.

2. Speck A. L., PLATON, A multipurpose crystallographic tool, 1980-2000.